STUDY OF TURBULENT SPOTS IN THE FLAT PLATE BOUNDARY LAYER

Thesis

Submitted by

JOHN BARROW, B.Sc. (Edinburgh)

For the degree of

Doctor of Philosophy

The Fluid Dynamics Unit
Department of Physics,
University of Edinburgh.

September, 1974.

C O N T E N T S

C O N T E N T S (Contd.)

PREFACE

The research described in this thesis was conducted in the Fluid Dynamics Unit of the Department of Physics, University of Edinburgh, under the supervision of Dr. M. A. S. Ross. It is the original work of the author except where specific reference is made to other sources. It has not been submitted, in part or in whole, for any degree at any other University.

John Barrow

John Barrow.

SYMBOLS

The following symbols are used to describe the quantities indicated in this list, unless otherwise stated in the text.

X - distance from the leading edge of the flat plate.

Y - distance from the centre line of the flat plate perpendicular to X and Z.

Z - distance from surface of the flat plate.

U_o - free stream velocity.

U_B - streamwise undisturbed velocity in the boundary layer.

U_{BI}, U_{BO} - U_B at inner and outer hot wires.

ΔU_I, ΔU_O - streamwise mean flow disturbance velocity at inner and outer hot wires.

ΔV - spanwise mean flow disturbance velocity.

W - mean velocity normal to the plate.

u_I, u_O - streamwise turbulent fluctuation velocities at the inner and outer hot wires.

v - spanwise turbulent fluctuation velocity.

u' - streamwise root mean square turbulent intensity.

δ - boundary layer thickness.

h_X, h_Y, h_Z - mean vorticity components.

CHAPTER 1

INTRODUCTION

Boundary layers have been studied for many years and, in particular, aspects of the boundary layer on a flat plate parallel to the free stream have been dealt with in detail by very many workers. The understanding of the physical processes which make a boundary layer cease to be laminar and become instead turbulent has increased but the processes are by no means fully understood.

In 1883 Osborne Reynolds[12] reported his studies of flow in a pipe. He was particularly concerned with the transition from laminar to turbulent flow and observed the intermittent nature of this transition.

Much later, G.I. Taylor[16] suggested that if the pressure gradients associated with disturbances in the free stream were large enough when combined with the main stream gradient to cause local transient separation, then transition would occur almost immediately. He obtained good agreement with the results of experiments on a sphere in a wind tunnel with a high degree of free stream turbulence.

In 1951, Emmons[5] observed by chance what he called 'turbulent spots' on a sloping water table. At random instants tiny spots of turbulence appeared and grew as they moved downstream. He observed that the downstream portion of the flow was soon covered with continually growing turbulent spots until eventually the whole of this area was

turbulent. On the basis of these observations, he suggested that the concept of the transition region lying between two imaginary lines which divided the completely laminar and completely turbulent regions was wrong. Instead, he proposed a probability transition theory describing transition in terms of the random occurrence of the turbulent spots.

Subsequent work by Schubauer and Klebanoff[14], who used hot wire anemometers to investigate the natural transition of a laminar boundary layer on a flat plate in air, confirmed Emmons' hypothesis. In addition, they provided information on the geometry and propagation velocities of turbulent spots. The spots they observed were produced by discharging a spark through the boundary layer on a flat plate in a wind tunnel. It was observed that each turbulent spot was followed by a region of unusual stability which they described as a 'calmed' region and in which transition would not occur. In this region the boundary layer was thinner, with a fuller velocity profile, than the laminar boundary layer at the same Reynolds' number based on downstream distance. Afterwards the boundary layer soon reverted to its laminar state.

Schubauer and Klebanoff also observed that Taylor's hypothesis of transient separation before transition[16] was not verified when an adverse pressure gradient shortened the transition region to a few inches. Under such conditions reversal of the flow near the surface was prevented by the action of the shearing stresses which become high at the same time that the disturbance amplitude is large enough to cause such a reversal.

In 1956 Townsend gave an account of the state of the knowledge of a number of turbulent flows in his book, 'The Structure of Turbulent Shear Flow'.[17] He developed a formal theory for homogeneous, but non-isotropic turbulence based on the Navier-Stokes equations and proceeded to analyse the results of measurements on a variety of turbulent shear flows in terms of this theory. He discussed correlation and spectrum measurements, rates of production and dissipation of turbulent energy, and also turbulent intensity and mean velocity distributions in the flows.

This was a statistical approach to fully turbulent flow and was used by a large number of workers who developed a clear statistical picture for a variety of such flows. In the middle to late 1950's it appeared that such an approach had gone about as far as possible in describing fully developed turbulent flows and the emphasis in turbulent flow investigations then shifted to the transition region and the origins of turbulence.

A typical study of the new type was that of Hama, Long and Hagarty[6] in 1957, who reported their observations of the transition from two to three dimensional flow in a boundary layer using dye filaments in water. Tripping the flow with a small diameter rod attached to the surface, and later using a small step in the surface, they observed the development of longitudinal spanwise waves which became hair pin shaped vortices, with their 'legs' pointing upstream.

Klebanoff, Tidstrom and Sargent[9] in 1962 reported studies of three dimensional disturbances introduced into

a two dimensional boundary layer in air, using the vibrating ribbon method with strips of adhesive tape on the surface beneath the ribbon. Using hot wire anemometers, they demonstrated the actual breakdown of the three dimensional wave motion into turbulence to be a consequence of a new instability which arises in this three dimensional wave motion.

Kovasznay, Komoda and Vasudeva[11] also used adhesive tape on the surface below a vibrating ribbon to produce three dimensional disturbances in a laminar boundary layer in air. Longitudinal vortices were induced as a result and point breakdown of the flow always occurred at the disturbance intensity 'peaks' developed by the vortices. They obtained maps of the flow by using a probe system capable of mounting ten hot wires simultaneously.

More recently, attention has been given to the laminar sub-layer and inner layer of turbulent boundary layers.

Kim, Kline and Reynolds[8], in 1971, discovered streamwise streaks in both regions, which, on breaking up, ejected 'parcels' of momentum away from the wall. This 'bursting' phenomenon had been seen also by Corino and Brodkey[4] in 1969, who used a high speed cine-camera to photograph the trajectories of very small particles suspended in the flow in the inner layer.

The development, during the 1960's, of an experimental and statistical technique known as 'conditional sampling', has assisted in the studies of the transition region using hot wire anemometry. The fluctuations of the hot wire voltage caused by the arrival of an event in the flow at

the hot wire, are sampled by the electronic circuitry. If this signal satisfies some pre-set condition, then the signal is recorded for statistical analysis.

This technique was used by Willmarth and Lu[18] in 1972 to study the flow near the wall in a turbulent boundary layer in air. They concluded that their results, along with those of Kim et al.[8] and Corino and Brodkey[4], indicated the presence of a hair pin shaped vortex near the wall with its legs pointing upstream.

Conditional sampling has also been used to investigate the outer layer of the turbulent boundary layer.

Kaplan and Laufer[7], in 1969, used digital techniques involving conditional sampling to find the mean velocity deficit in the turbulent bulges in the outer flow field and the statistics related to the shape of the bulges.

Kovasznay, Kibens and Blackwelder[10], in 1970, obtained similar results using analogue techniques. They found the average structure of the large eddies in the outer flow field, using space-time and cross correlations of streamwise, normal velocity components and the intermittency function.

Blackwelder and Kovasznay[2], in 1972, showed that the Reynolds' shearing stress in the intermittent region is associated almost exclusively with the turbulent portions of the flow and that there is a mean rotational flow inside an "average" bulge in the interface between turbulent and non-turbulent flow. The large scale spanwise eddies were found to travel much more than ten boundary layer thicknesses before losing their identity; however the decay times were

different for the various velocity components associated with the large eddies. Also, evidence supporting the hypothesis that the violent bursting in the inner layer is ultimately associated with the outer intermittent structure was given.

The present work has something of the character of conditional sampling in that only fully developed turbulence, in the form of turbulent spots, was examined. The spots were initiated by injecting a small amount of air through a hole in the flat plate on which a laminar boundary layer was formed. A typical hot wire trace, resulting from the passage of a turbulent spot, is shown in Fig. (1.1). The trace is similar to that shown by Schubauer and Klebanoff[15] although the methods by which the spots were produced were different. A PDP8 digital computer was used to control experiments and record data. Many turbulent spots were observed at each chosen position in the boundary layer and mean flow velocities and turbulent intensities were computed from the digitised data. Crossed constant temperature hot wires gave streamwise and spanwise mean velocity components and the streamwise fluctuation component. The normal mean velocity was computed using the equation of continuity.

Diagrams and contour maps showing distributions of streamwise, spanwise and normal mean velocity, streamwise root mean square fluctuation and streamwise, spanwise and normal mean vorticity components at selected positions downstream are presented.

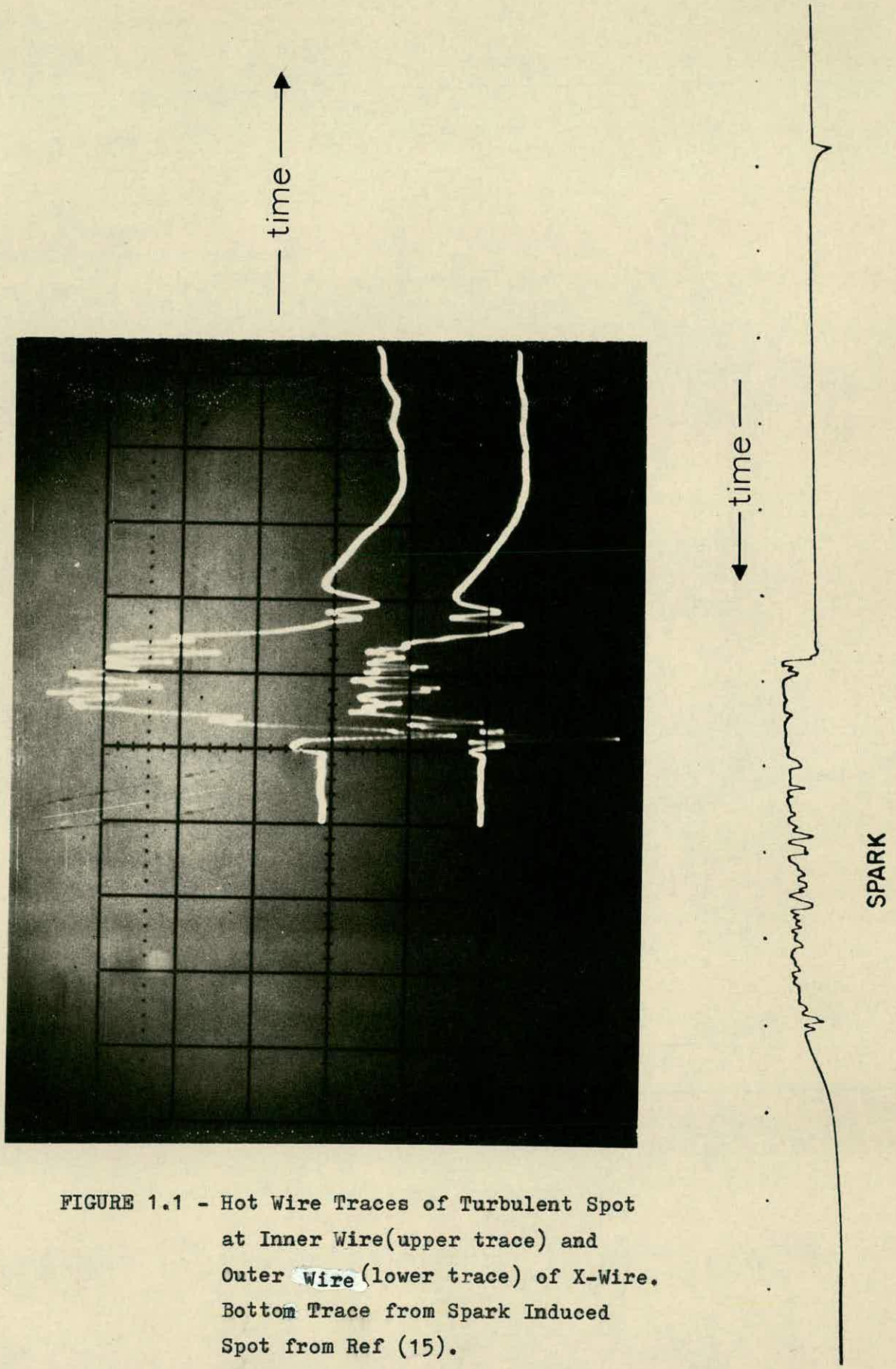

FIGURE 1.1 - Hot Wire Traces of Turbulent Spot at Inner Wire(upper trace) and Outer Wire (lower trace) of X-Wire. Bottom Trace from Spark Induced Spot from Ref (15).

CHAPTER 2

DESCRIPTION OF EQUIPMENT

This chapter contains a brief description of the wind tunnel. A more detailed description is given by Barnes[1].

1a. The Tunnel

The closed circuit wind tunnel was designed specifically for low turbulence work. The ratio of the cross-sectional areas of the settling chamber and working section was 15:1. Three fixed screens made from 41 mesh, 36 s.w.g. phosphor bronze wire were placed in the expansion section, immediately upstream of the settling chamber to prevent flow separation here. Two other screens, of the same mesh size and material as the fixed screens, acted as moveable smoothing screens and were placed two feet apart in the settling chamber. The blockage coefficient was 0.508.

Values of the total residual turbulence level, above 8 Hz., are

$$1/3 \times (u'^2 + v'^2 + w'^2)^{\frac{1}{2}}/U_o \times 100^o/o = 0.027^o/o \text{ at } 65 \text{ ft/s.}$$

$$= 0.006^o/o \text{ at } 30 \text{ ft/s.}$$

(see Barnes[1]).

An airline diagram of the tunnel is shown in Fig. 2.1.

1b. Drive and Control

The drive came from a hydrostatic servo-system, based on an N.E.L. design, which provided a complete hydraulic analogue of the Ward-Leonard System. The pump was driven

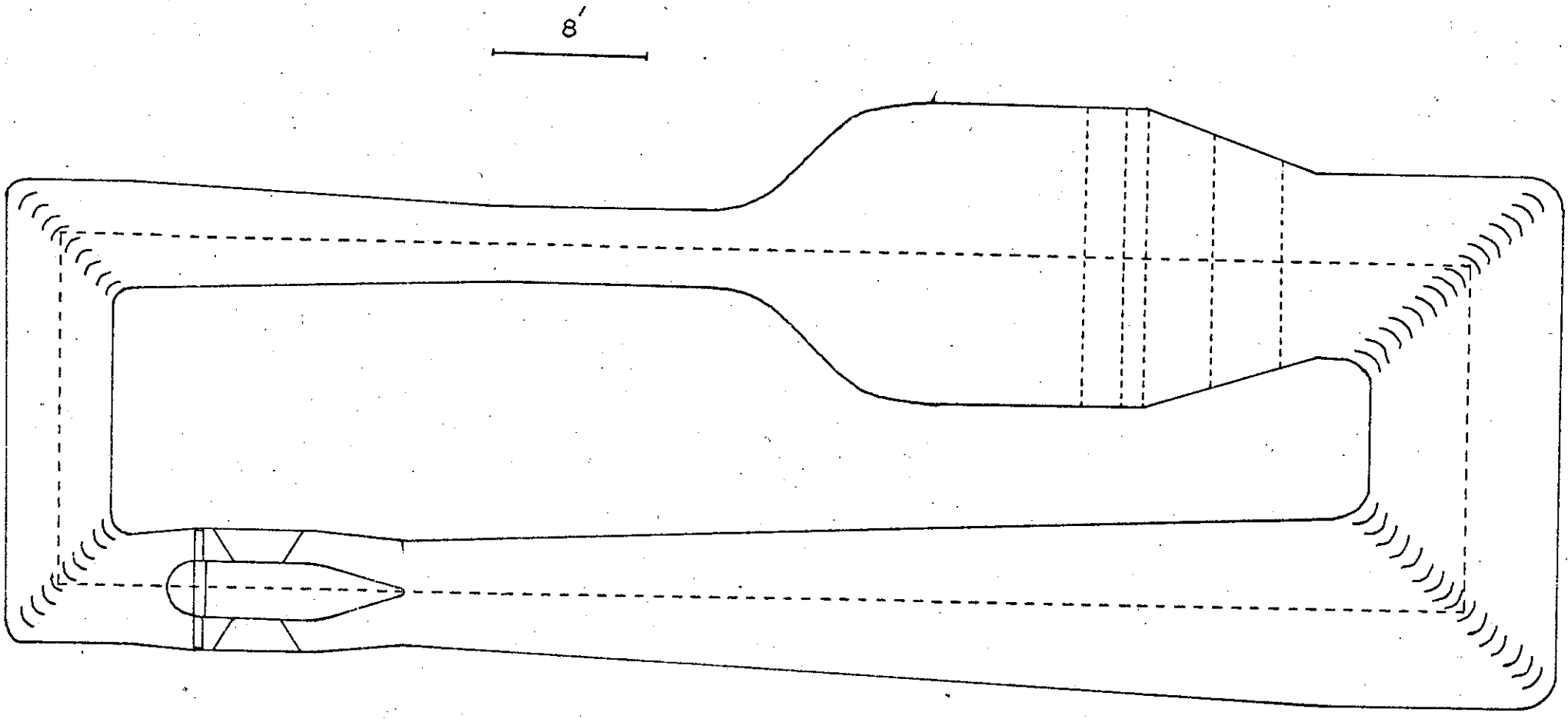

FIGURE 2.1 - Airline Diagram of the Tunnel.

at a constant speed by 35 H.P. squirrel cage induction motor, and the pump in turn drove the hydrostatic motor coupled to the fan. The fan was designed to absorb 30 H.P. at 750 r.p.m.

Two speed controls were used. The angle of the swash plate was altered by the coarse control and changed the rate of flow of oil through the pump and consequently the speed of rotation of the fan. Two pairs of relays controlled the operation of the 230 volt motor that drove the swash plate. One pair of relays could be energised/de-energised manually from the control panel in the control room, and the PDP8 computer controlled the other pair. A control panel switch, via one of these relay pairs, controlled the swash plate motor.

The fine control adjusted the amount of oil by-passing the hydrostatic motor, using an electrically controlled, variable aperture, moog valve situated between the high pressure delivery and low pressure return pipes of the pump and either of two variable 2000 ohm resistors controlled the current supply to the moog valve. The selection of the resistors was from a control panel switch. One resistor was varied through a 50:1 right angled gear box by a 12 volt stepper motor, controlled by the PDP8 computer. The fine control allowed a variation of $\pm$ 0.1 r.p.m. in the speed of revolution of the fan.

In case of emergency, a temperature controlled switch cut out the fan motor if the oil became too hot.

1c. The Working Section

The working section was basically of 4 ft. square section and 10 ft. long with a slight expansion along its length to allow for boundary layer growth on the walls. In order to maintain as near zero pressure gradient as possible along the length of the working section, adjustable fillets were set into the corners, making the cross-section octagonal. Each fillet could be flexed $\pm$ 1 inch providing a 2°/o variation in the area of the working section. The mean area of the working section was 13 square feet.

Two doors, one at either end of the working section, gave access for the insertion of apparatus. The pressure in the control room and the working section was equalised by breather holes at the rear end of the working section. The pressure in the tunnel was brought to atmospheric between the third and fourth corners, where the velocity was lower than in the working section. Consequently, the pressure in the control room was lower than atmospheric, and the room was sealed.

The designed maximum speed attainable in the working section was 140 ft/s.

2. The Flat Plate

The flat plate was a piece of perspex 9 feet long, 4 feet broad and $\frac{1}{2}$ inch thick. The leading edge was symmetrically tapered over the front 6 inches to a $\frac{1}{32}$ inch diameter cylindrical tip. The trailing edge was tapered

over the back $7\frac{1}{2}$ inches to a $\frac{1}{64}$ inch cylindrical tip. The plate was suspended from a heavy L-shaped duralumin bracket bolted to the roof and off-set from the centre-line of the working section by $\frac{1}{4}$ inch. Along its bottom edge, the plate was wedged by a series of small dulalumin brackets screwed to the floor. The leading edge was $5\frac{1}{2}$ inches from the upstream end of the working section.

3. The Traversing Mechanism

a. The Carriage

The carriage was designed to be used with the PDP8 computer. To reduce any influence of the carriage on the flow, its leading and trailing edges were streamlined. The carriage was 44 inches high, 1.75 inches thick and 20.5 inches long (see Fig. 2.2).

3b. The x Movement

The carriage moved on ball races along a 1 inch diameter steel rod fixed to the floor of the tunnel, 4 inches from the plate and parallel to it. A loop capstan drive allowed the carriage to be moved in the X direction by a SLO-SYN type SS25/1011 24 volt stepper motor via a 12:1 reduction gear.

3c. The y Movement

The unit carrying the Y traversing mechanism ran between vertical rails $\frac{1}{2}$ inch in diameter. A $\frac{1}{20}$ inch

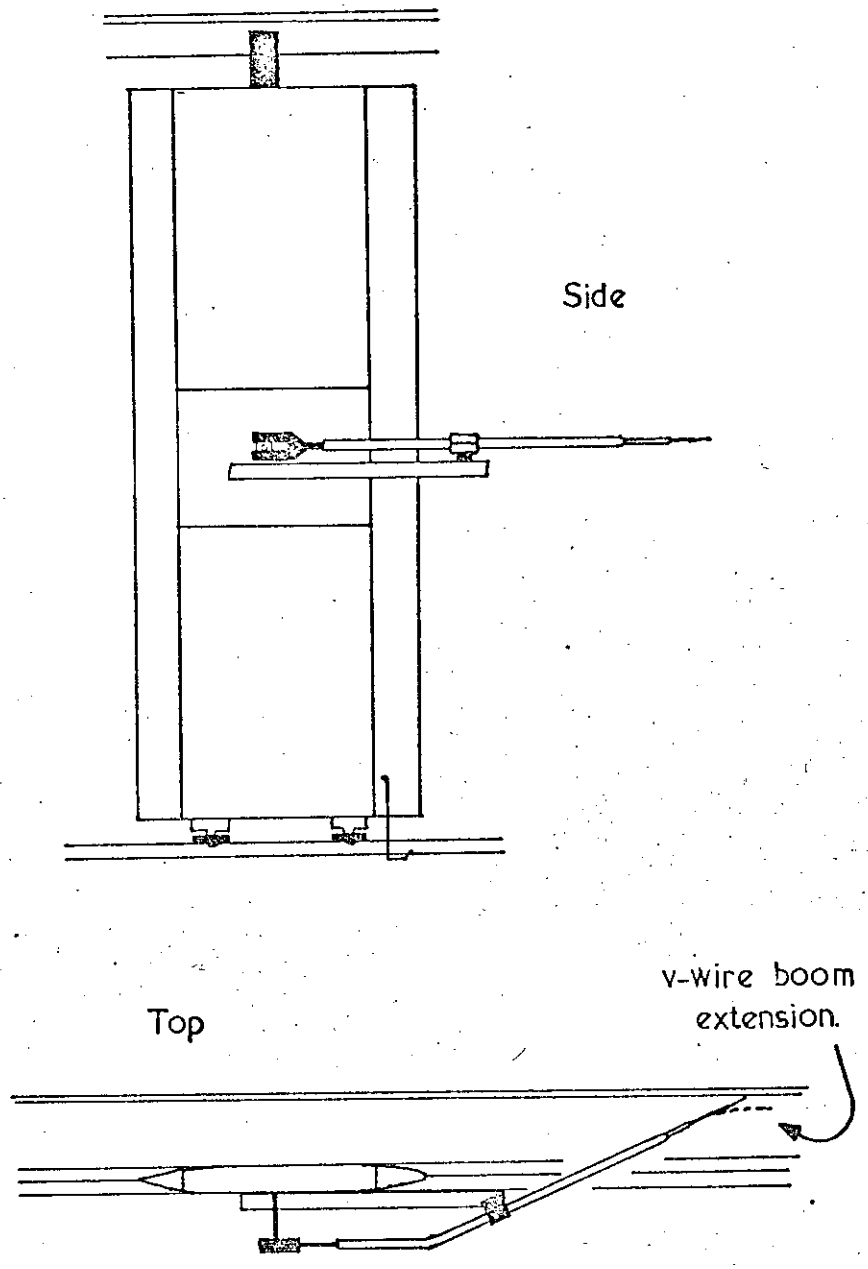

FIGURE 2.2 - The Carriage

diameter steel cable, connected to a 1 inch diameter threaded drum, supported the unit. The drum was rotated by a 24 volt Muirhead stepper motor, type 11M3004, acting through an 80:1 Vactric reduction gearhead and a 12½:1 reduction gearbox. During the course of the work described in this thesis, a fault occurred in this stepper motor and also in the stepper motor which moved the boom in the Z direction. These motors were later replaced by 28 volt DC motors (Vactric 11P101).

Sliding cover-plates attached to the unit maintained the streamlining of the carriage.

3d. The z Movement

The boom mounting is shown in Fig. 2.3. The end of the boom was pivoted on the drive nut, which was driven by the rotation of a 2 inch long micrometer screw of 0.05 inch pitch. The screw was rotated by a Muirhead 24 volt stepper motor type 11M3004 acting through a 100:1 right angled worm reduction gearbox. As mentioned in subsection 3c, this motor was replaced with a D.C. motor after developing a fault.

As the drive unit moved along the screw, the distance between the end of the boom and the pivot on the drive nut changed. The boom was made in two parts to allow for this; the end section attached to the drive nut could slide inside the part which was pivoted and carried the hot wire probe. The change in total length of the boom was small and a closely linear relationship existed between the distance

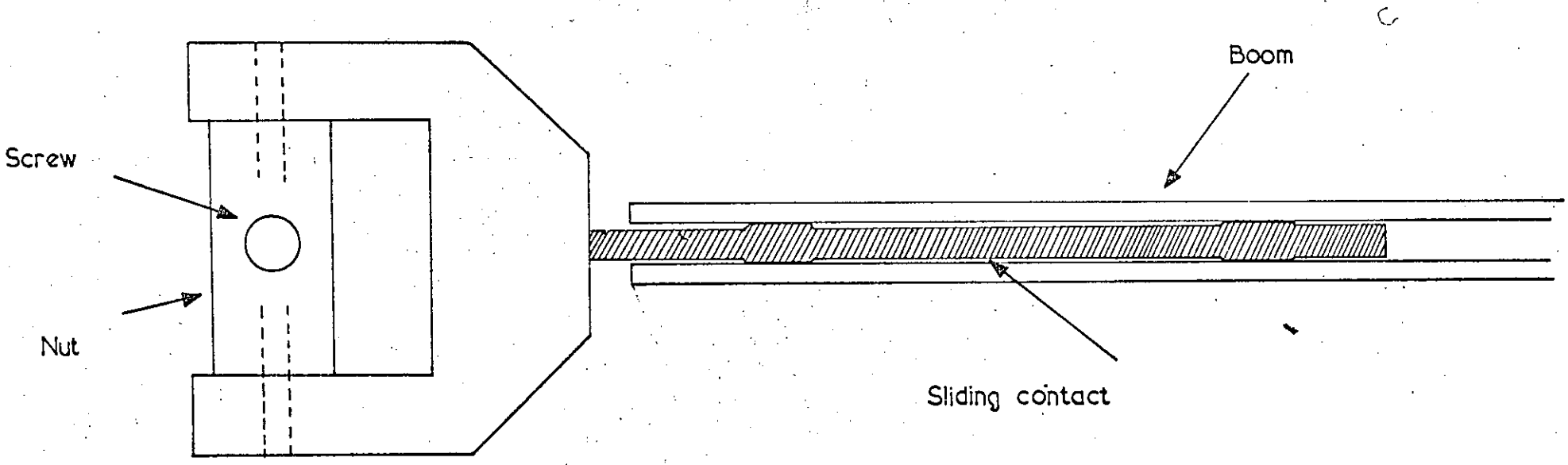

FIGURE 2.3 - Boom and Drive Nut Assembly.

moved by the drive, and the short distance (typically 1 cm.) moved by the hot wire probe in an experiment.

The hot wire probe carried at the end of the boom could be positioned with an accuracy of 0.05 inches in the x direction, 0.02 inches in the y direction and 0.001 inches in the z direction.

Fig. 2.4 shows the experimental coordinate system. This is not a right-handed coordinate system and the positive y direction was reversed to correct this during the data analysis.

3e. The Carriage Control Unit

The control unit has been described in detail by Ross[14]. It allowed the three 24 volt stepper motors which positioned the hot wire probe, to be operated either manually or by the PDP8 computer. The stepper motors were driven by 24 volt pulses supplied to their four terminals in a given order. Two pairs of transistors functioning as bistable multivibrators were incorporated in the manual drive circuit. These multivibrators supplied pulses to either of the two stepper motor terminals associated with each stator of the motor. A free running multivibrator supplied 15 volt triggering pulses to the bistable multivibrators and the frequency of the triggering pulses controlled the speed at which the stepper motors were driven. The direction of drive of the stepper motors was determined by the order in which pulses were supplied to the four terminals of the motors.

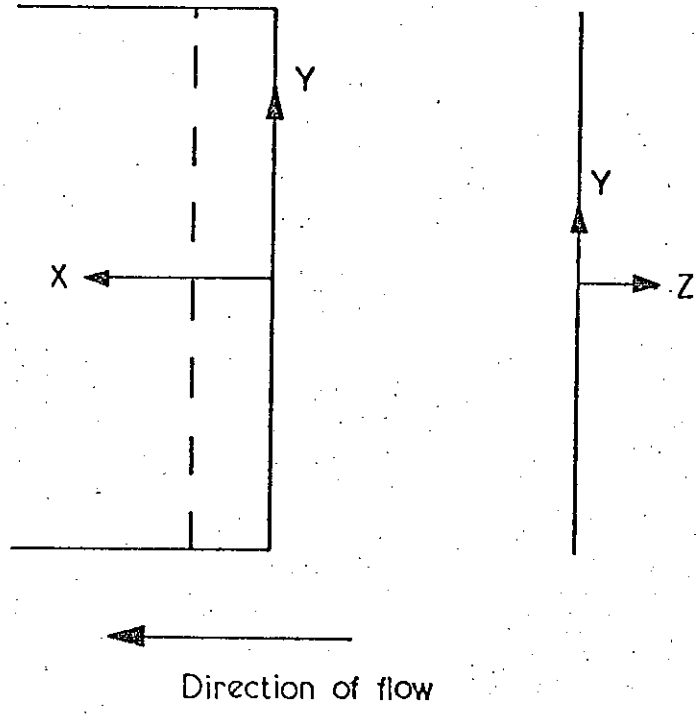

FIGURE 2.4 - The Experimental Coordinate System.

When the y and z motors were replaced with D.C. motors, the control unit was used to control the x movement only.

The D.C. motors could be driven either manually, via switches which selected the motor and the direction of drive, or via the PDP8 computer which performed the same function through three RS Type 40 relays. The speed at which the motors were driven manually was controlled by a variable resistor and by a 91 ohm, 9 watt fixed resistor in the automatic mode. The selection of manual or computer operation was made by a toggle switch. In the manual mode a second toggle switch applied 24 volts through the variable resistor to a third toggle switch which reversed the voltage, or otherwise, depending on the direction in which it was desired to drive the motor. The fourth, and last, toggle switch in the series selected the motor to be driven, so that when the second toggle switch was made, the selected motor was driven for any desired length of time at a speed which could be varied.

In the computer mode, selection of direction of drive and motors was accomplished by energising or de-energising the appropriate relays. Finally, by energising the on/off relay for a given time using a delay cycle in the PDP8 computer, written by Dr. J.G. Burns, 24 volts was applied to the selected motor through the fixed resistor. The delay cycle was programmed so that no other program could interrupt the cycle and so the selected D.C. motors were moved by the same amount each time the cycle was initiated.

The length of the delay could be altered by making a minor alteration to the 'control' program. The hot wire probe could therefore be moved through any desired step-length.

This system was devised by Dr. I. Grant. Fig. 2.5 gives the circuit diagram.

3f. The Measurement of Position

The x position was measured using a potentiometer. The potentiometer wire ran the length of the rail and was stretched, $\frac{1}{4}$ inch from the rail, between two supports. A D.C. voltage of approximately 2 volts was maintained across the wire and a contact attached to the carriage base slid along the wire.

The length of the potentiometer wire was derived by comparing measurements made with a travelling microscope with those of the voltage tapped by the sliding contact at small intervals. The graph of distance v. voltage was a straight line as in Fig. 2.6 and knowledge of its gradient and the total voltage drop across the wire gave an estimate of the length of the wire. From this method, the length of the x potentiometer wire was of the order of 99 inches.

The point of injection of the disturbance into the boundary layer, through a brass plug set in the plate, served as a reference position 12 inches from the leading edge of the plate. The x measurement was calibrated by moving the hot wire probe to coincide with the point of injection of the disturbances and reading the potentiometer voltage V_{XR} at that position and the total potentiometer voltage, V_{TR}.

The position of the carriage was calculated from the formula

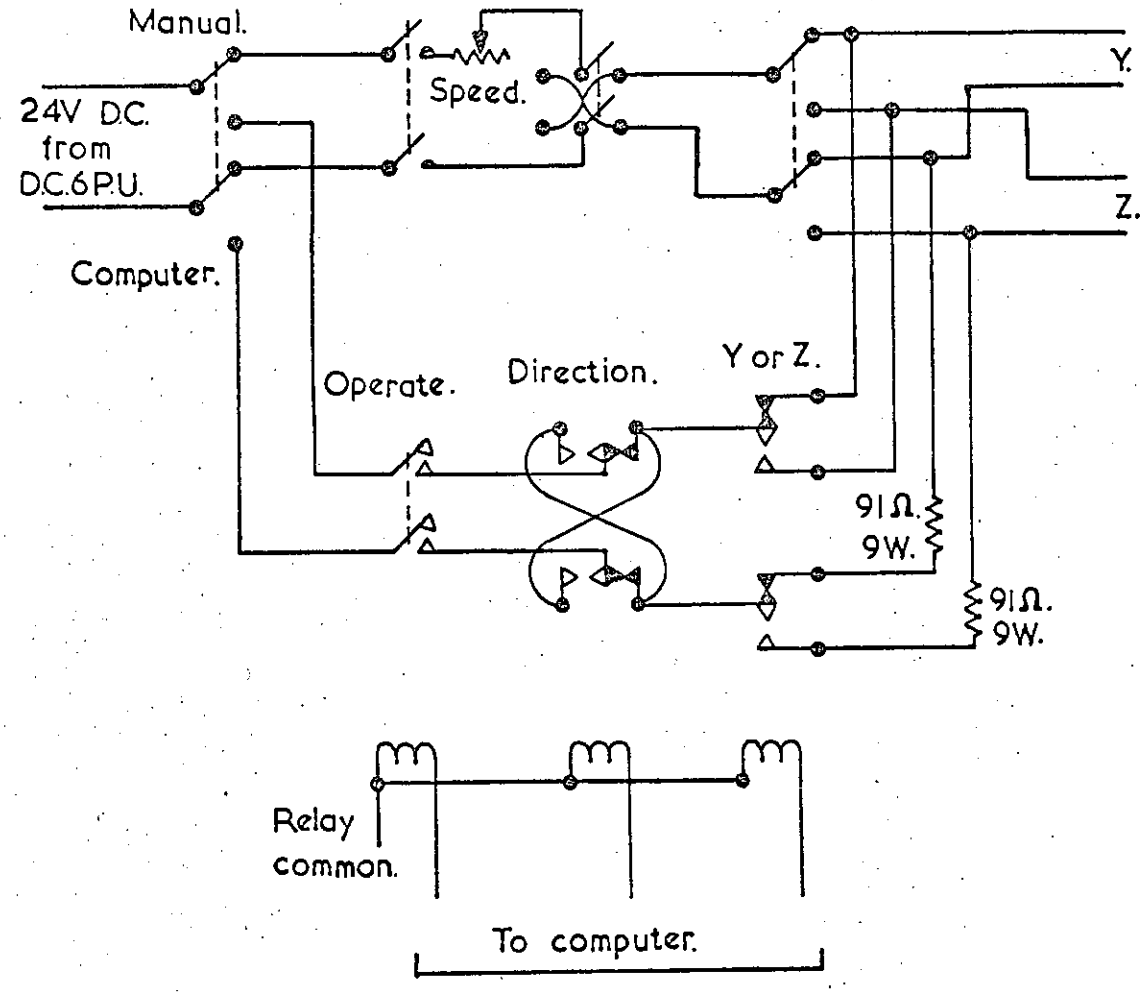

FIGURE 2.5 The DC Motor Circuit.

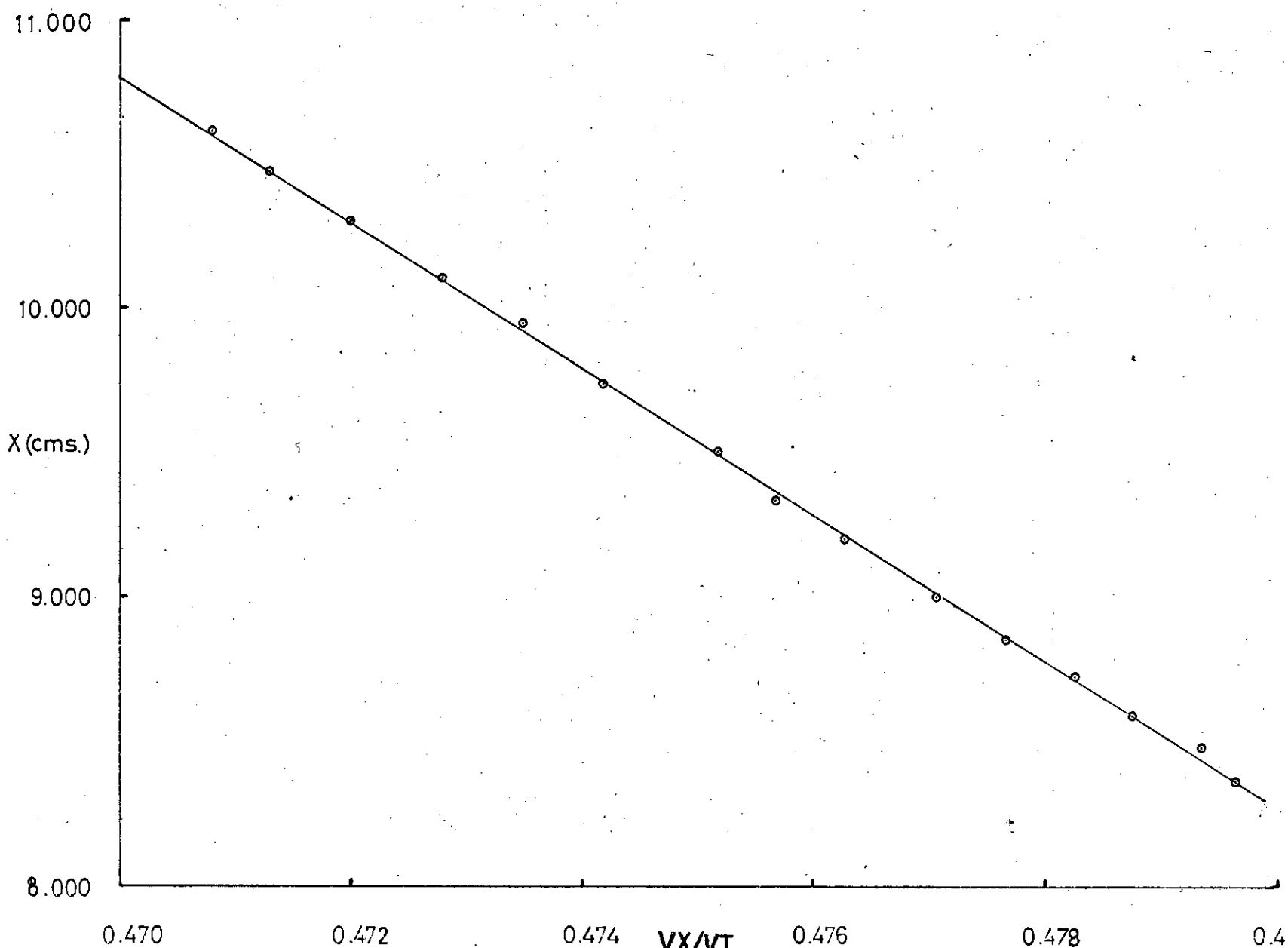

FIGURE 2.6 The X-Potentiometer Circuit.

$$X = (V_X - V_{XR}) \times L/V_{TR} + 12 \text{ inches},$$

where L is the length of the potentiometer wire in inches. The x coordinate could be measured with an accuracy of $\pm$ 0.05 inches.

The y coordinate could also be measured using a potentiometer wire held vertically in the carriage. The point of injection of the disturbance was taken as the reference position for the vertical movement. The relevant formula is

$$Y = (V_{YR} - V_Y) \times L_1/V_{TR} \quad \text{inches},$$

where L_1 is the length of the y potentiometer wire in inches. The y coordinate could be measured to an accuracy of $\pm$ 0.05 inches.

The z coordinate was the distance from the plate to the hot wire probe. Since the probe broke when it touched the plate, the zero position could not be found and precluded direct measurement of the z position. Instead a method dependent on the characteristics of the Blasius boundary layer was used and is described in Chapter 3.1c. The quantity which could be measured directly was the number of steps or, later in the work, the number of computer delays, necessary to move the probe a certain distance. This parameter should have a linear relationship with the distance the probe is moved. This is found to be so, as in Fig. 2.7, over the distance moved in a typical experiment (approximately 1 cm.), by measuring with a

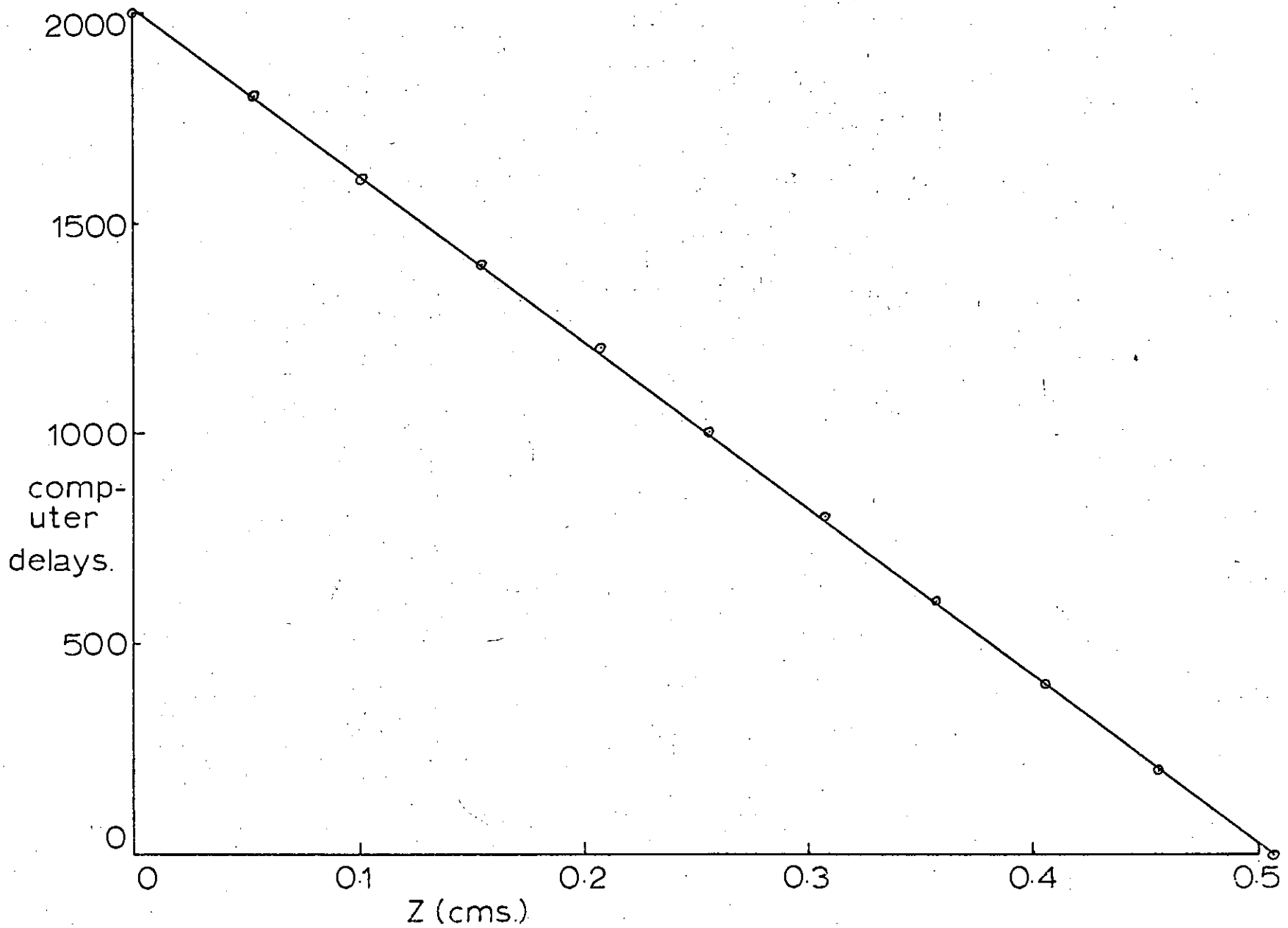

FIGURE 2.7 - Z DC Motor Calibration.

travelling microscope, the distance by which a large number of steps or computer delays moved the probe (see Fig. 2.7). The average of several such measurements was taken and it was found that one pulse to the stepper motor moved the hot wire probe 0.22×10^{-3} inch and one computer delay moved the hot wire probe 0.1×10^{-3} inch.

4. The Boundary Layer Perturbation

The boundary layer was perturbed by injecting a small amount of air through a hole of diameter 0.041 inch in a brass plug set flush in the plate. A 3 inch diameter transistor radio loudspeaker, driven by rectangular pulses from a pulse generator, injected the disturbance. The pulse generator was constructed in the departmental workshop and the circuit is given in Fig. 2.8. The loudspeaker was securely taped to the back of the plate so that the loudspeaker cone was situated symmetrically behind the brass plug as shown in Fig. 2.9.

An amplifier was inserted between the pulse generator and the loudspeaker and was simply a transistor switch which was switched on by the leading edge of a pulse from the pulse generator. In switching on, current flowed in the collector/emitter circuit of the switching transistor for as long as it was switched on, i.e. for as long as the pulse lasted. Thus, by putting the loudspeaker in series with the transistor power supply, a pulse of the desired height and length could be obtained across the loudspeaker coil and hence the circuit was effectively amplifying the

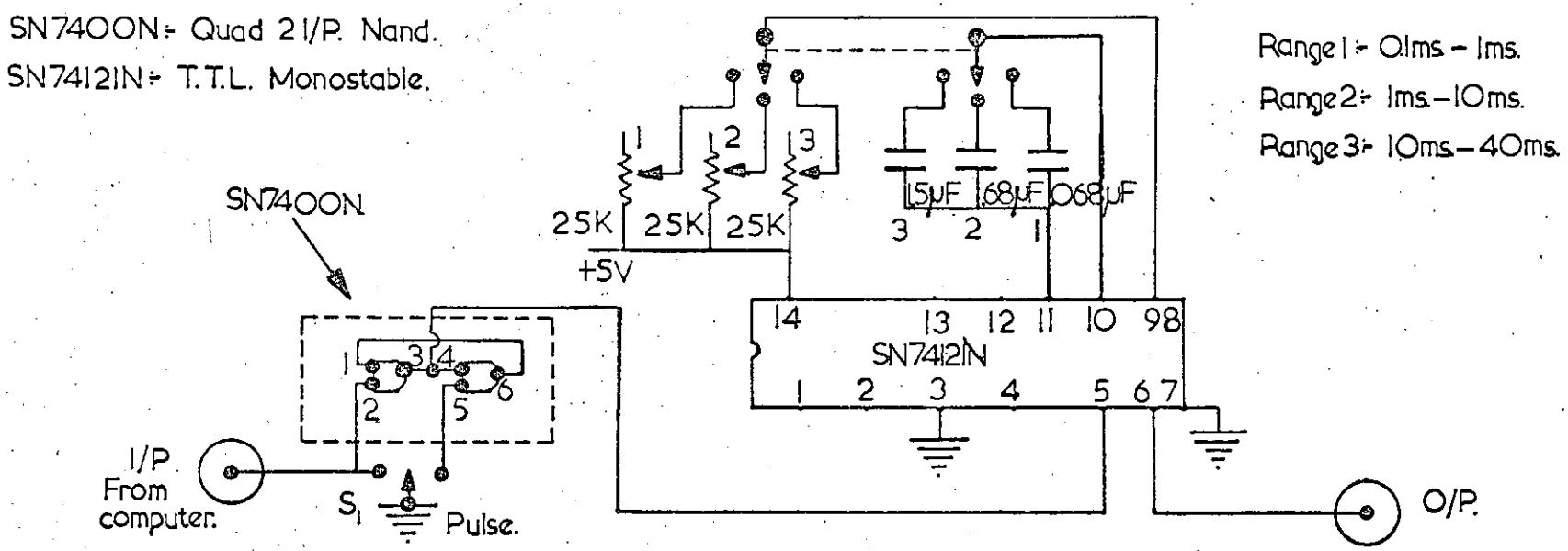

FIGURE 2.8 - The Pulse Generator Circuit.

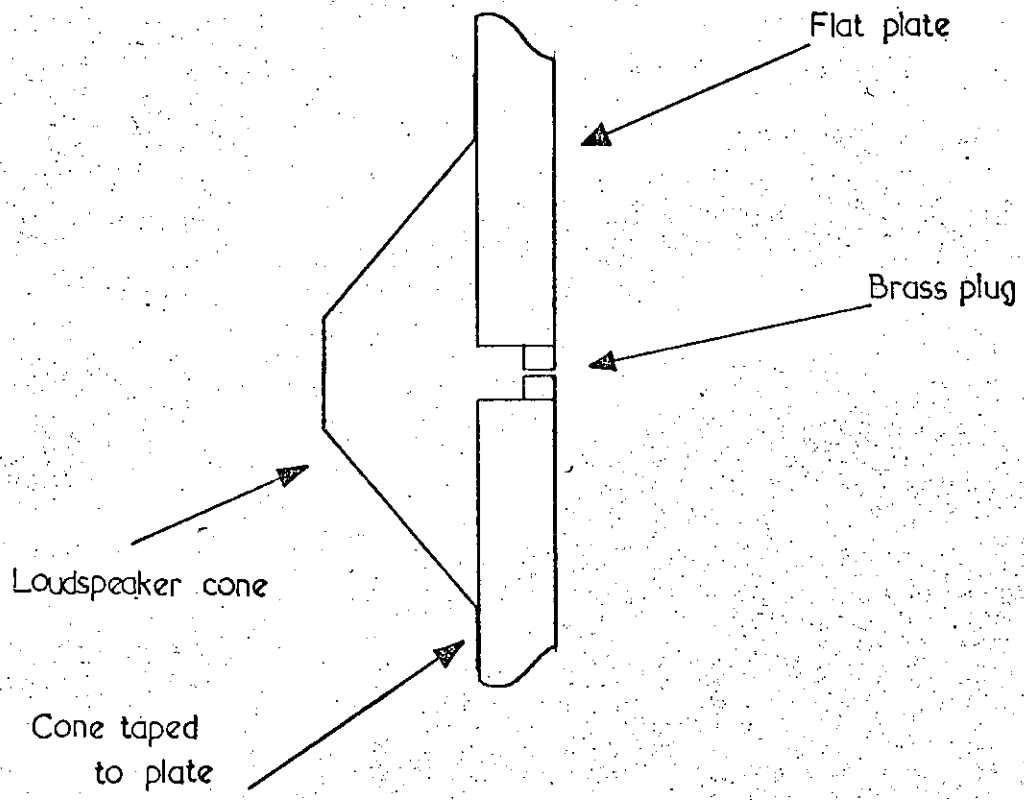

FIGURE 2.9 - The Loudspeaker Mounted Behind the Plate.

original applied pulse. The pulse height and length were variable, but a pulse of height 14 volts and 1 ms in length was found to be satisfactory when applied to the loudspeaker.

A diode was put across the loudspeaker coil to prevent 'backlash' when the transistor switched off. The loudspeaker was connected into the amplifier circuit so that its initial movement was towards the plate.

The pulse generator could be controlled manually or automatically by the PDP8 computer. In the manual mode, making a switch on the front control panel of the pulse generator produced a pulse. When used automatically, the PDP8 computer grounded a relay connected to an input in the front control panel of the pulse generator to produce a pulse.

The amplifier/switch circuit is given in Fig. 2.10. The hot wire trace due to the injected disturbance with no external flow can be seen in Fig. 2.11. This photograph was taken with a constant temperature hot wire probe close to the brass plug. A pulse was fired and the hot wire output digitized at 8 kHz.

5. Hot Wire Anemometry

For a constant temperature hot wire anemometer, King's well known law becomes

$$V^2 = V_o^2 + BU^n$$

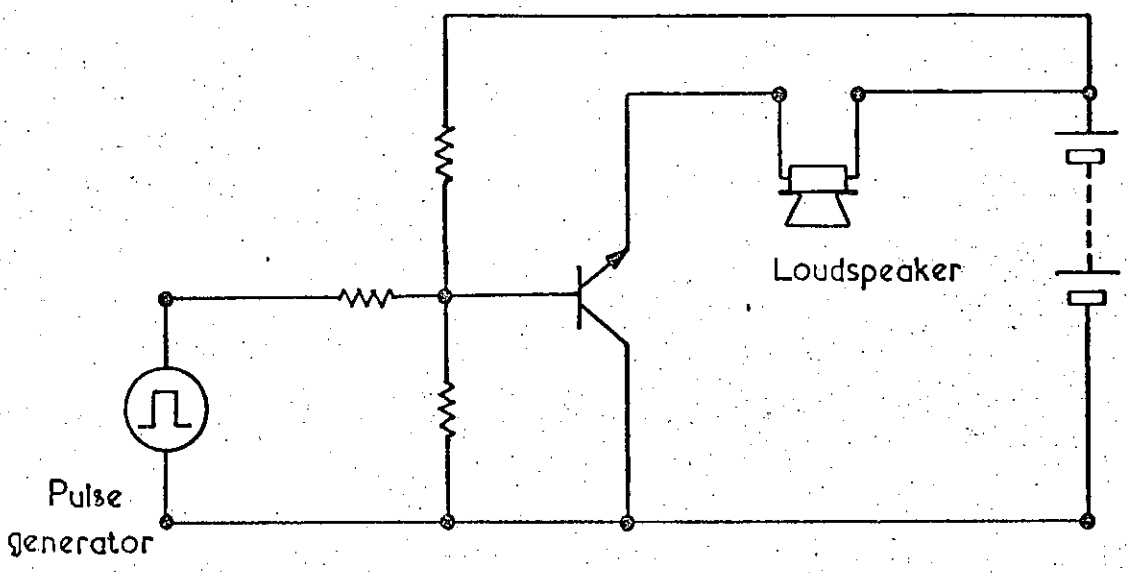

FIGURE 2.10 The Pulse Amplifier Circuit.

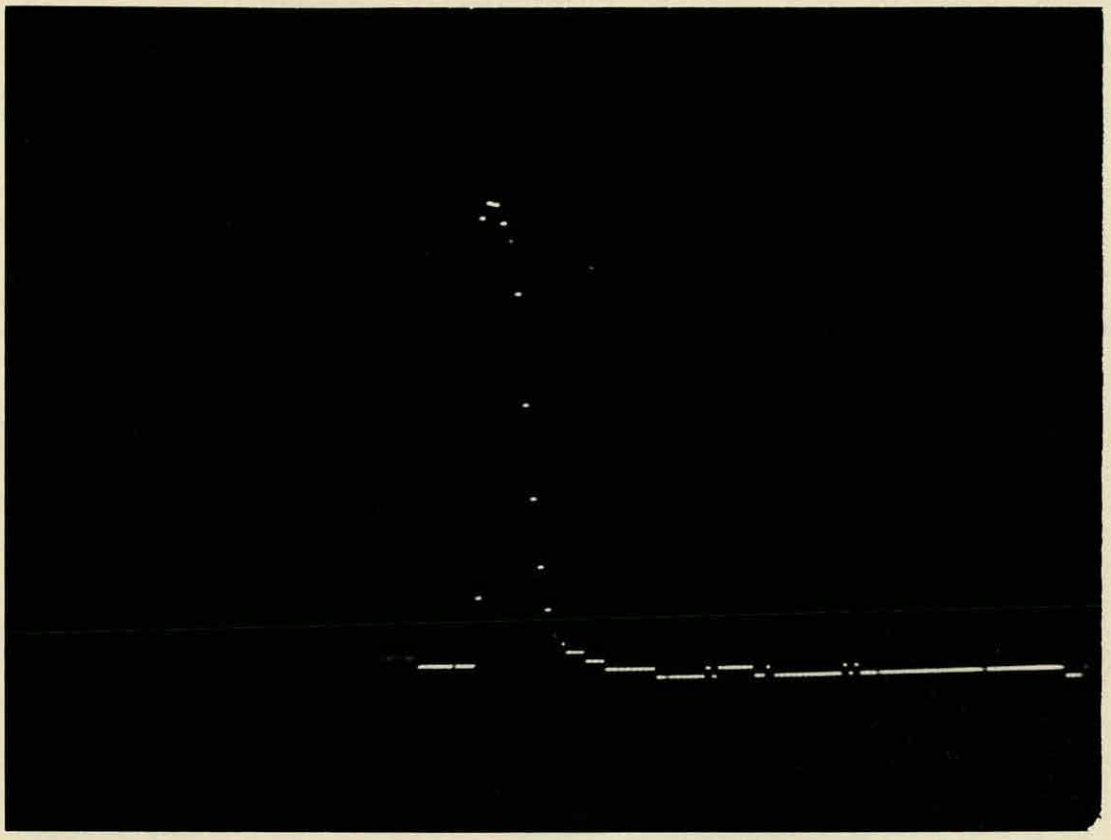

FIGURE 2.11 The Injected Disturbance.

where V is the hot wire voltage corresponding to the flow velocity U and V_o^2 and B are constants.

Collis and Williams (1959) showed that, when the Reynolds' number, based on wire diameter and the flow velocity, is in the range $0.02 < R < 44$, then King's law should be modified by putting $n = 0.45$.

$$V^2 = V_o^2 + BU^{0.45}$$

was therefore the equation used to analyse the hot wire data.

6. The Hot Wire Anemometer

The single U component hot wire was carried in a 'head' which screwed into a coaxial plug at the end of the boom attached to the carriage. Two prongs, one hard soldered to the stainless steel case of the head, the other to an insulated central pin, carried the hot wire. The prongs were nickel plated number 6 sewing needles. A streamline perspex cap, fitted tightly into the steel case, completed the assembly, the whole being held together with Araldite. The head is shown in Fig. 2.12.

Wollaston wire of 0.002 inch diameter was soft soldered to the prongs, and the central part of the silver coating was removed by electrolytic etching in a fine jet of 10% nitric acid. The etched portion of the wire was typically 0.1 inch long, and its diameter was 0.0022 inch. After etching, the wire was washed with water to remove any excess acid.

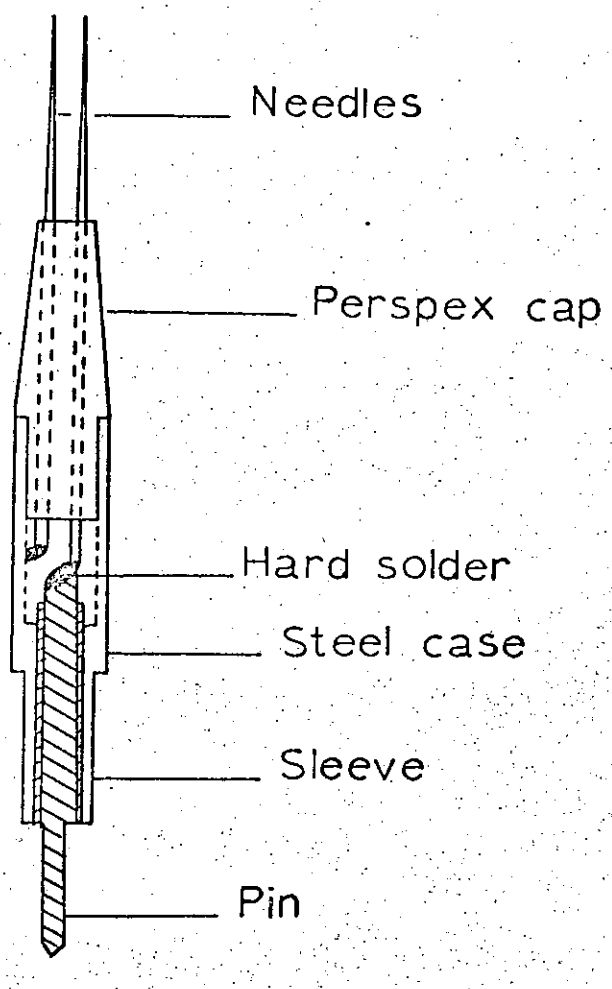

FIGURE 2.12 The Single Wire Head.

An attempt was made to make conventional X-wire probes to measure the U and V velocity components in the flow, using sewing needles, but difficulties with the manufacture of such probes prompted their re-designing. Instead of using sewing needles as probe supports, four pieces of malleable core from a multi-core cable were used. The pieces of core were securely bound together and insulated from each other with insulating tape and Araldite. This assembly was secured in a hollow head with Araldite after four short leads were soldered to the pieces of core. B.N.C. miniature plugs connected the leads to the coaxial cables going to the control units. A complete X wire head is shown in Fig. 2.13.

The end few millimetres of the probes were bent at right angles to the axis of the head to prevent the head touching the plate before the inner wire was sufficiently close to the plate. The inner hot wire, sensitive to both U and V flow velocity components, was carried at approximately 30° to the direction of the mean flow and the outer wire, sensitive only to the U flow velocity component, was carried vertically. The angle of the sloping probe was derived from measurements made with a travelling microscope after the head had been put into the boom on the carriage. This angle could be obtained quite quickly by using the vertical wire as a reference. The accuracy of this measurement was $3^{\circ}/o$. The wire separation was similarly measured at this point.

Advantages of the re-designed probes over the conventional X-wire configuration are

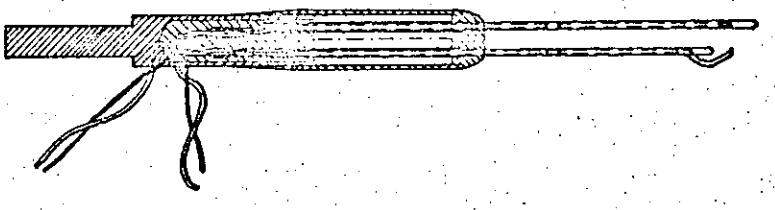

Side view.

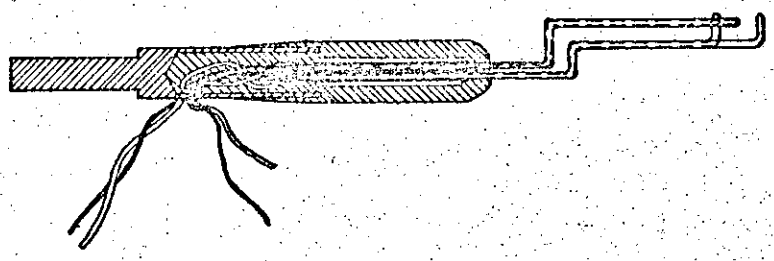

Top view.

FIGURE 2.13 - The X-Wire Head.

1) Probe interference can be made less by bending in the malleable supports.

2) Etching the central part of the Wollaston wire was simplified. By tracking along the U component wire, with the etching current off, until the sloping wire was reached, the two wires could be etched simultaneously.

3) The malleable core took solder more readily without copper plating than sewing needles.

4) The malleability of the wire supports enabled a better configuration of wires and supports, in relation to the plate, to be achieved. Trying to bend sewing needles so that the probe could be positioned close to the plate proved frustrating and laborious, whereas by judiciously cutting and bending the core material this was easily achieved.

The control units for the hot wires were manufactured by DISA and the hot wires were used with an overheat ratio of 0.8.

The data analysis methods which were used meant that matching of the hot wires was not required.

7. Windspeed Control

A device developed by Dr. T. Robertson and Dr. J.G. Burns allowed on-line control of the air speed during the course of experiments[13].

The device consisted of a constant current hot wire situated behind a circular cylinder mounted with its axis normal to the flow. The hot wire signal, caused by eddy-

shedding from the cylinder, was amplified and passed to the PDP8 computer interface, which also received 1 sec. gating pulses from a Venner frequency meter. An interface register counted the number of pulses in 1 sec. intervals, a Schmidt trigger on the input excluding the noise.

The computer compared this count with a number given to it at the start of the experiment, and the fine control of the fan motor was adjusted accordingly to set the velocity.

CHAPTER 3

DESCRIPTION OF EXPERIMENTS AND DATA ANALYSIS

3.1a The Experiments

All the experiments from which results were obtained for this thesis were performed in the closed circuit wind tunnel described in Chapter 2. The PDP8 computer was used for on-line control and data collection as well as for data reduction. Two free stream velocities were used, 28.5 ft./s. and 43.5 ft./s. The boundary layer was disturbed by injecting a small amount of air through a small hole in the flat plate as described in Chapter 2, section 4. The voltage across each hot wire probe was passed first to a Tetronix Type 122 low noise preamplifier with a gain of 100 and a bandwidth from 0.2 Hz to 10 KHz. The signal from the preamplifier was then passed to an attenuator made from resistors of $1^{o}/o$ tolerance before being passed to the analogue to digital converter in the PDP8. The attenuator was used to reduce the signal from the preamplifier so that it was in the range $\pm$ 5 volts, which was the range of operation of the analogue to digital converter. Finally, the digitised signal was recorded on magnetic tape on the PDP8. A Solartron digital voltmeter, which could be operated manually or automatically, measured the hot wire voltages in the undisturbed boundary layer; these voltages enabled the hot wire positions relative to the plate to be determined as described in section 1c of this chapter.

The computer program which controlled the data collection could be easily modified by changing certain machine code instructions given to the PDP8. A flow diagram is given in Fig. (3.1), showing the sequence of operations in a typical experiment using two constant temperature hot wires. There were three main steps in such an experiment:

(1) Check the windspeed using the device mentioned in Chapter 2, section 6, and measure the voltage across the hot wire(s).

(2) Fire a series of pulses; digitise and record the hot wire voltages; check the windspeed and measure the undisturbed hot wire voltage(s).

(3) On completion of (2) at a given station in the boundary layer, move the hot wire(s) out to the next position and repeat the sequence from (1).

The windspeed was checked every ten pulses. The undisturbed voltages were measured five times every time the wind speed was checked, and the average of these measurements was calculated at the end of the series of pulses. An average voltage was taken here to eliminate the effect of small fluctuations in the instantaneous measurements of the undisturbed voltages.

A small machine code sub-routine, written by Dr. J.G. Burns, delayed digitisation for a given time, enabling the disturbance to reach the probes before digitisation began.

The program could be halted by making a switch in the control room or, by over-riding this switch with machine code instructions, remote control from the computer could be

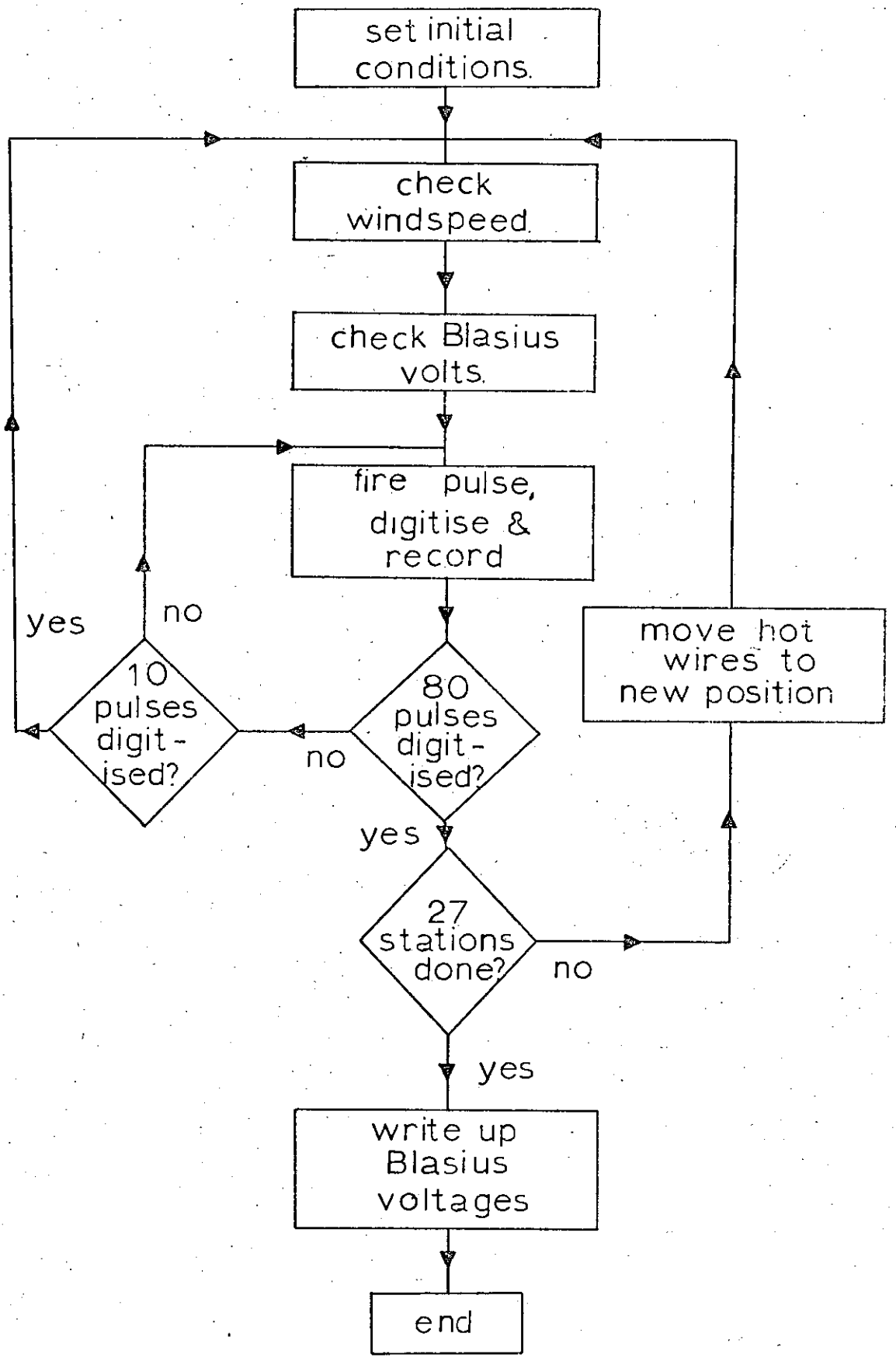

FIGURE 3.1 - Flow Diagram for Experimental Control Program.

exercised. This facility was particularly useful in setting the initial conditions of the experiment. The halt stopped the program with the digitised hot wire signal displayed on the oscilloscope attached to the PDP8, allowing inspection of the signal and ensuring that the correct delay had been used before digitisation (see above).

One experiment consisting of 80 pulses at each of 27 stations through the boundary layer took approximately 30 minutes. Six such traverses were performed at spanwise positions around the centre line of the plate. The instruments were calibrated before the six traverses were started and on the completion of every second one.

27 stations through the boundary layer were selected for the following reasons.

The format of the magnetic tapes used for storage on the PDP8 meant that only 1474 blocks of data of 128, 12 bit binary words could be stored on one tape. Since two hot wires were being used two such blocks were used to store the data from one digitised pulse, effectively giving 128 data words per hot wire. The turbulent spots passed the hot wires in approximately $^{1}/_{7}$ second or less and were digitised at 3KHz., or 1.5 KHz. per hot wire, so 128 data words covered the central length of the spot, being 128/1500 second. Using 80 pulses to get a smooth average pulse meant that one tape had room for 9 such runs, viz. $9 \times 80 \times 2 = 1440$ blocks with a little space left over. The PDP8 had three magnetic tape units so $27 \times 80 \times 2$ blocks of 128, 12 bit binary data words were recorded in one experiment. On the third, and final tape, the undisturbed hot wire voltages

were written in the space left at the end of the tape after all the digitised pulses had been recorded. Thus, just over half a million numbers were recorded on the PDP8 in one experiment for subsequent reduction. (One 12 bit binary word ≡ one four digit number.)

Originally, the time to complete six such experiments was approximately $4\frac{1}{2}$ hours. However, some machine code changes to the program reduced this time considerably, so that the final time became approximately $3\frac{1}{2}$ hours.

The subsequent data reduction took approximately $1\frac{1}{2}$ hours per experiment. In this time the data reduction program produced ensemble average and mean square voltages from the raw data for conversion later into mean flow and root mean square velocities.

The ensemble average was the average of 80 data points at the same point after digitisation. This gave the mean flow information.

The mean square was computed using

$$x_{rms} = \overline{x_i^2} - \overline{x}^2, \quad \text{where } \overline{x} = (\sum_i x_i)/N,$$

where $N = 80$ and $i = 1, 2, 3, \ldots, 80$. (See Fig. 3.2)).

The reduced data was transmitted to the Edinburgh Regional Computing Centre's (E.R.C.C.) computers (I.B.M. 370/155 and later 370/158) for storage on magnetic tape. Transmission was effected via the E.R.C.C.'s remote terminal facility which treated the PDP8 as a punched card reader connected to the E.R.C.C.'s machines. This allowed easy handling of large quantities of binary data, as well as programs. The conversion from voltage to velocity was performed by a program written using E.R.C.C. machines in

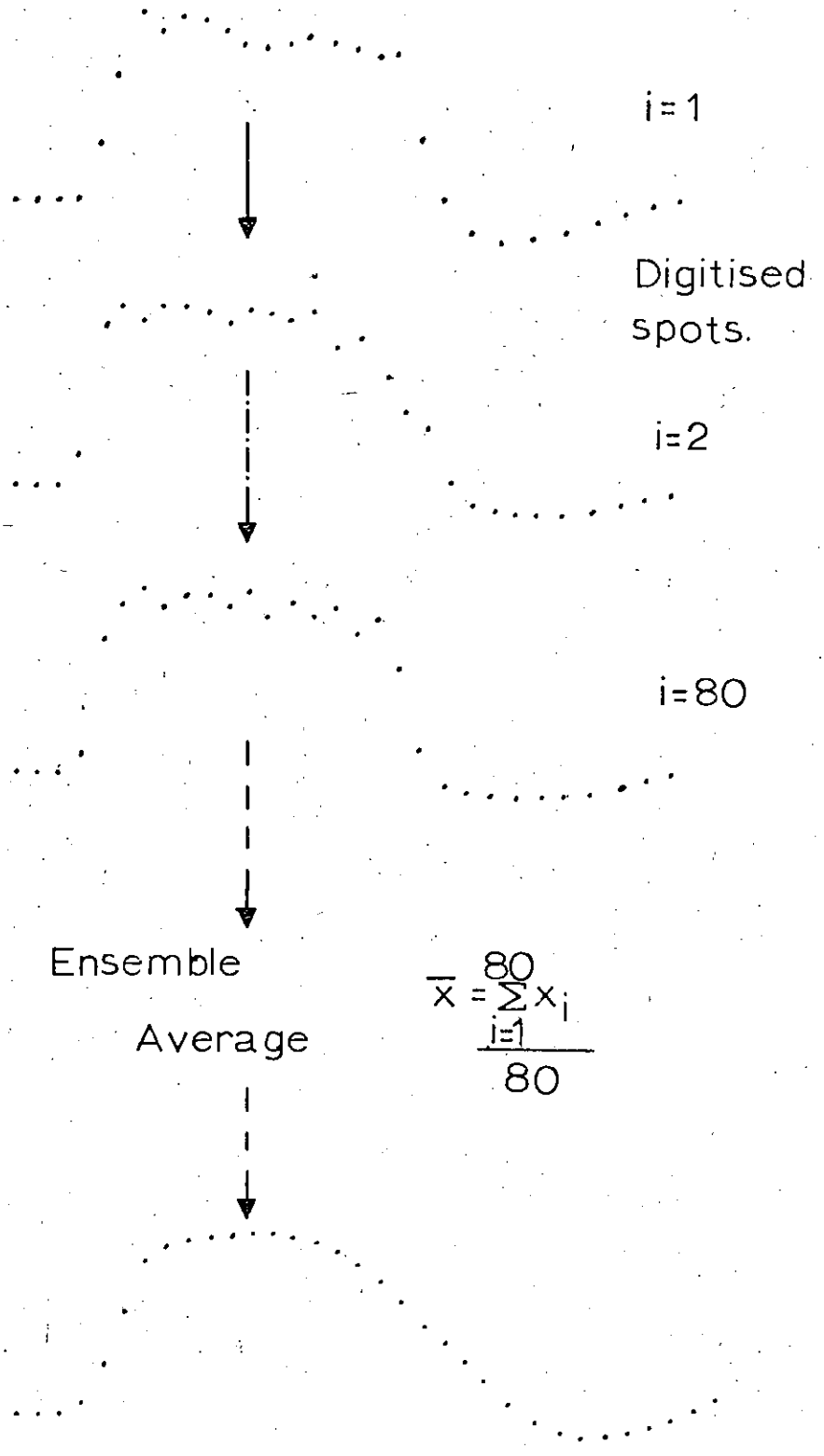

FIGURE 3.2 - Calculation of Ensemble Average.

the E.R.C.C. language 'IMP'.

3.1b. The Shape and Velocity of the Turbulent Spots

Some work was done on the shape and velocity of propagation of the spots but since this was not the main subject of this thesis a detailed investigation was not performed.

The program, mentioned earlier, which was used to control the main experiments was used now to control single, constant temperature hot wires which were sensitive only to the streamwise velocity component. Ten turbulent spots were digitised and stored on magnetic tape on the PDP8 for replaying on to the computer oscilloscope for observation. Knowing the length of delay before digitisation and the rate of digitisation enabled the time of arrival of the leading and trailing edges of the spots to be measured. From these measured times the spot geometry was deduced in the following manner (see Fig. (3.3)).

The velocity with which the leading edges moves downstream is assumed to be constant at a given z/δ position in the boundary layer. The line AB is a small section of the leading edge of the spot. At A, the velocity of the leading edge is x_1/t_1, where x_1 is the downstream distance from the point of origin of the spot and t_1 the time to travel x_1. At B, the probe is situated vertically above A in the xy plane and the leading edge of the spot arrives at a time t_2 from the point of origin where $t_2 > t_1$. Thus, because the leading edge of the spot slopes upstream away from the centre line, it appears to travel at a velocity decreasing along its length. The assumption is that this is not so and

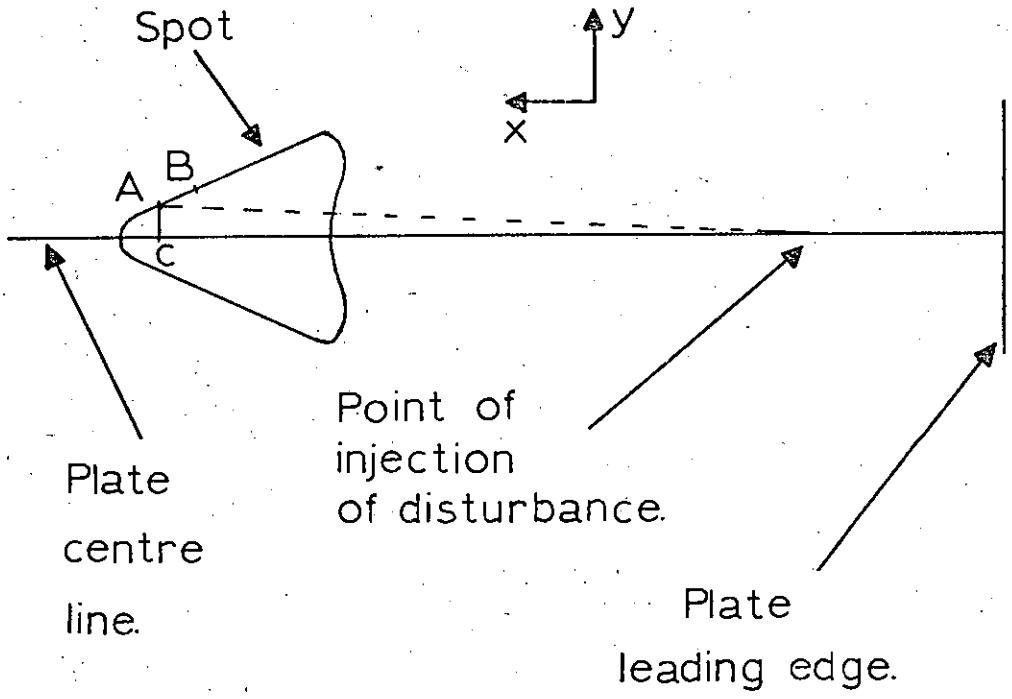

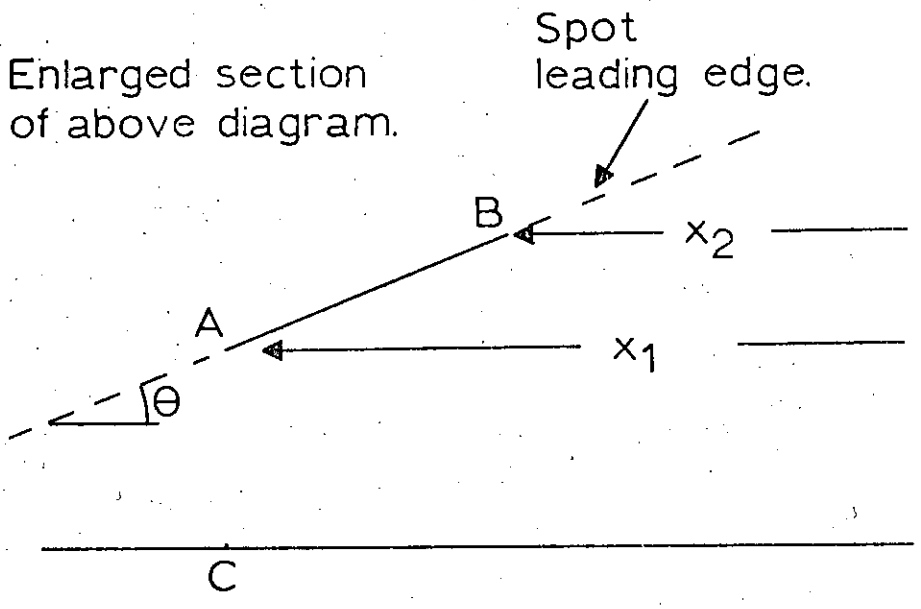

FIGURE 3.3 - Calculation of Spot Geometry.

$\frac{x_1}{t_1} = \frac{x_2}{t_2}$, where x_2 is the downstream distance of the leading edge of the spot from the origin when the leading edge is at A, x_1 from the origin. It is assumed that the angle subtended by the distance, AC, from A to the centre line, at the origin is small.

Therefore, $x_1 - x_2 = x_1 - x_1 \times \frac{t_2}{t_1}$.

Now $\tan \theta = \frac{y}{x_1 - x_2}$, where θ is the angle between AB and the downstream direction and y is the vertical separation of A and B, so

$$\tan \theta = \frac{y}{x_1 - x_1 \times \frac{t_2}{t_1}} = \frac{y}{x_1 - U_1 t_2},$$

where U_1 is the velocity of the leading edge.

Rearranging this equation gives

$$y = x_1 \tan \theta - U_1 \tan \theta \times t_2 .$$

Plots of x_1 against t_1 at various distances from the plate, on the centre line gave values for U_1. On the centre line $y = 0$ and $t_2 = t_1$. The velocity of the trailing edge of the spot can be similarly determined.

At constant x_1, plots of y against t_2 gave $\tan \theta$. These results are discussed in Chapter 4.

3.1c. Hot Wire Calibration

The hot wire was calibrated in the free stream by measuring the voltages across it at six wind speeds. The wind speeds were derived from pressure measurements made with a Pitot-static tube permanently situated 5 ft. from the front of the working section, 2.75 ft. from the floor

of the working section and 8 inches from the tunnel wall. The Pitot-static tube was connected to a Combustion Instruments 'Combist' micro-manometer. At the same time atmospheric pressure and the air temperature in the working section were measured.

V_o^2 and B from the hot wire equation (see Chapter 2, section 5) were obtained by plotting V^2 versus $U_o^{0.45}$ where V is the hot wire voltage and U_o the free stream velocity. The constants V_o^2 and B, were then used along with the measured boundary layer undisturbed voltages to compute the non-dimensional velocity U_B/U_o, where U_B is the velocity at a point in the boundary layer and U_o the free stream velocity.

In the experiments from which the undisturbed hot wire voltages were taken, the first ten stations in the boundary layer were in the region $0 < U_B/U_o < 0.4$. When using the X-wire array this was easily achieved with the inner wire but the outer wire did not entirely satisfy this limit although most of the outer wire stations lay in the above range. Keeping the hot wire in this range for the first ten stations enabled a comparison of the experimental curve with the theoretical Blasius velocity distribution where the Blasius curve is nearly a straight line. Computing straight lines from the ten points, using a least squares method and so obtaining the gradients, allowed the data, after comparison with the gradient of the Blasius curve here, to be sorted into good and bad fits to the Blasius curve. The program, which performed the above

calculation, then selected the best four curves, using the above criterion involving the gradients and drew them on the Calcomp graph plotter attached to the I.B.M. 370/158 at E.R.C.C. The best of these four curves was then selected by eye and examples of the inner and outer wire calibrations are given in Figs. (3.4a) and (3.4b).

The area under the computed Blasius curve was numerically integrated, using Simpson's Rule, to obtain the boundary layer momentum thickness which was used to compute the boundary layer thickness, δ. Distances normal to the plate were non-dimensionalised using δ.

3.2 Theoretical Background to the Experiments.

a. The Mean Flow

As stated in Chapter 2, section 5, the equation governing the operation of a constant temperature hot wire anemometer is

$$V^2 = V_o^2 + BU^{0.45} \quad \text{or} \quad V^2 = A + BU^{0.45}.$$

When more than one velocity component is required, more than one anemometer must be used and each anemometer then has its own equation which is solved with the other(s) to obtain the velocity components.

The instantaneous equation for the inner sloping wire in this work is

$$S_{TI}^2(t) = A_I + B_I\, U_{TI}^{0.45}(t) \quad \text{at time} \quad t. \qquad (3.1)$$

$U_{TI}(t)$ is the total instantaneous velocity and is

$$U_{TI}(t) = [U_{BI} + \Delta U_I(t) + u_I(t)] \sin\theta - [\Delta V(t) + v(t)] \cos\theta$$

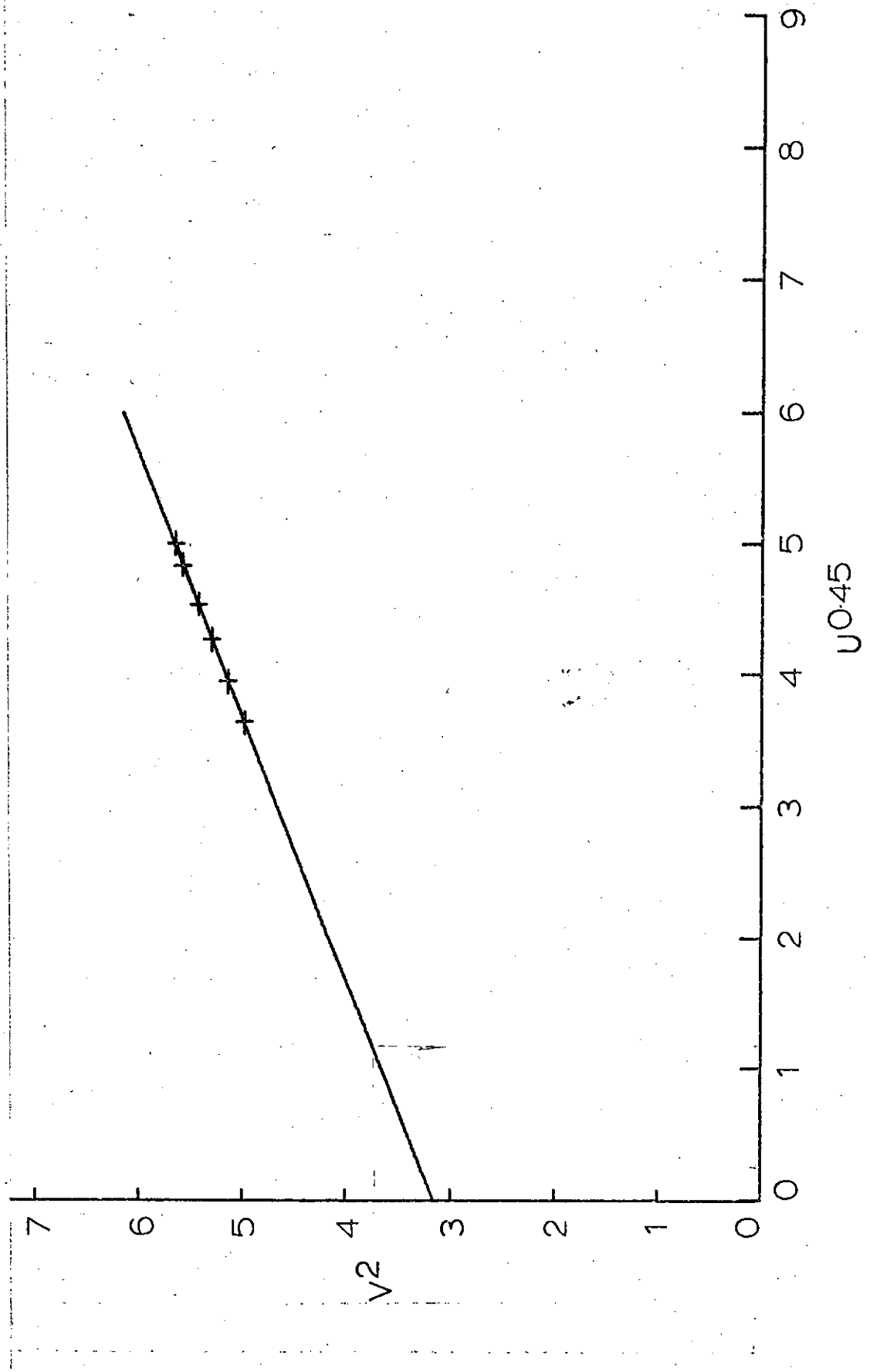

FIGURE 3.4a(i) - Calibration Curve for Inner Wire.

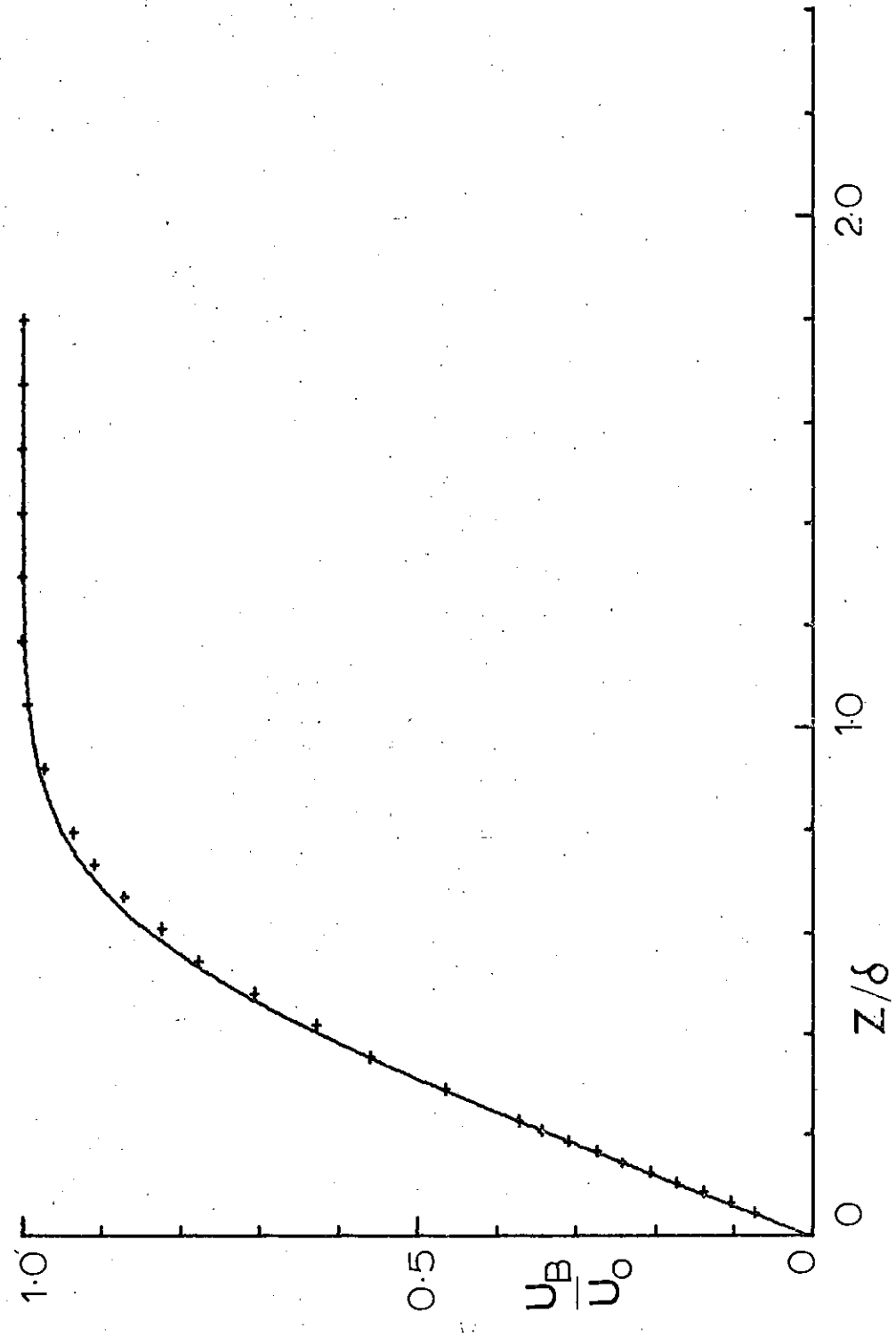

FIGURE 3.4a(ii) - Blasius Fit for Inner Wire.

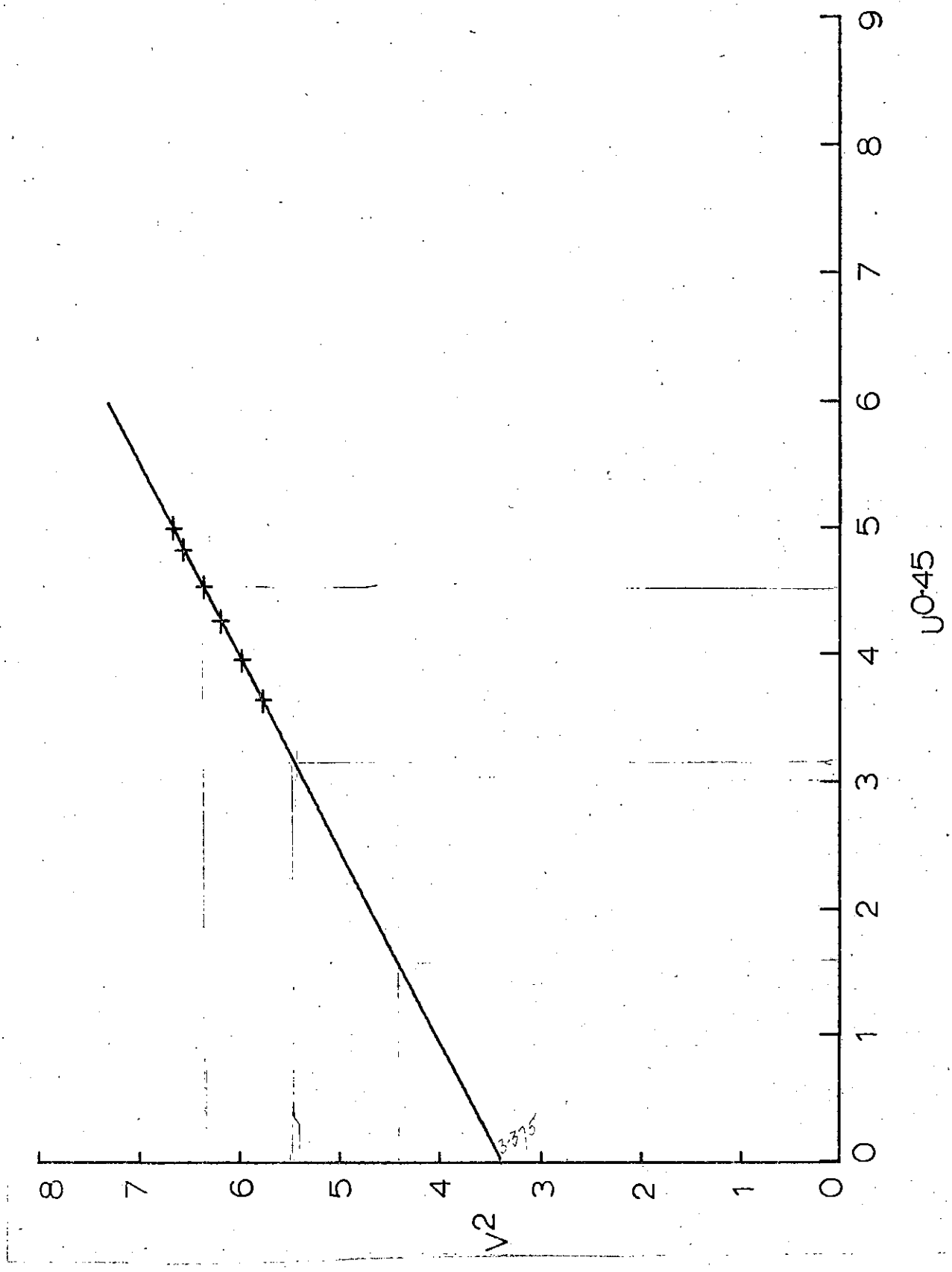

FIGURE 5.4b(i) - Calibration Curve for Outer Wire.

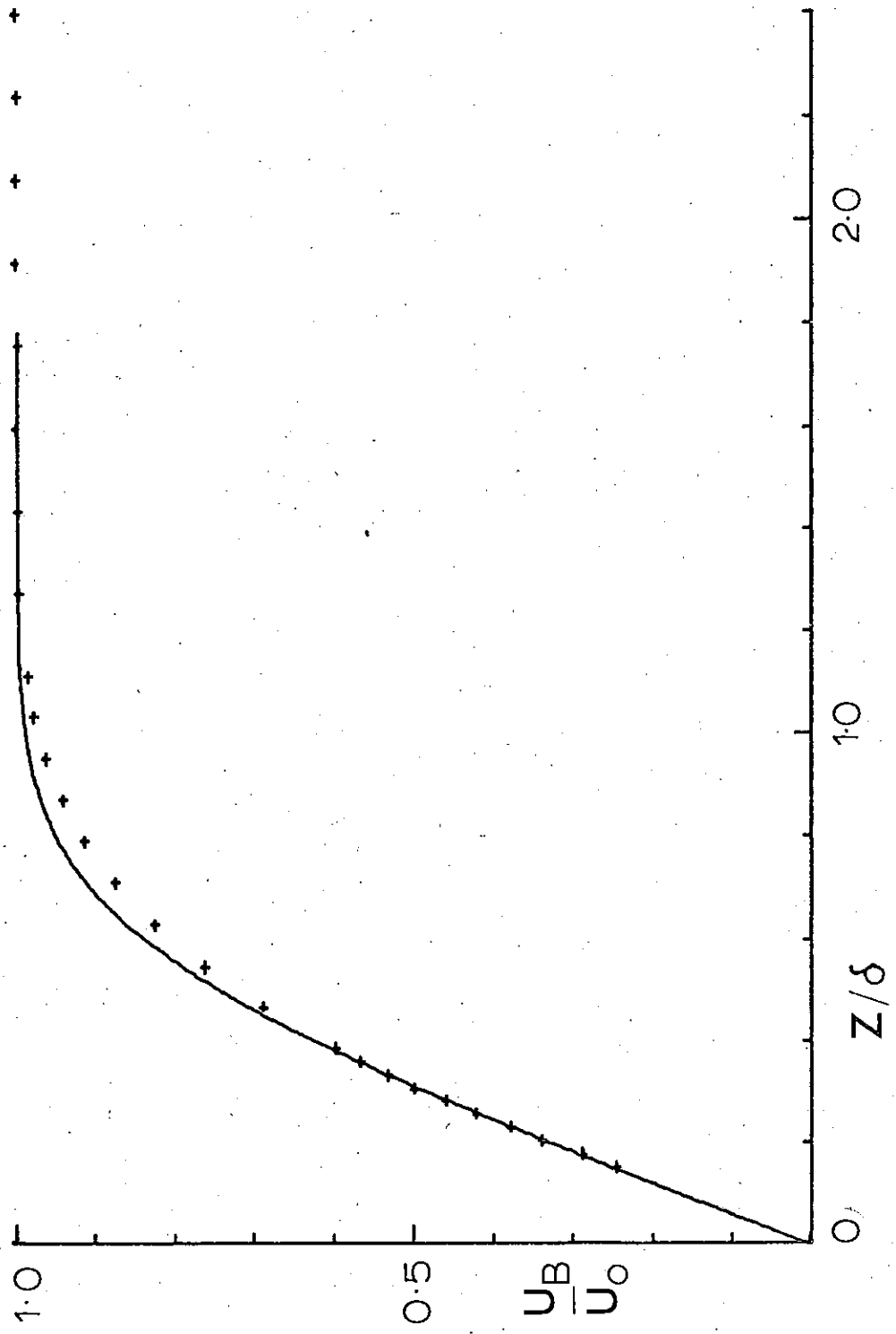

FIGURE 5.4b(ii) - Blasius Fit for Outer Wire.

where U_{BI} is the velocity in the undisturbed Blasius boundary layer, $\Delta U_I(t)$ is the velocity of the mean flow disturbance at time t, $u_I(t)$ is the streamwise turbulent fluctuation velocity at time t, $\Delta V(t)$ is the spanwise mean flow disturbance velocity at time t, $v(t)$ is the spanwise turbulent fluctuation velocity at time t, and θ is the angle the wire makes with the mean flow direction. S_{TI} is used here to avoid confusion with V.

The equivalent equation for the outer wire, sensitive to the streamwise components only is

$$S_{TO}^2(t) = A_o + B_o U_{TO}^{0.45}(t) \qquad (3.2)$$

where $U_{TO}(t) = U_{BO} + \Delta U_o(t) + u_o(t)$ with the same meanings as above.

To solve these equations data only from positions in the boundary layer where the inner hot wire moves into a position previously occupied by the outer wire is used (see Fig. (3.5)). It is assumed, at positions which match like this, that

$$U_{BI} = U_{BO} = U_B \quad \text{and} \quad \Delta U_I(t) = \Delta U_o(t) = \Delta U \ ,$$

where it is understood that ΔU is observed at time t. By taking ensemble averages over 80 spots the mean flow data is effectively filtered from the turbulent data and so the equations for the two hot wires for the mean flow are

$$S_{MI}^2 = A_I + B_I \left[(U_B + \Delta U)\sin\theta - \Delta V \cos\theta\right]^{0.45} \qquad (3.3)$$

and

$$S_{MO}^2 = A_o + B_o(U_B + \Delta U)^{0.45} \qquad (3.4)$$

where S_{MI} and S_{MO} are the mean flow voltages and it is

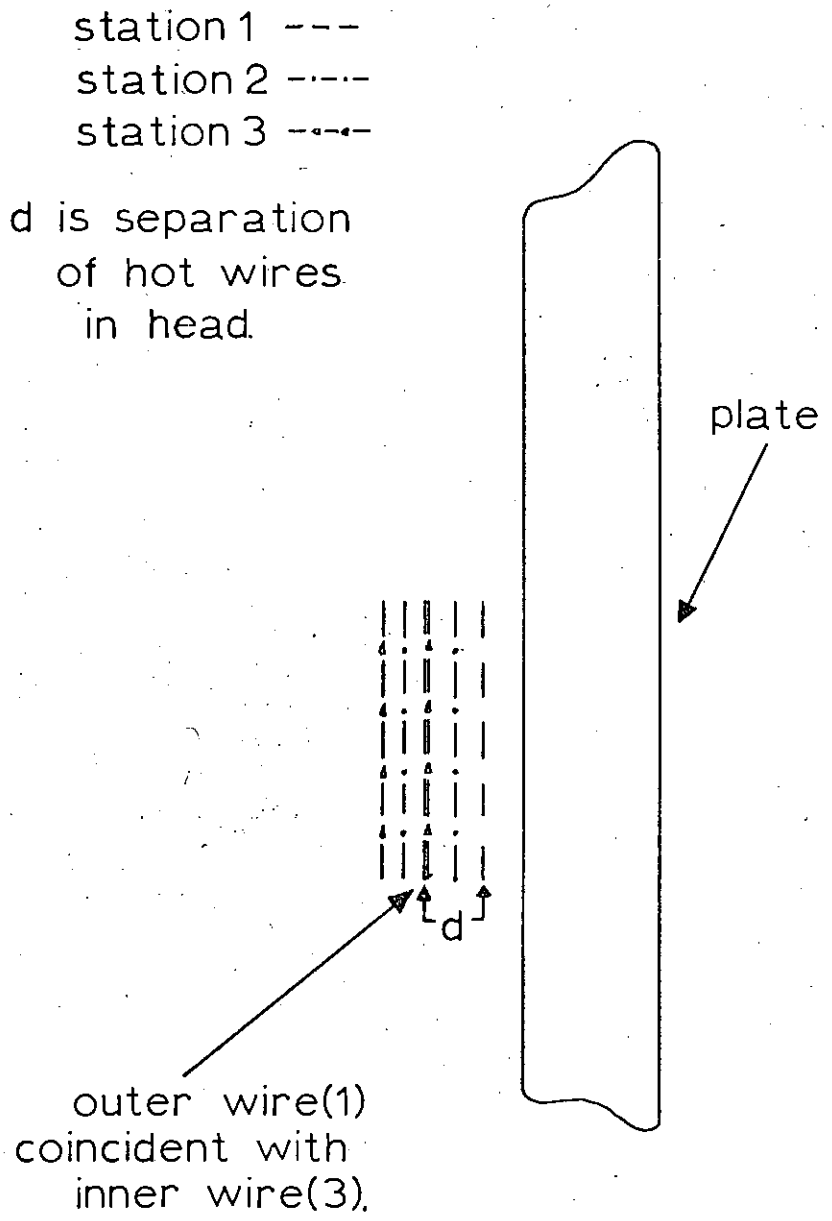

FIGURE 3.5 - Diagram Illustrating Inner and Outer Hot Wire 'Coincidence'.

understood that they are measured at time t.

Also $$S_{BI}^2 = A_I + B_I(U_B \sin\theta)^{0.45} \tag{3.5}$$

and $$S_{BO}^2 = A_o + B_o U_B^{0.45} \tag{3.6}$$

where S_{BI} and S_{BO} are the undisturbed flow voltages.

Equations (3.3), (3.4), (3.5) and (3.6) can now be solved for ΔU, ΔV and U_B.

From (3.3),

$$S_{MI}^2 - A_I = B_I(U_B \sin\theta)^{0.45}\left[1 + \Delta U/U_B - \frac{\Delta V}{U_B}\cot\theta\right]^{0.45},$$

which becomes, using (3.5)

$$\frac{S_{MI}^2 - A_I}{S_{BI}^2 - A_I} = \left[1 + \frac{\Delta U}{U_B} - \frac{\Delta V}{U_B}\cot\theta\right]^{0.45}.$$

This becomes, on simplification,

$$\left(\frac{S_{MI}^2 - A_I}{S_{BI}^2 - A_I}\right)^{2.222} - 1 = \frac{\Delta U}{U_B} - \frac{\Delta V}{U_B}\cot\theta. \tag{3.7}$$

Similarly, from (3.4) and (3.6),

$$\left(\frac{S_{MO}^2 - A_O}{S_{BO}^2 - A_O}\right)^{2.222} - 1 = \frac{\Delta U}{U_B}. \tag{3.8}$$

By subtracting (3.7) from (3.8),

$$\frac{\Delta V}{U_B} = \tan\theta\left\{\left[\frac{S_{MO}^2 - A_O}{S_{BO}^2 - A_O}\right]^{2.222} - \left[\frac{S_{MI}^2 - A_I}{S_{BI}^2 - A_I}\right]^{2.222}\right\} \tag{3.9}$$

Thus equations (3.8) and (3.9) express the streamwise and spanwise mean flow disturbance velocities in terms of measurable quantities. The total streamwise mean flow disturbance is given by

$$\frac{U_B + \Delta U}{U_B} = 1 + \frac{\Delta U}{U_B}$$

which is easily obtained from equation (3.8).

The component of mean velocity normal to the plate was calculated using equations (3.8) and (3.9) with the equation of continuity and all three components were expressed in terms of the free stream velocity U_o, viz: $1 + \Delta U/U_o$, $\Delta V/U_o$ and W/U_o by multiplying each by U_B/U_o, the value of the undisturbed Blasius non-dimensional velocity.

b. Root Mean Square Fluctuations (r.m.s.)

To evaluate the root mean square turbulence intensity the hot wire equation is used as the starting point,

$$S^2 = A + BU^{0.45)} \quad . \qquad (3.10)$$

Differentiation of (3.10) gives

$$2S.dS = 0.45BU^{-0.55}.dU \quad .$$

Multiplying the right hand side of this equation by $\frac{U^{0.45}}{U^{0.45}}$ gives,

$$2S.dS = 0.45BU^{0.45}.\frac{dU}{U} \quad .$$

If dS is taken as the root mean square fluctuation voltage, then dU is the root mean square turbulent intensity and

$$\frac{dU}{U} = \frac{u'(t)}{U(t)} = \frac{444.4 \times S(t) \times s'(t)}{B\,U^{0.45}(t)} \ ^{o}/_{o} \quad . \qquad (3.11)$$

As mentioned in subsection (a) of this section, the

averaging process effectively filters the mean flow information from the turbulent information. Thus $U(t)$ in equation (3.11) is the total streamwise mean flow disturbance $(U_B + \Delta U)$, with $S(t)$ as the corresponding hot wire voltage.

The spanwise component of the r.m.s. turbulence intensity cannot be obtained by ensemble averaging from the X-wire configuration used in these experiments. Two oppositely sloping wires must be used to do this, but by calculating the instantaneous velocities and then averaging, this component can be found with the hot wire configuration used in this work.

In the above derivation, no account is taken of the distortion of the signal arising from the non-linearity of the hot wire calibration curve in the region of large velocity fluctuations but the corrections of Champagne and Sleicher[3] for sloping hot wires in turbulent flows were applied. For turbulent intensities of the order of 20°/o, DISA estimate that r.m.s. measurements made without corrections for non-linearity will be approximately 5°/o in error (see Chapter 4, section 2).

3.3 Interpolation of Data

The first interpolation of the data was performed during the running of the data reduction program. Data from the inner wire was parabolically interpolated so that the data points matched in time those obtained from the outer wire. This matching was necessary because the analogue

to digital converter digitised in a series, and not a parallel, fashion. In other words, the inner wire voltage was digitised first, then the outer and back to the inner and so on. A parabolic interpolation was used since a linear process does not represent a rapidly fluctuating signal as closely. The Newton-Gregory equation, terminated after the third term, was used for the interpolation.

Later, after the conversion from voltage to velocity, the Newton-Gregory equation, for unequal intervals was used to produce equi-spaced data at intervals in z/δ of 0.05 to simplify data handling. Again, the equation was terminated after the third term. With data in this form, the programs utilising the contour subroutine, which was used extensively, were considerably simplified. The interpolated data was stored on magnetic tape at E.R.C.C.

The contour subroutine, written by Mr. S.T. Hayes and modified by E.R.C.C. personnel, required equi-spaced data arrays to be given to it. It performed a scaling operation on the data, using information about the real extent of the data and drew contours through the data, using linear interpolation.

Furthermore, the program written to compute the vorticity components was simplified by using the equi-spaced interpolated data in that it was not necessary to give all the positions through the boundary layer at which data was taken, but only the interval in z/δ, 0.05, at which data now existed. Because positioning the hot wires at the same positions normal to the plate in a spanwise series of experiments was difficult to achieve and not attempted,

computing spanwise velocity gradients could not have been accomplished without using equi-spaced data.

At both free stream velocities used, the point of closest approach, for the X-wire array, at which data was taken and used, lay in the range $0 < z/\delta < 0.15$ and depended on the downstream distance. The greater the distance downstream for the X-wire array, the smaller the separation became of the individual hot wires in terms of z/δ. Consequently the point of closest approach moved towards the plate as the downstream distance increased.

In order to have equi-spaced data from the plate outwards, the interpolation process 'generated' data where no data was taken in the experiments, between the plate and the point of closest approach of the X-wire array to the plate. Thus, at $z/\delta = 0.05$, the data, while reflecting the influence of the data boundaries at $z/\delta = 0$, where the velocity components are zero, and $z/\delta < 0.15$, is strictly speaking fictitious, but in experiments where a close approach was possible, the data is in good agreement with the interpolated values from other runs where such a close approach to the plate was not possible.

CHAPTER 4

EXPERIMENTAL OBSERVATIONS

4.1 Geometry of the Turbulent Spot and Streamwise Component of Total Mean Velocity

The coordinate axes were: positive x, downstream to the left; positive y, spanwise downwards and positive z, normal to the plate as in Fig. 4.1. The Reynolds' Number, R, is based on the total thickness of the laminar layer measured at $0.99U_o$, where U_o is the free stream velocity and then

$$R = \frac{U_o \delta}{\nu},$$ where ν is the kinematic viscosity.

The plan and velocities of propagation of the leading and trailing edges of the spot were deduced from measurements of the time taken for the spot to travel from its origin to a single hot wire probe, sensitive only to the streamwise mean velocity component. The voltage across the hot wire as the spot arrived at the probe was recorded digitally by the PDP8 at a known digitization rate and the time when the voltage changed measured.

The spot was nearly triangular in plan with the apex or nose at the downstream end flattened, and the upstream trailing end slightly indented. The semi-angle of the leading edge was approximately 14.5^o at $z/\delta = 0.3$, $U_o \sim 30$ ft/s. and increased slowly with increase of U_o. This plan was maintained as the spot moved downstream as shown in Fig. 4.2.

The velocity of the leading edge at the nose varied from approximately $0.88U_o$ at $z/\delta = 0.1$ to approximately

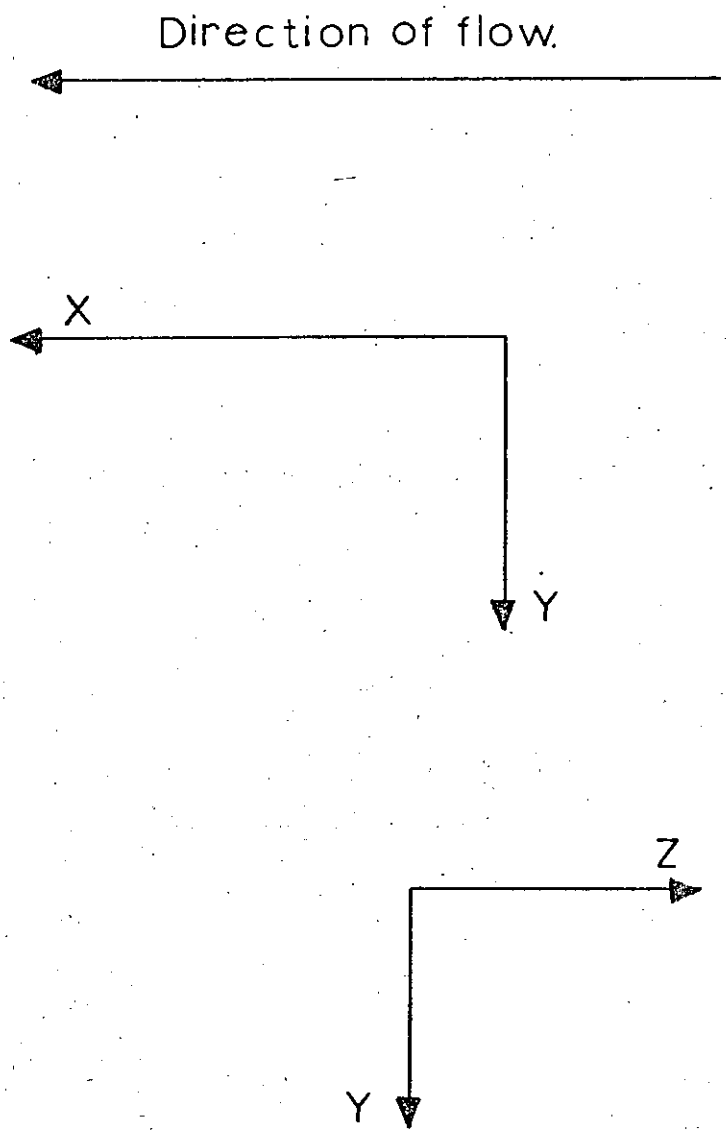

FIGURE 4.1 - Coordinate System Used in Data Treatment.

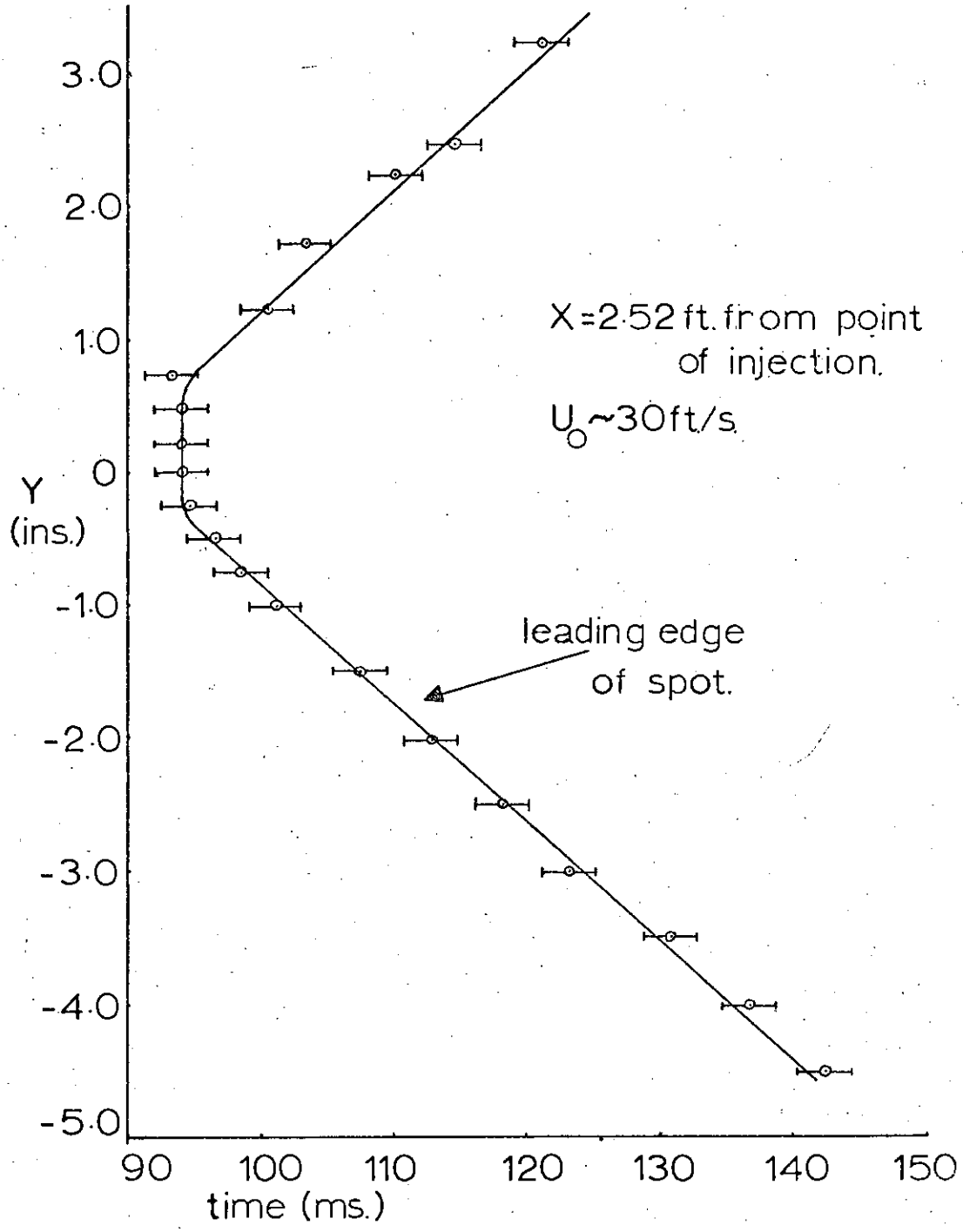

FIGURE 4.2 - Plan of Front of Spot.

$0.99U_o$ at $z/\delta = 0.7$, while the velocity at the trailing edge appeared to have no variation and the trailing edge itself remained normal to the plate through the boundary layer. The velocity of the trailing edge was approximately $0.5U_o$.

The turbulent spot extended well outside the laminar boundary layer with the upper surface rising gradually to a definite hump near the centre. The exact extent of the of the upper surface was difficult to determine because of the intermittency and weakness of the fluctuations in the uppermost regions. However, it was evident that the spot grew normally to the plate as it moved downstream, reaching $z/\delta \sim 2.0$ at $R = 1157$ and $z/\delta > 3.0$ at $R = 1485$, as shown in Fig. 4.3.

These observations agree in general with those made by Schubauer and Klebanoff in Ref. 4.

As mentioned previously, an interpolation process was used to produce values of constant velocity components at equal intervals in z/δ of 0.05. A typical contour diagram of this kind for the streamwise component is shown in Fig. 4.5.

Close investigation of the contour maps of streamwise total mean velocity revealed that the shape of the leading edge in the xz plane through the nose was like a parabola whose axis coincided with the plate surface and was not a straight line as indicated in Ref. 15. The parabola could be conveniently divided into two sections - a lower section, $0 \leqslant z/\delta \leqslant 0.3$, of mean slope approximately 9^o,

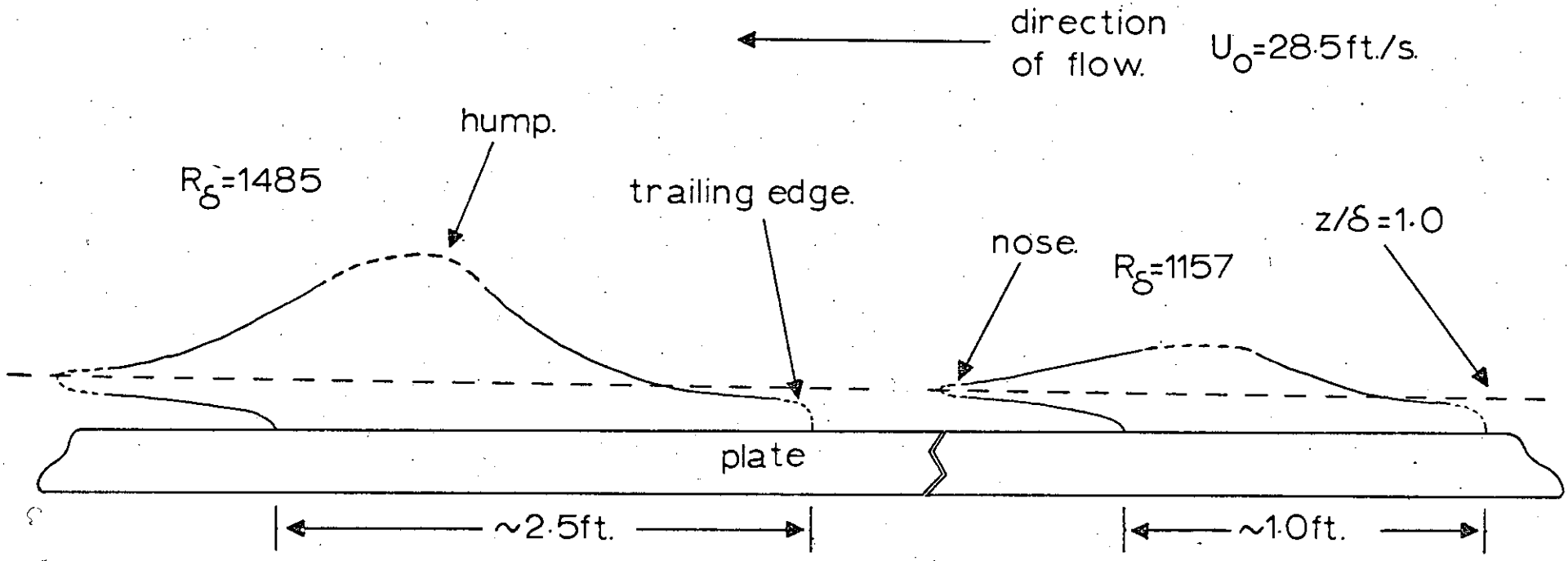

FIGURE 4.3 - Growth of Spot Downstream.

(Not to scale)

and an upper section, $0.3 \leqslant z/\delta \leqslant 0.95$ of mean slope approximately 2°. At $z/\delta \sim 0.95$ the outer section began to curve upwards when it merged into the envelope of the top of the spot, as shown in Fig. 4.4.

Measurements taken from the contour maps of streamwise total mean velocity showed that, for a given U_o, the distance AF, as shown in Fig. 4.5, increased as the spot moved downstream. While precise measurement was not easy on these contour maps, it seems that the distance AF varies approximately as the square of the distance travelled by the spot downstream as shown in Fig. 4.6.

The distance AF increased with time and varied approximately inversely with the free stream speed as shown in Fig. 4.6.

At E, in Fig. 4.5, the contours of streamwise total mean velocity for $U > 0.7U_o$ came very close to the plate. The gradient of velocity across the layer becomes very steep and viscosity then acts to quench the turbulence. The point E represents the effective upstream limit of the turbulence in the spot and beyond E the turbulence drops to a very low level. Upstream from E, the boundary layer becomes very thin and laminar; this is consistent with the findings of Schubauer and Klebanoff in Ref. 15.

Immediately downstream from A in Fig. 4.5 and between the plate and $z/\delta \sim 0.15$, the contours of streamwise total mean velocity become closer together than in the laminar boundary layer, and remain so from the point A to the point E. In this region these contours had numerous small wave-like irregularities which reached up to $z/\delta \sim 0.2$

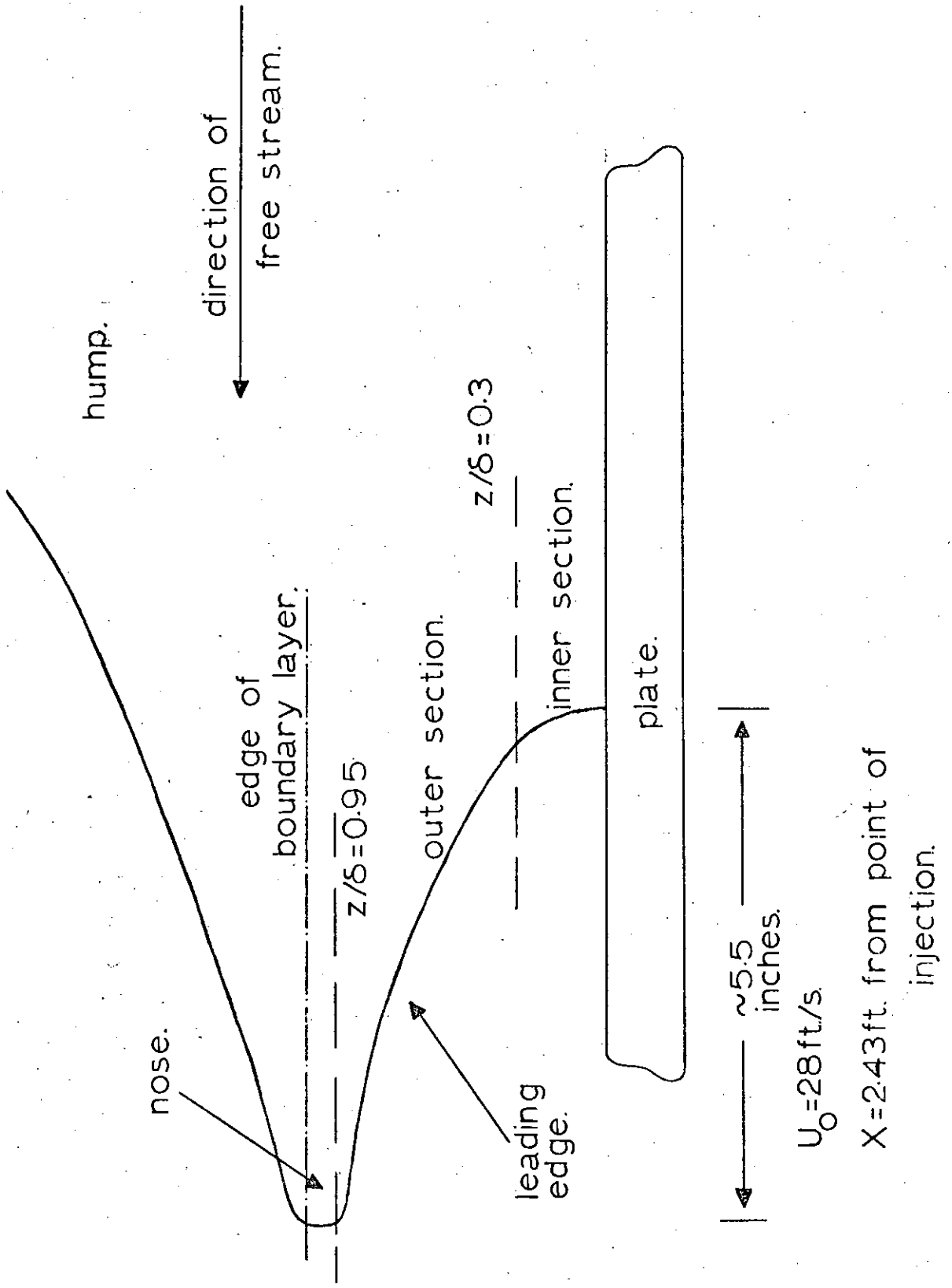

FIGURE 4.4 - Enlarged Section of Spot showing Inner and Outer Sections of Leading Edge and Merging of Outer Section with Top of Spot on Spot Centre Line (Not to Scale).

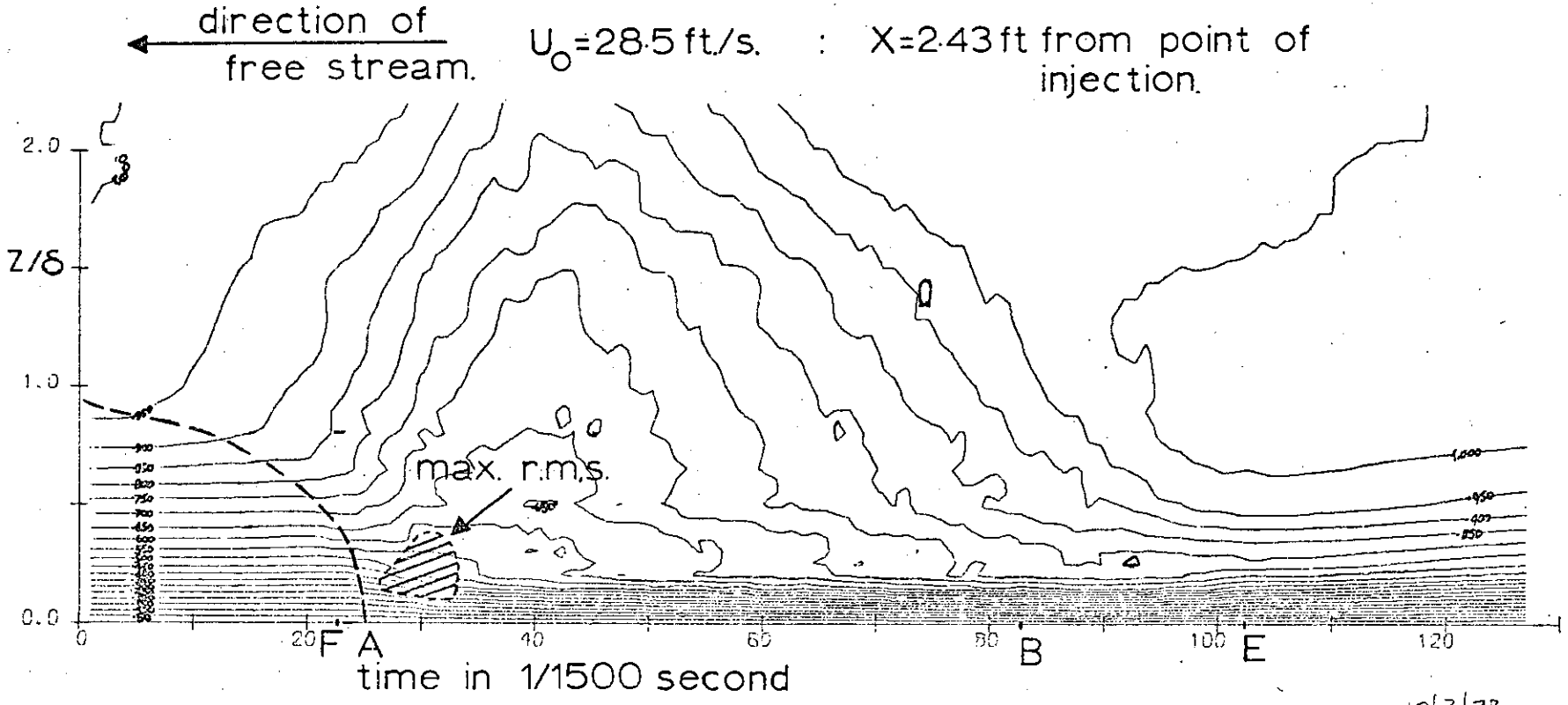

FIGURE 4.5 - Contours of Streamwise Total Mean Velocity U/U_o on Spot Centre Line.

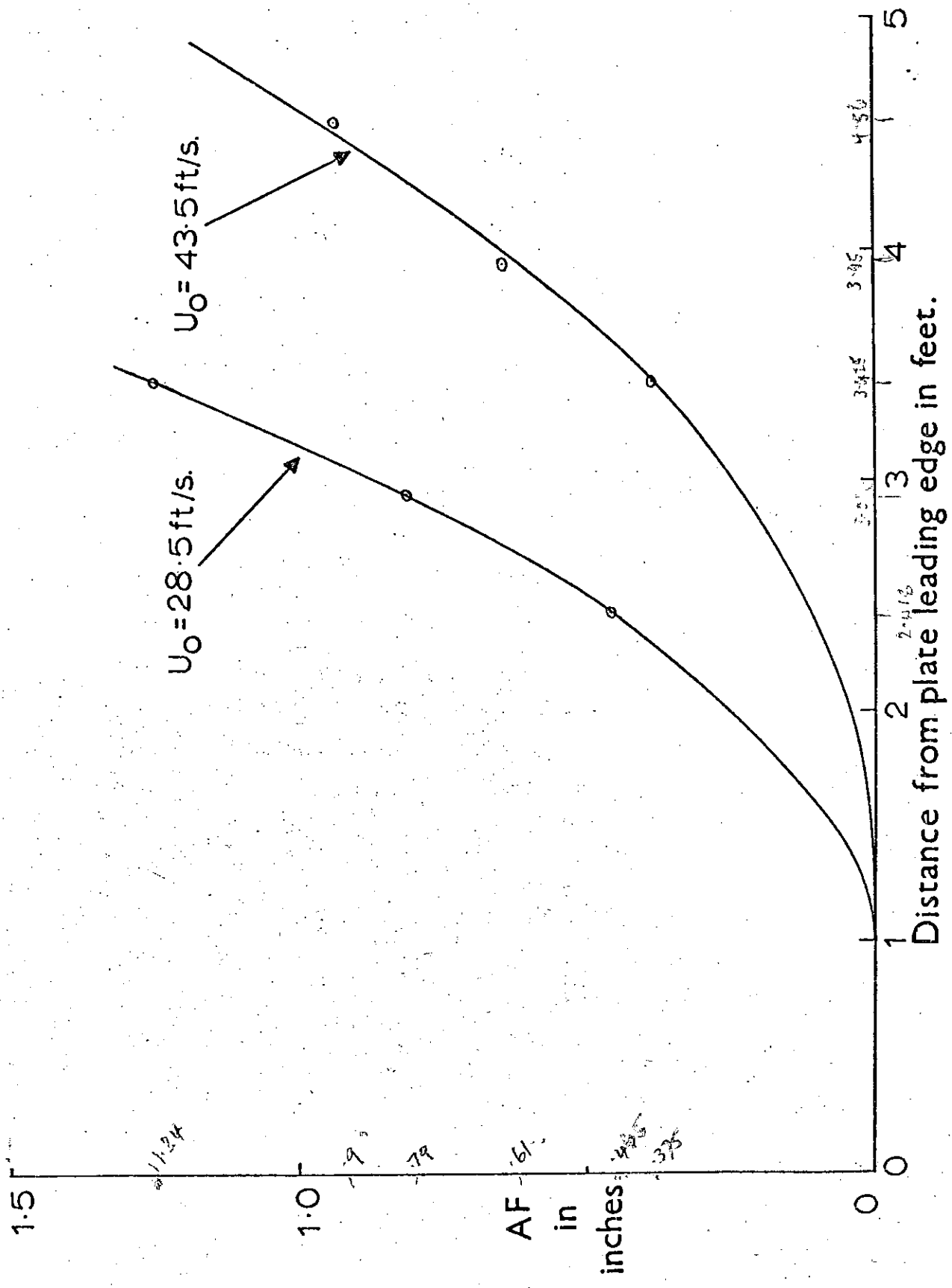

FIGURE 4.6 - Graph of Focal Distance AF Against Downstream Distance.

but rarely beyond.

Just behind the parabolic leading edge and in the range $0 < z/\delta \leqslant 0.3$, there was a general, but not necessarily smooth, acceleration of flow. Above $z/\delta = 0.2$ and between points A and B in Fig. 4.5, the normal gradient of streamwise total mean velocity, $\partial U/\partial z$, drops quickly as the contours become more widely spaced than in the laminar boundary layer. From the leading edge of the spot the contours show a deceleration of flow in the downstream direction which lasts until the region under the hump is reached. In the hump the contours reach their furthest point from the plate and then begin to converge.

There are large variations in the contours in the heart of the spot - between points A and B and in the range $0.2 \leqslant z/\delta \leqslant 1.5$. Generally these variations are not seen in the leading edge contours but are evident in the contours behind the hump, although to an increasingly smaller degree as the contour values increase.

The spanwise contour maps of streamwise total mean velocity show a spanwise waviness in the central region of the spot as shown in Fig. 4.7. This waviness was symmetrical about the centre line of the spot. Above $z/\delta \sim 0.7$ the waviness largely disappears and below $z/\delta \sim 0.2$ it is not apparent. The wavelength is approximately 1.0 inch and does not vary with the spot development.

A similar waviness appears in the leading edge contours around $z/\delta = 1.0$. Again, this is symmetrical about the centre line of the spot but its wavelength varies with the spot development, so that well downstream the wave is drawn

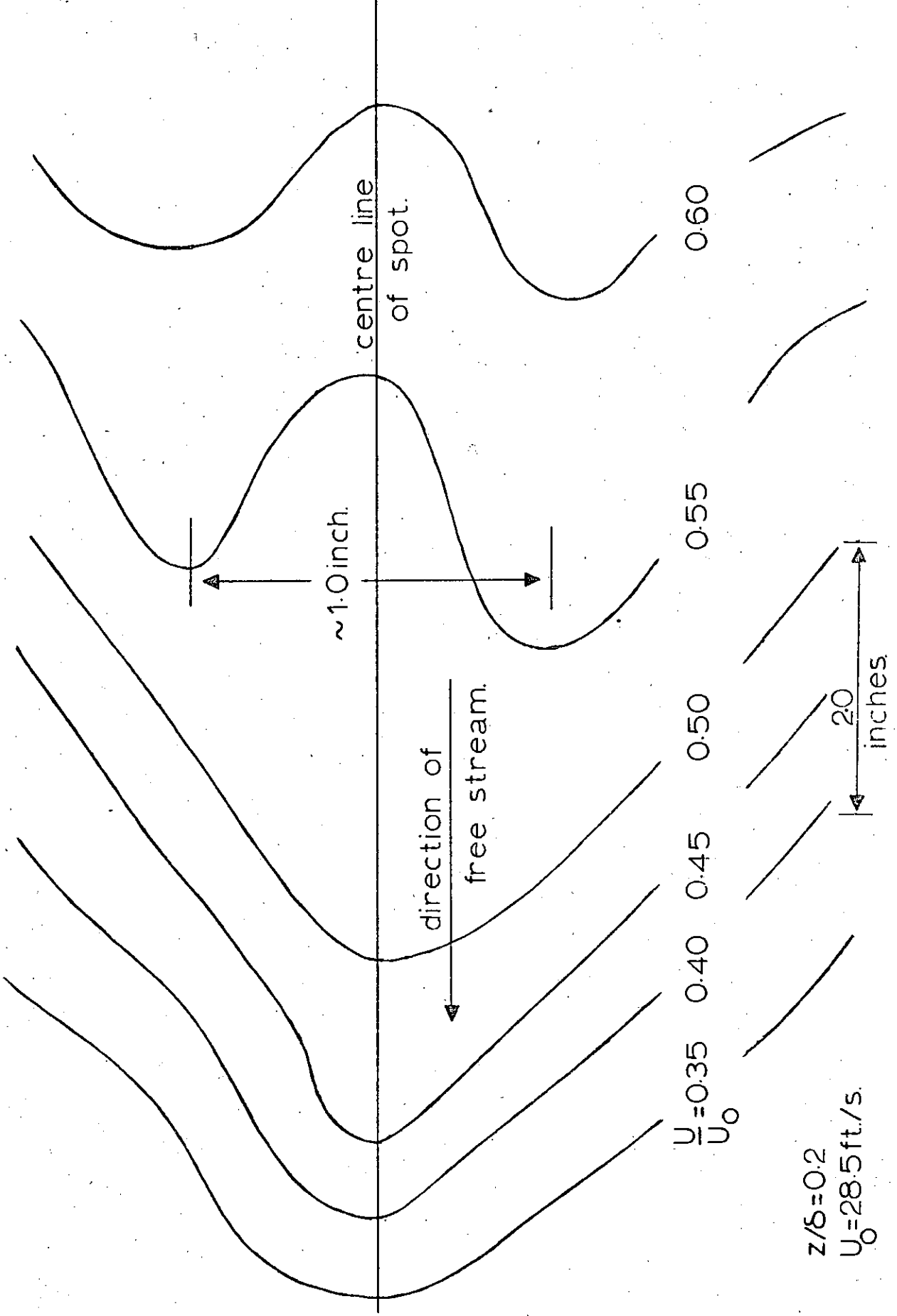

FIGURE 4.7 - Diagram Showing Spanwise Waviness in Contours of Total Streamwise Mean Velocity U/U_o at $z/\delta = 0.2$.

out along the leading edge. In this case also the wavelength is of the order of 1.0 inch.

Curves of the distribution of streamwise total mean velocity against z/δ at given times through the spot which give an indication of the development in time of the mean flow, are shown in Fig. 4.8. Initially, before the spot arrives, the curves are Blasius velocity distributions. On the arrival of the spot the distribution changes quickly to that typical of turbulent mean velocity and this distribution is maintained during the passage of the spot until point E of Fig. 4.5 is reached.

The greatest distortion in these curves occurs under the hump and good agreement is reached here with Kovasznay et al., in Ref. 11, who presented similar curves.

4.2 Streamwise Root Mean Square Fluctuations

The contours of the r.m.s. turbulence level in the xz plane between the plate and $z/\delta = 0.15$ show variations which appear to have a definite connection with the variations in this region mentioned earlier in the streamwise total mean velocity contours. Under the highest points of these r.m.s. level variations, there are dips in the streamwise total mean velocity contours. Immediately behind such rises in the r.m.s. level there are often regions where enhanced turbulence appears to spread upwards. The mean velocity contours pass through these regions of enhanced turbulence as they rise from the above mentioned dips.

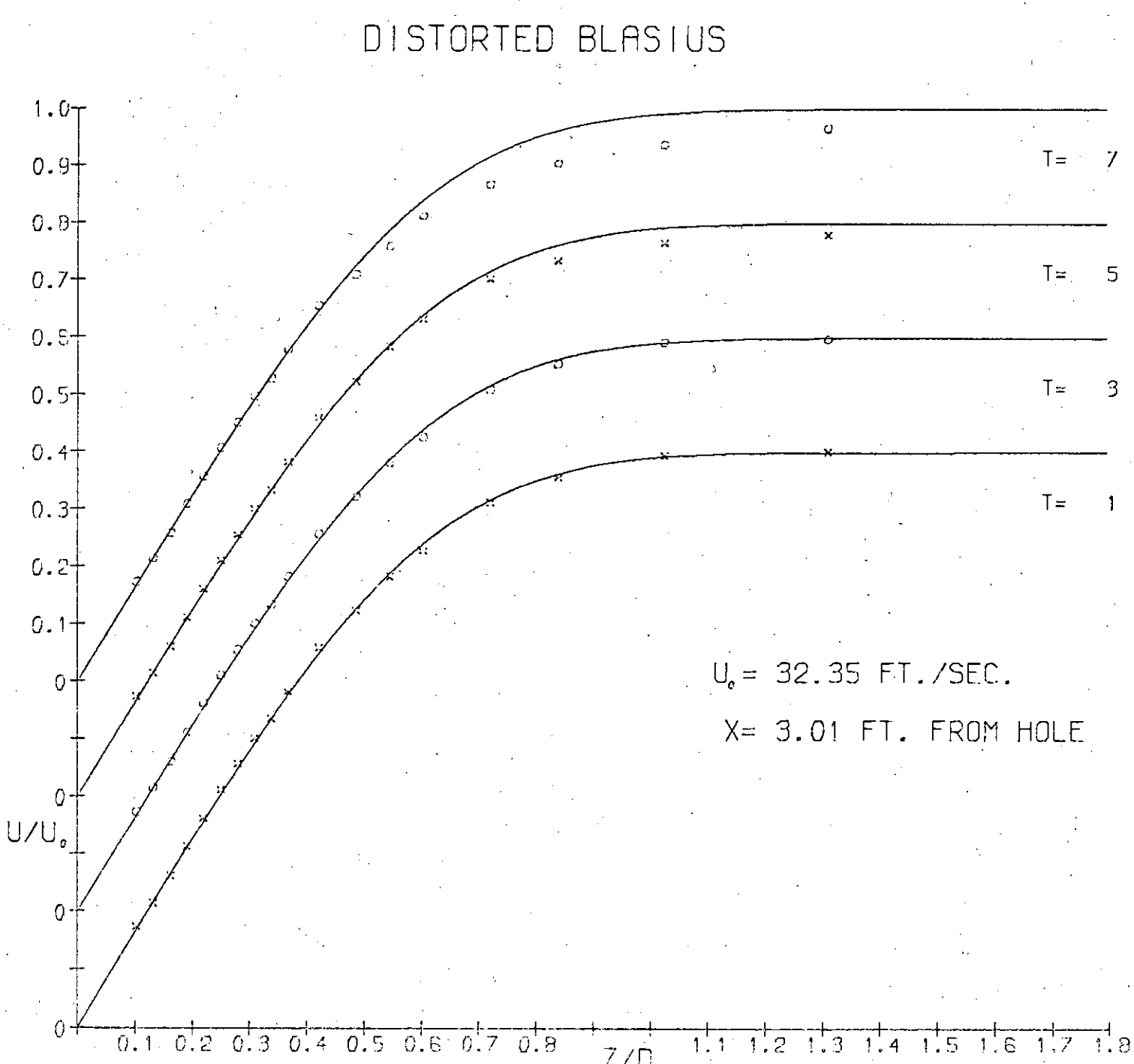

FIGURE 4.8(i) - Distributions of Streamwise Total Mean Velocity U/U_o at Intervals in Time.

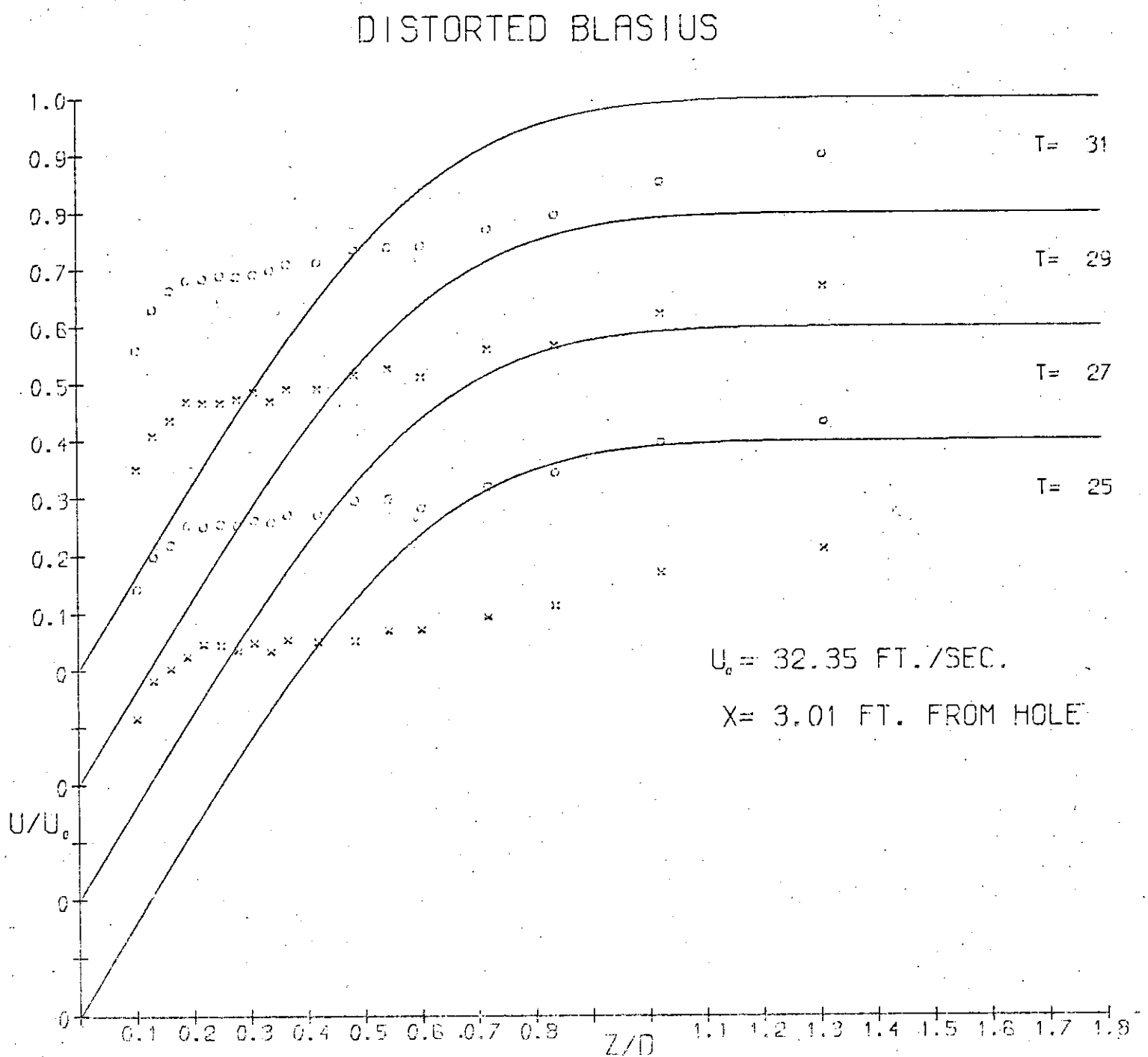

FIGURE 4.8(ii) - Distributions of Streamwise Total Mean Velocity U/U_o at Intervals in Time.

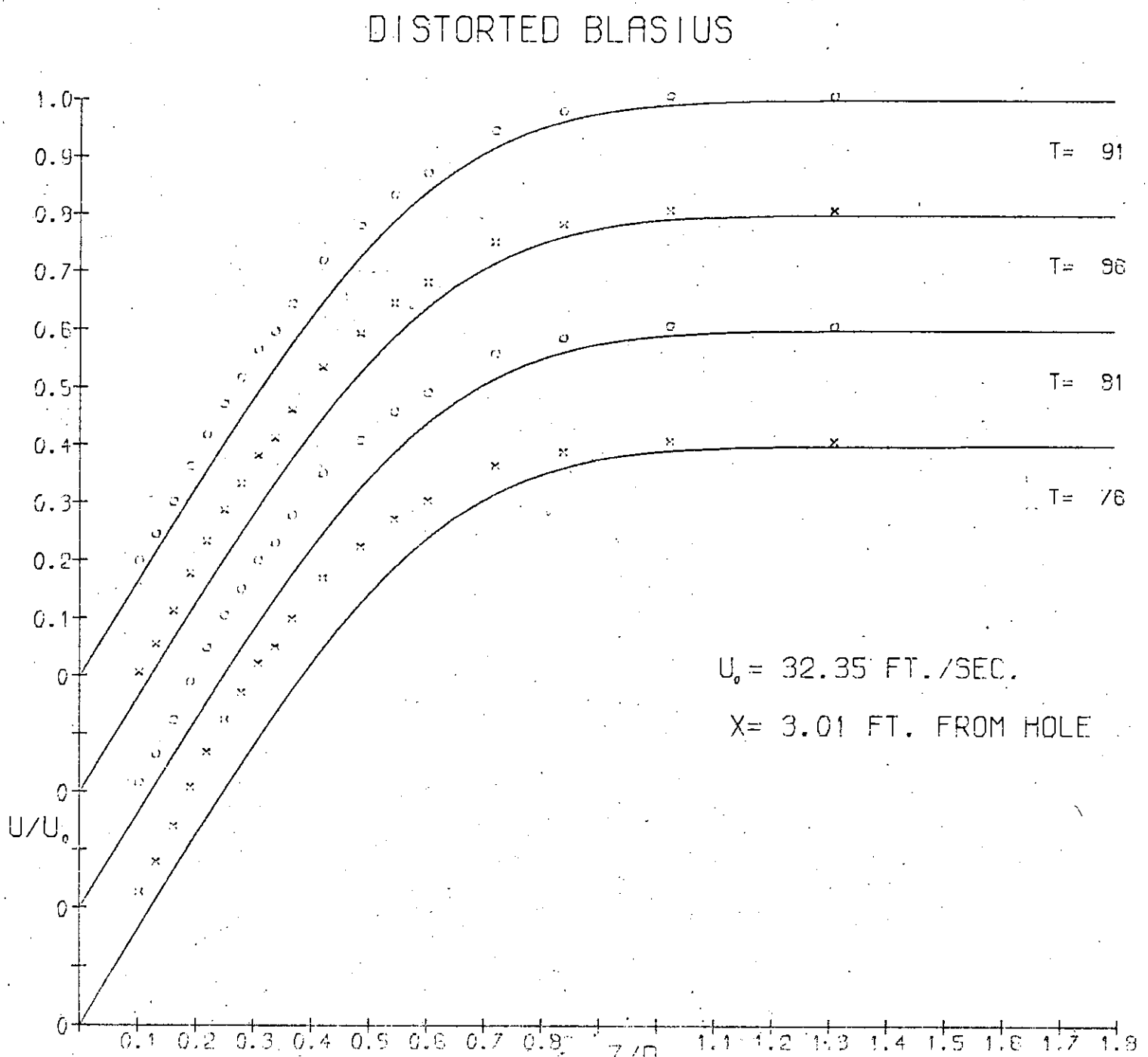

FIGURE 4.8(iii) - Distributions of Streamwise Total Mean Velocity U/U_o at Intervals in Time.

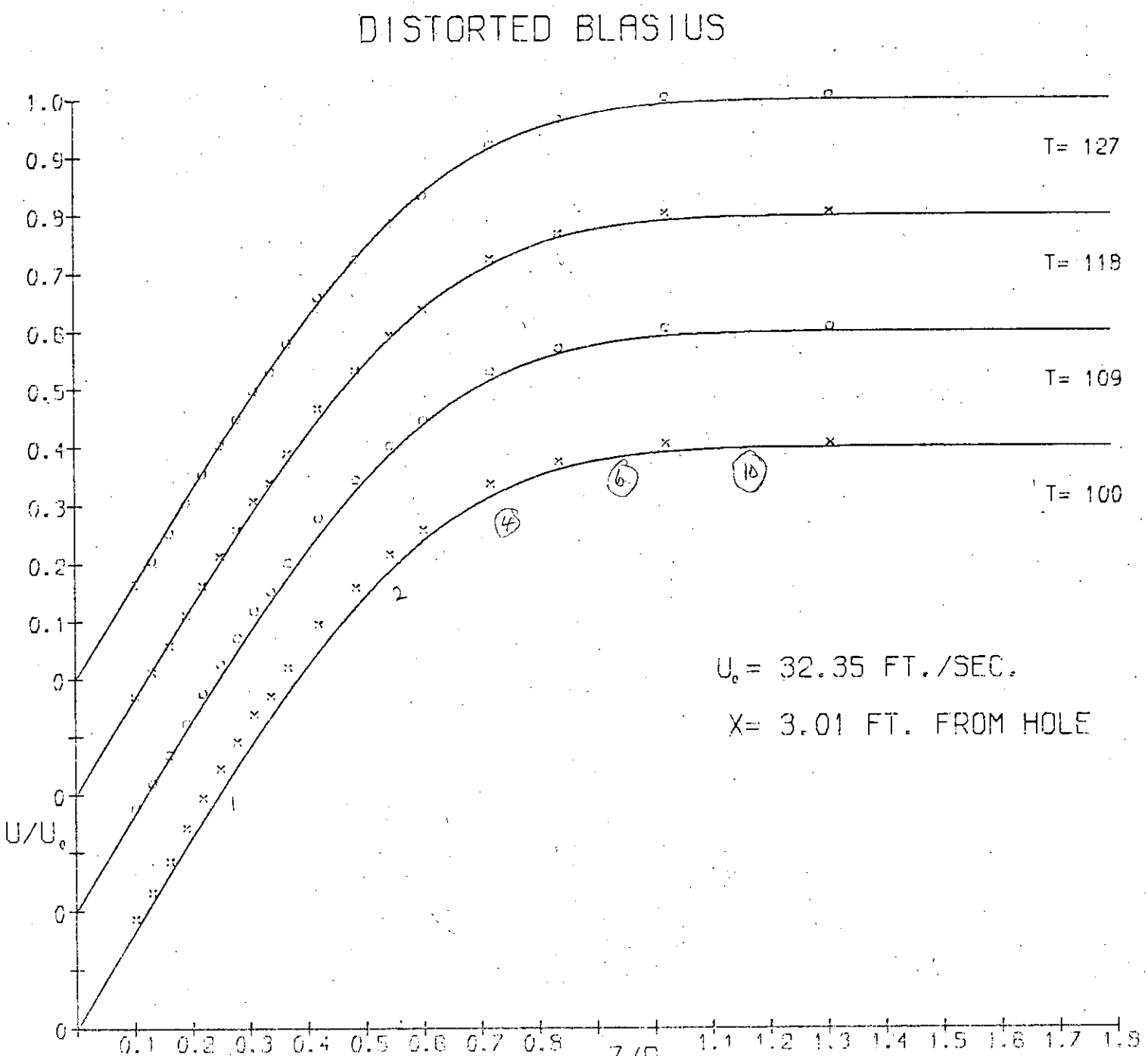

FIGURE 4.8(iv) - Distributions of Streamwise Total Mean Velocity U/U_o at Intervals in Time.

Often the streamwise total mean velocity contours reach their furthest extent from the plate in the region where the r.m.s. level enhancement is greatest.

The region of the maximum r.m.s. level lies approximately 0.1 of the distance AE (see Fig. 4.5) behind the leading edge of the spot with its centre at approximately $z/\delta = 0.2$. Typically the maximum r.m.s. level is 16°/o of the free stream velocity, U_o, and tends to be localised in the range $0.15 \leqslant z/\delta \leqslant 0.30$. The region of high turbulence intensity extends spanwise on both sides of the centre line of the spot. In addition to this principal maximum there are subsidiary maxima of the r.m.s. level forming the regions of enhanced r.m.s. level mentioned earlier. The principal maximum appears to maintain a constant height above the plate as the spot develops.

Above $z/\delta = 0.3$, turbulence can be detected throughout the volume of the spot, although its intensity decreases as z/δ increases.

Quite large irregularities in the r.m.s. levels appear in the upper regions of the spot (above $z/\delta \sim 0.5$). In these cases, high intensity turbulence is invading low intensity regions but there does not appear to be the strong connection with the irregularities in the streamwise total mean velocity that was observed nearer the plate. The volume occupied by these events decreases towards the outside of the spot at both the front and back.

Localised upward displacements of the r.m.s. level

contours around $z/\delta = 0.2$ are observed in successive contours up to, and above, $z/\delta \sim 0.6$.

4.3 Spanwise Component of Mean Velocity

The spanwise component of the mean velocity at the leading edge of the spot is towards the centre line of the spot in the region z/δ 1.0 and is away from the centre line below about $z/\delta = 0.8$, as shown in Fig. (4.9).

Towards the rear of the spot, the structure of the spanwise component is less clear but the motion seems to be away from the centre line of the spot above $z/\delta \sim 0.8$.

In the middle of the spot the spanwise component behaves differently in three main regions.

Above $z/\delta \sim 0.35$ the spanwise component is mainly away from the centre line of the spot, but below this region such symmetry is not found in the spanwise component.

Around $z/\delta = 0.3$, the flow is upwards across the plate through the spot, while below $z/\delta \sim 0.3$, the spanwise motion is predominantly downwards across the plate through the spot, although there are some irregularities. The anti-symmetry is most marked near the spot centre line.

4.4 Normal Component of Mean Velocity

The normal component is directed towards the plate in front of the hump and remains so down to about $z/\delta = 0.3$, although here it becomes weaker as z/δ decreases, as shown in Fig. (4.10).

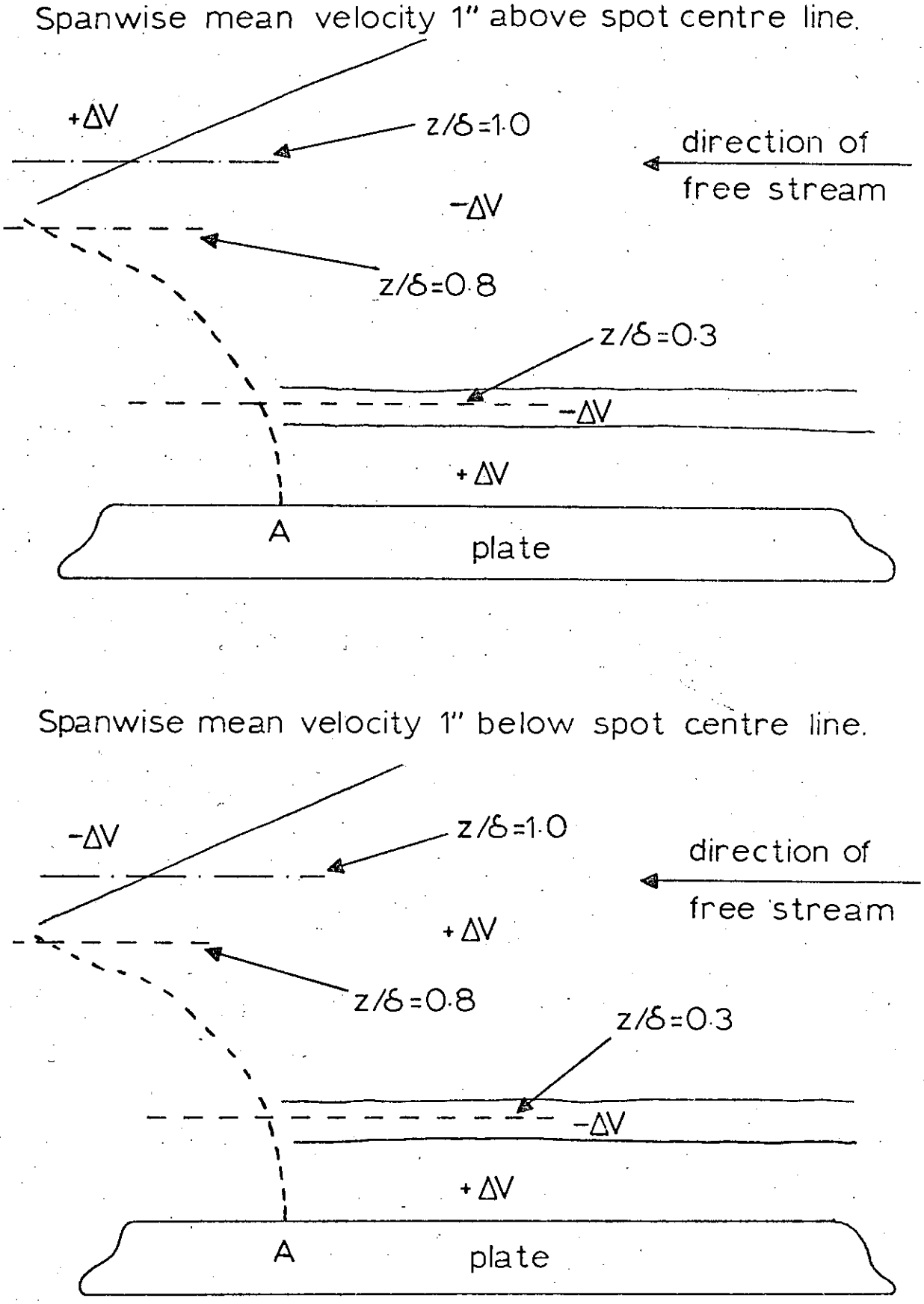

FIGURE 4.9 - Schematic Diagram of Spanwise Mean Velocity ΔV.

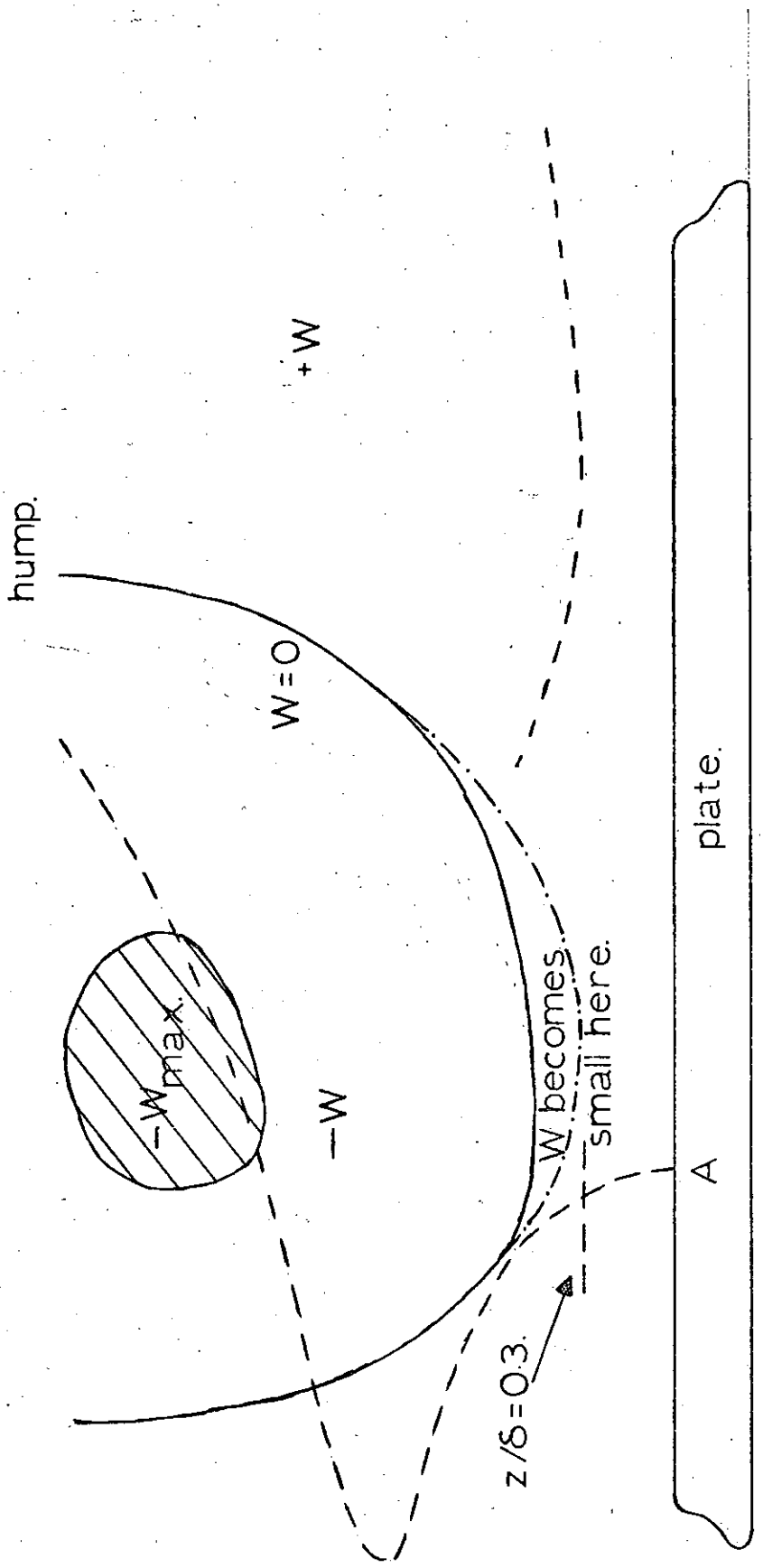

FIGURE 4.10 - Schematic Diagram of Normal Mean Velocity W/U_o on Spot Centre Line.

In and behind the hump the normal component is directed away from the plate and does not appear to vary much in the spanwise direction. In this region its magnitude decreases towards the plate and also towards the rear of the spot. Below $z/\delta \sim 0.3$, it is less than $0.01U_o$ and is within the limits of experimental uncertainty (see Appendix A for discussion of errors).

Spanwise contour maps of the normal component show that the zero contour, dividing the two opposing motions, approximately follows the shape of the leading edge of the spot, and lies just in front of or just within the hump, but not behind the hump.

CHAPTER 5

INTERPRETATION AND DISCUSSION OF OBSERVATIONS

The turbulent spot in a laminar boundary layer is a complex phenomenon. It is a compact example of transition from laminar to turbulent flow followed by the subsequent re-laminarisation of the boundary layer after the spot has passed. To assist in the interpretation of the observations presented in Chapter 4, the streamwise, spanwise and normal mean vorticity components

$$h_X = \partial W/\partial Y - \partial \Delta V/\partial Z \ ,$$
$$h_Y = \partial U/\partial Z - \partial W/\partial X \ ,$$
$$h_Z = \partial U/\partial Y - \partial \Delta V/\partial X \ , \quad \text{where}$$

$U = U_B + \Delta U$, were computed.

The shape of the leading edge of the spot around the nose suggests that a spanwise vortex here would be stretched, that the cross-section of the vortex filaments would be contracted, and that the spanwise component of mean vorticity in this region would be large in comparison with the spanwise vorticity at a corresponding height in the Blasius layer. This was not found and it is possible that the design of the experiments may account for this and could be improved. As mentioned in Chapter 3, section 1a, 27 stations were taken through the boundary layer and the first 10 stations lay in the range $0 < z/\delta \leqslant 0.3$. The greatest z/δ position was approximately 2.5 so that 17 stations covered the range $0.3 \leqslant z/\delta \leqslant 2.5$. The first 9 stations of these 17 were at intervals in z/δ of approximately 0.08 and the last 8 stations were at intervals in z/δ of approximately 0.16. Thus the change from intervals in z/δ of approximately 0.08 to 0.16

occurred around $z/\delta = 1.0$. The nose of the spot is localised around $z/\delta = 1.0$ so it is possible that the the experimental resolution was insufficient in this region. In the rest of the spot the resolution appears to be commensurate with the scale of the phenomena observed. The instantaneous recordings of the hot wire voltages as the spot passed indicated that in a group of 80 spots, successive spots were not duplicated exactly. It is possible that there were small fluctuations of the position of the nose around $z/\delta = 1.0$ and that therefore the averaging process, used in the initial stages of data reduction, decreased the real effect of the flow in the nose. The mean velocity components in the region of the nose are, however, well defined and provide other evidence of the motion in this region.

Around the nose of the spot, at $z/\delta \sim 1.0$, the spanwise mean velocity component is directed towards the centre line of the spot and the normal mean velocity component is directed towards the plate as stated in Chapter 4 and as shown in Fig. 5.1. Around $z/\delta = 0.8$ the spanwise mean velocity component is directed away from the centre line of the spot. These observations, when considered with the symmetrically swept shape of the leading edge of the spot, suggest a spanwise vortex directed upwards across the plate (negative vorticity) and forming the leading edge of the spot.

Around the hump and to the rear of the spot, the spanwise and normal mean velocity components suggest a spanwise vorticity having the same sense as the vorticity in the laminar boundary layer. This is opposite to the sense of the vorticity in the nose and calculation of the streamwise

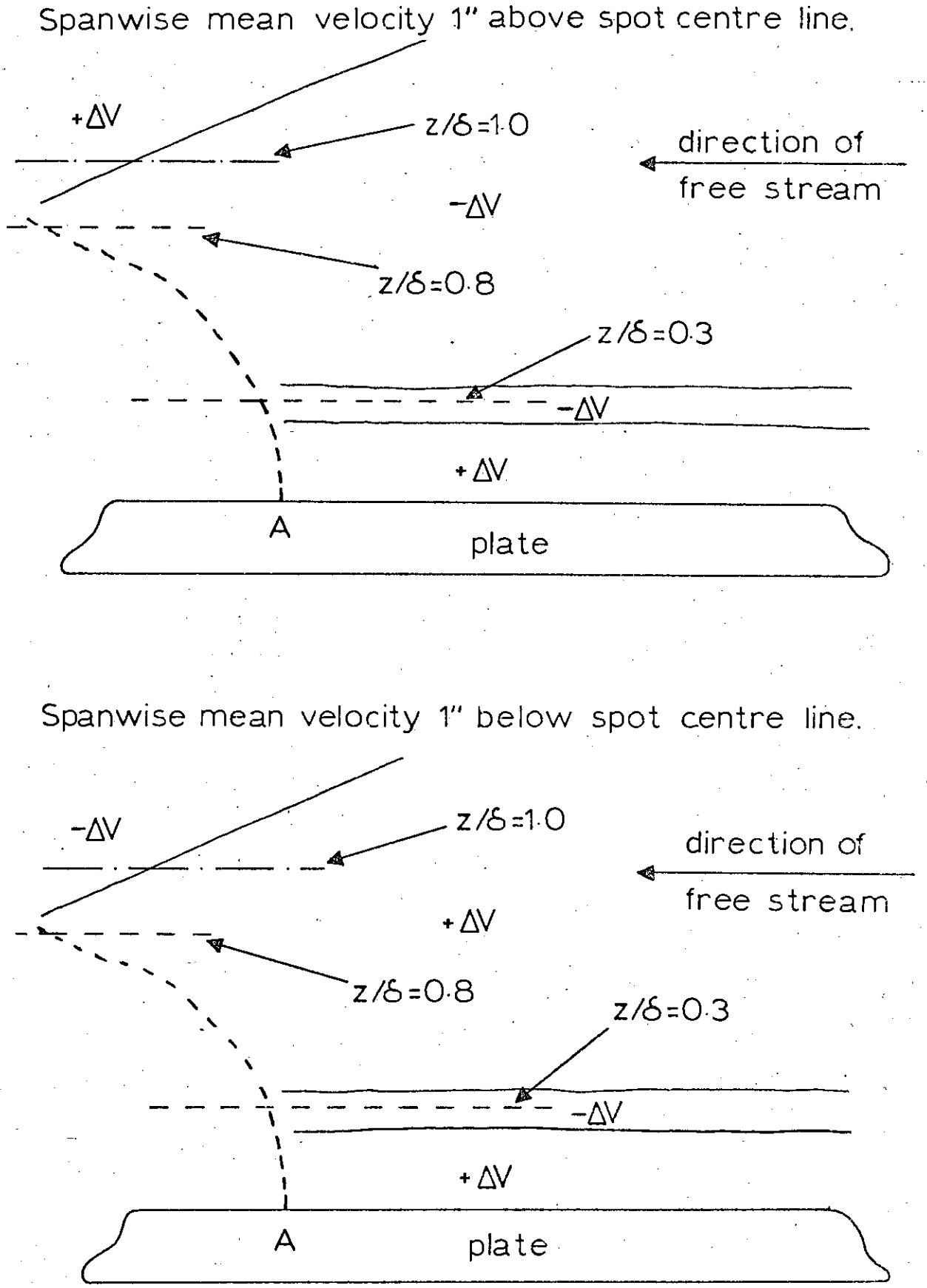

FIGURE 5.1 - Schematic Diagram of Spanwise Mean Velocity ΔV.

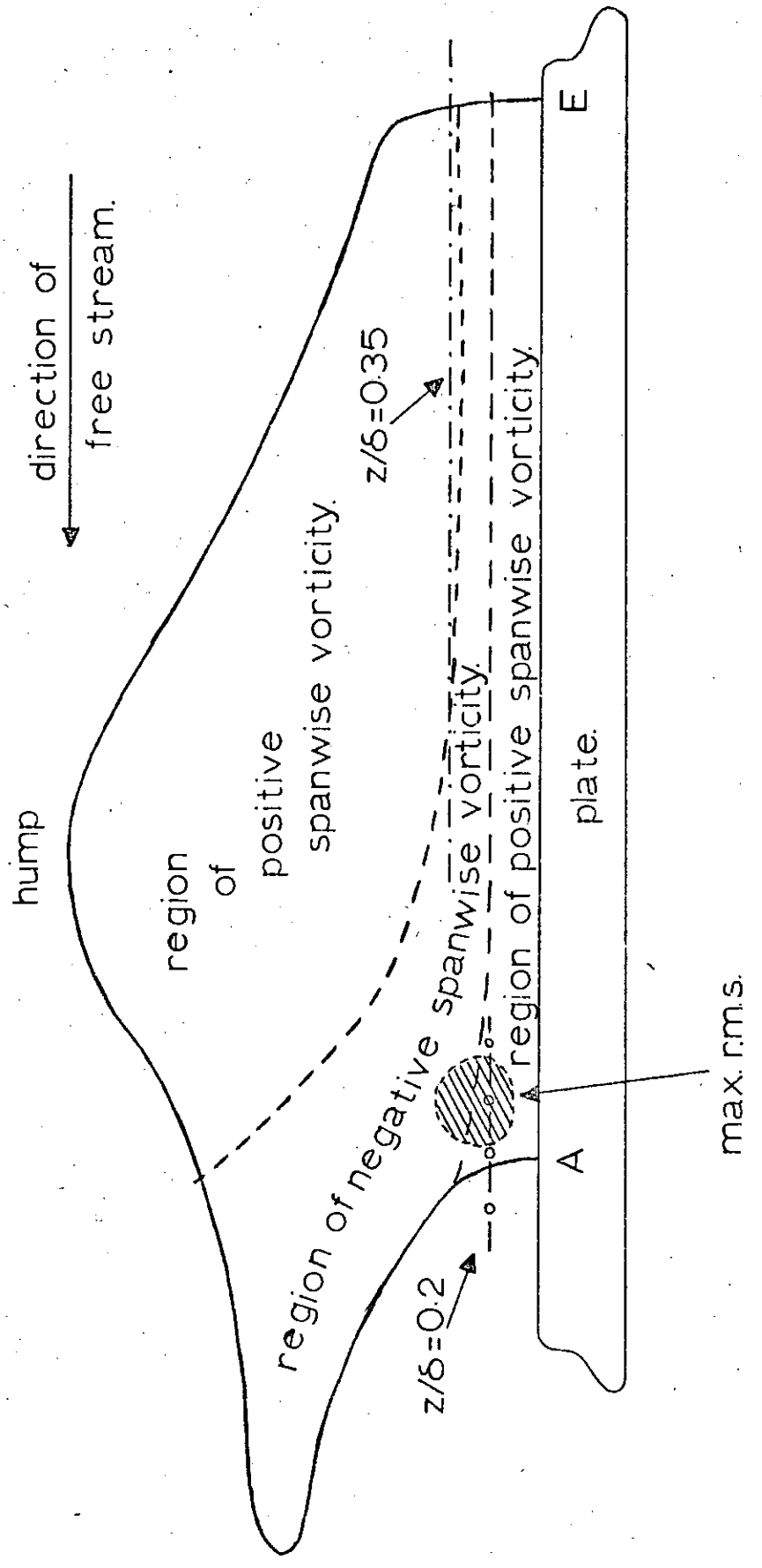

FIGURE 5.2 - Schematic Diagram showing Main Mean Vortices in Spot and Position of Region of Maximum r.m.s..

and spanwise mean vorticity components confirms this. The normal mean vorticity component shows that the vortex in this region is tilted so that it is furthest from the plate around the hump and extends upstream from the hump to the rear of the spot. No evidence of a change in the sense of the spanwise mean vorticity could be found in this region. This vortex is closest to the plate around $z/\delta = 0.35$ in the rear of the spot (see Fig. 5.2).

Spanwise mean vorticity directed upwards across the plate is found from about $z/\delta = 0.7$ to $z/\delta \sim 0.2$ underneath this positive vorticity in the hump. The spanwise mean vorticity contours in this region show regions in the downstream direction with alternate and negative vorticity, but vorticity of the opposite sense to that in the hump appears to be induced under the vortex which forms the hump. This induced vortex exists from the nose to the trailing edge of the spot underneath the upper vortex (see Fig 5.2).

It is thought that the upper surface of the turbulent spot consists of two spanwise vortices of the opposite sense, which slope down towards the plate and extend upstream to the trailing edge of the spot as shown in Fig 5.2. The leading edge of the spot is formed from a vortex with a spanwise vorticity of the opposite sense to that in the laminar boundary layer while the region around the hump and back to the trailing edge of the spot is formed from a vortex having spanwise vorticity of the same sense as the laminar boundary layer and extends through the major part of the spot volume. This interpretation may be compared with the work of Hama et al.[6] who observed 'milk bottle' vortices with vorticity of the same sense as that in the laminar boundary layer. They

observed that the downstream head of such vortices lifted away from the plate into faster fluid and the tail moved towards the plate. This comparison should be treated with caution however, since the methods of producing the vortices are different. Hama et al. moved faster fluid into the surface using a trip wire, and later a step in the surface, whereas in the work described in this thesis slow fluid was pushed from the surface into the upper region of the laminar boundary layer.

Spanwise mean vorticity with the same sense as that in the laminar boundary layer is found in the range $0 < z/\delta \lesssim 0.20$. The magnitude of this vorticity component increases towards the plate and is a manifestation of the large positive normal gradient of the spanwise mean velocity, $\partial U/\partial Z$, and the very small streamwise gradient of the normal mean velocity $\partial W/\partial X$, here. Around $z/\delta = 0.2$, the streamwise mean vorticity component is directed upstream down to about $z/\delta = 0.1$ when it reverses. Above $z/\delta \sim 0.3$, the streamwise mean vorticity component is more complicated developing a spanwise periodicity which is found well into the upper regions of the spot. Between the plate and $z/\delta \sim 0.25$, where the normal component of mean velocity is very small, the normal component of mean vorticity is more complex than higher in the spot where the normal mean velocity component becomes larger

The region of spanwise vorticity between the plate and $z/\delta \sim 0.2$ thickens slightly at the leading edge of the spot and follows the lower surface of the vortex of opposite sense above it.

The turbulent spot thus appears to consist mainly of three mean vortices as shown in Fig. 5.2 - the two mentioned earlier and the third, with the same sense as the vortex

forming the hump, between the plate and $z/\delta \sim 0.2$. The middle vortex is contained in the central region around the centre line of the spot and reaches up to the nose from there. Since vortex lines do not end in a fluid, it is conjectured that the three vortices must merge in the rear of the spot. No evidence was found which indicated the vortices merging in the front region of the spot.

The maximum r.m.s. region ($z/\delta \sim 0.2$) seems to occur between the two lower vortices as shown in Fig. 5.2. From this region to the trailing edge of the spot the region where the r.m.s. level is high is drawn out along the interface between the two lower vortices while decreasing towards the trailing edge. Fluid entrained in the nose region by the action of the vortices there maintains the maximum r.m.s. level although in an indirect way. The maximum r.m.s. level lies around the region where the normal mean velocity component towards the plate is very small so the energy transported by this component from the free stream must be absorbed at a higher z/δ position than that at which the maximum r.m.s. level lies. It thus appears that the 'gear wheel' system of the three main mean vortices already mentioned, transfers the energy from the entrained fluid into the region of maximum r.m.s. intensity. The streamwise mean velocity component distributions show that in the heart of the spot, where the r.m.s. level is high, the mean velocity increases very slowly with z/δ. The kinetic energy of the entrained fluid must contribute to the generation of turbulence. It is concluded therefore that the r.m.s. level is maintained at its high level by the action of the main vortices bringing in higher energy fluid to the region of strongest gener-

ation of turbulence. Towards the rear of the spot the high, but decreasing, r.m.s. level is produced more by the action of the two lower vortices and less by the energy of the entrained fluid. Around point E of Fig 4.5 the streamwise gradient of the streamwise velocity, $\partial U/\partial X$, is increasing at the expense of $\partial \Delta V/\partial Y$ and $\partial W/\partial Z$ and the vortex structure is beginning to break down.

The irregularities and variations mentioned in Chapter 4 and shown in Fig 5.3 in the streamwise mean velovity component and the r.m.s. level close to the plate are believed to be manifestations of the phenomenon of 'bursting' which has been shown to exist in this region ($z/\delta \lesssim 0.15$) by various workers[4],[8]. The upward displacements of the r.m.s. contours observed in the region $z/\delta \lesssim 0.15$ could be the result of ejections of fluid of low mean velocity away from the plate as found by Kim et al.. If this assumption is true, then the dips in the streamwise mean velocity contours which are connected with these r.m.s. displacements must represent the streamwise acceleration which has been observed to be associated with such bursting. Higher in the spot the localised upward displacements of the r.m.s. contours mentioned at the end of section 2, Chapter 4, provide evidence that the bursting events closer to the plate are influencing the flow in the region up to $z/\delta \sim 0.6$. Similar, more detailed, observations were made by Blackwelder and Kovasznay[2].

The experimental work produced a very large amount of data. The printed results were too voluminous to handle within the scope of this thesis and contour diagrams gave a more condensed presentation. The interpretation has relied heavily on these contour diagrams, and is therefore more

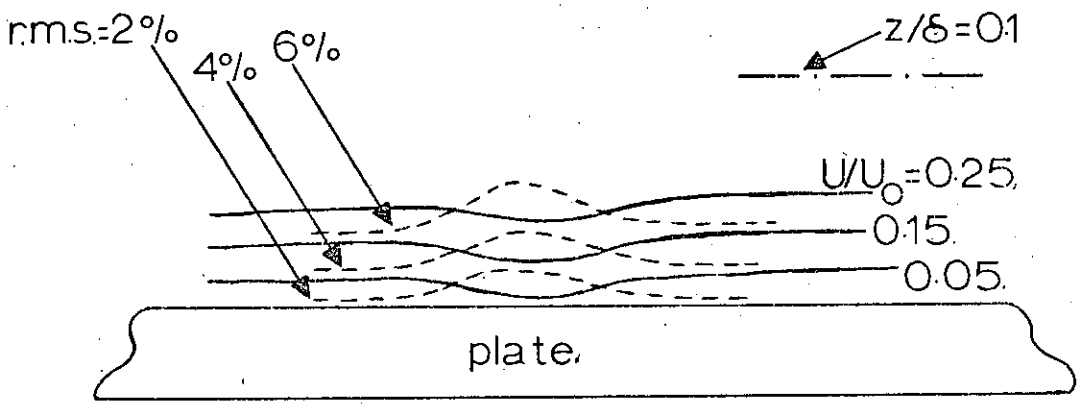

FIGURE 5.3 - Schematic Diagram of Irregularities in Contours of Streamwise Total Mean Velocity U/U_o and r.m.s. level Contours Near Plate.

qualitative than quantitative. It is hoped, however, to carry out a more detailed investigation to give a more quantitative explanation of the structure of the turbulent spot.

APPENDIX A

Estimation of Experimental Errors

Starting with the hot wire equation

$$S^2 = A + B\,U^{0.45}$$

where S is used in place of V to avoid confusion later in this Appendix, an expression can be derived for the non-dimensional velocity in the Blasius boundary layer for the outer hot wire, viz.

$$\left(\frac{S_{BO}^2 - A_o}{S_{OO}^2 - A_o}\right)^{2.222} = \frac{U_{BO}}{U_o}\,,$$ where S_{OO} is the voltage of the outer hot wire at the free stream velocity U_o.

The error formula

$$\sigma_f = \sqrt{\left(\frac{\partial f}{\partial a}\right)^2 \sigma_a^2 + \left(\frac{\partial f}{\partial b}\right)^2 \sigma_b^2 + \ldots\ldots} \qquad (A.1)$$

where $f = f(a, b, \ldots.)$ and σ_a, σ_b etc. are the reading errors in a, b, ..., etc., is now used to compute the error in U_{BO}/U_o. The error in A_o is small enough to be ignored.

$$\sigma_{(U_{BO}/U_o)} = \frac{4.444}{(S_{OO}^2 - A_o)} \sqrt{S_{BO}^2 \left(\frac{S_{BO}^2 - A_o}{S_{OO}^2 - A_o}\right)^{2.444} \sigma_{S_{BO}}^2 + S_{OO}^2 \left(\frac{S_{BO}^2 - A_o}{S_{OO}^2 - A_o}\right)^{4.444} \sigma_{S_{O}}^2}$$

Typical data near the plate ($U_{BO}/U_o = 0.206$) is

$$S_{BO} = 2.2036 \text{ volts}$$

and $A_o = 3.394$ with $S_{OO} = 2.5243$ volts. The reading error of the Solartron digital voltmeter for S_{BO} and S_{OO} is

$$\sigma = \pm 0.001 \text{ volts.}$$

Near the plate therefore,

$$\sigma_{(U_{BO}/U_o)} \sim \pm 0.0016, \text{ or approximately } 0.8^{\circ}/o.$$

The matching of the hot wire stations, mentioned in Chapter 3, section 2, allows the assumption that the errors, $\sigma_{(U_{BO}/U_o)}$ and $\sigma_{(U_{BI}/U_o)}$, are of the same order at the same z/δ position, say $1^{\circ}/o$. This gives the error, $\sigma_{(U_B/U_o)}$, in the average non-dimensional velocity, U_B/U_o, measured by the two hot wires to be

$$\sigma_{(U_B/U_o)} = \sqrt{\frac{\sigma^2_{(U_{BO}/U_o)}}{4} + \frac{\sigma^2_{(U_{BI}/U_o)}}{4}} .$$

Therefore $\sigma_{(U_B/U_o)} \sim \pm 0.7^{\circ}/o$ near the plate.

In the free stream $S_{BO} = S_{OO} = S$ and $U_{BO}/U_o = 1.0$, giving

$$\sigma_{(U_{BO}/U_o)} = \frac{4.444}{(S^2 - A_o)} \sqrt{2 \times \sigma^2 \times S} ,$$

which gives $\sigma_{(U_{BO}/U_o)} = \pm 0.005$ or $0.5^{\circ}/o$. Using the assumption that the errors for the two hot wires are the same at the same z/δ position gives the error in the average value of the non-dimensional free stream velocity to be

$$\sigma_{(U_B/U_o)} \sim \pm 0.5^{\circ}/o.$$

To calculate the error in $(U_B + \Delta U)/U_o$, equation (3.8) is used as the starting point,

$$\Delta U/U_B = \left(\frac{S_{MO}^2 - A_o}{S_{BO}^2 - A_o}\right)^{2.222} - 1.$$

Equation A1 then gives,

$$\sigma_{(\Delta U/U_o)} =$$

$$\frac{4.444}{(S_{BO}^2 - A_o)}\sqrt{S_{MO}^2\left(\frac{S_{MO}^2 - A_o}{S_{BO}^2 - A_o}\right)^{2.444} \times \sigma_{S_{MO}}^2 + S_{BO}^2\left(\frac{S_{MO}^2 - A_o}{S_{BO}^2 - A_o}\right)^{4.444} \times \sigma_{S_B}^2}$$

Near the plate S_{MO} is greater than S_{BO} for most of the spot and $S_{MO} = S_{BO} + \Delta S$, where ΔS is the mean disturbance voltage obtained from the ensemble average procedure. Typically $\Delta S_{max} = 0.05$ volts near the plate.

$\sigma_{S_{MO}}$ is a combination of the reading error, $\sigma_{S_{BO}}$, from the digital voltmeter and a quantisation error, $\sigma_{\Delta S}$, from the analogue to digital converter. This quantisation error is negligible since the analogue to digital converter was used in its full scale mode, producing 12 bit binary words from the input signal. A full scale deflection is 4096 discrete voltage levels with a standard deviation of 0.29 of one scale unit. This is clearly an insignificant error, being of the order of $0.3/4096 = 7.5 \times 10^{-5}$ for maximum signals, rising to 0.15°/o for signals of 1/4 full scale. A further maximum error is quoted by the manufacturer as $\pm$ 0.025°/o for 12 bits for switching point error. $\sigma_{S_{MO}}$ can therefore be written $\sigma_{S_{BO}}$. Using the same data as before then gives

$$\sigma_{(\Delta U/U_B)} \sim \pm 0.011 \text{ near the plate.}$$

Now $\Delta U/U_o = \Delta U/U_B \times U_B/U_o$, therefore

$$\sigma_{(\Delta U/U_o)} =$$

$$\sqrt{\left(\frac{U_B}{U_o}\right)^2 \times \sigma_{(U/U_B)}^2 + \left(\frac{\Delta U}{U_B}\right)^2 \times \sigma_{(U_B/U_o)}^2} \quad , \quad (A.2)$$

and $\sigma_{(\Delta U/U_o)} \sim \pm$ 0.005 or 0.9°/o.

In the free stream, $S_{BO} = S_{OO}$ and S_{MO} is less than S_{OO}. The estimated error becomes $\sigma_{(\Delta U/U_B)} \sim \pm$ 0.005. Using equation (A2) gives $\sigma_{(\Delta U/U_o)} \sim \pm$ 0.005 or 0.5°/o.

To estimate the error in the spanwise mean flow velocity component, ΔV, equation (3.9) is used as the starting point along with equation (A1). The error in $\Delta V/U_o$, $\sigma_{(\Delta V/U_o)}$, is approximately 3°/o at higher values of $\Delta V/U_o$ ($\Delta V/U_o \sim 0.15$) and approximately 7°/o at $\Delta V/U_o \sim 0.04$, near the plate. In the free stream the range of the estimated error in $\Delta V/U_o$ is the same as near the plate.

To estimate the error, $\sigma_{(W/U_o)}$, in W/U_o, the equation of continuity is used as the starting point and is re-written so that

$$W/U_o = \mathbf{d}U/dX + \mathbf{d}\,V/dY \; dZ, \text{ where } U = (U_B + \Delta U)/U_o$$

and $V = \Delta V/U_o$. This gives the error in W to be

$$\sigma_{(W/U_o)} = dZ \times \sqrt{\sigma^2_{(dU/dX)} + \sigma^2_{(dV/dY)}},$$

where $dZ = 0.05$. Using this expression it is found that $\sigma_{(W/U_o)} \sim \pm$ 3°/o for $W/U_o \sim$ 0.05 and $\sim \pm$ 7°/o for $W/U_o \sim$ 0.01. The range of the estimated error, $\sigma_{(W/U_o)}$, in the free stream is of the same order as near the plate.

APPENDIX B

The diagrams contained in this appendix are representative of the contour maps of mean velocity components mentioned in the text. They were not included with the text because it was felt they contained too much detailed information. A short description of these contour maps is given here and their relation to the text is indicated. The position of the spot leading edge and centre line is marked on the contour maps.

On page 45 of the text (chapter 5), reference is made to the direction of the spanwise mean velocity component. In figs. B1a-d, these directions can be seen. At $z/\delta = 0.8$, below the spot centre line at $T \sim 30$, the spanwise mean velocity component is directed downwards across the plate, while above the spot centre line it is directed upwards across the plate. The zero contour separates these two regions by following approximately the centre line of the spot through the nose. As z/δ increases, these two regions of spanwise mean velocity become less marked until at $z/\delta = 1.0$, the pattern of this velocity component about the spot centre, manifest at $z/\delta = 0.8$, has virtually disappeared. By $z/\delta = 1.5$, however, a pattern has reappeared in which the spanwise mean velocity both above and below the centre line is now directed towards the spot centre line.

The region about the centre line and around the leading edge of the spot in which the normal mean velocity component is non-zero and directed towards the plate, decreases as

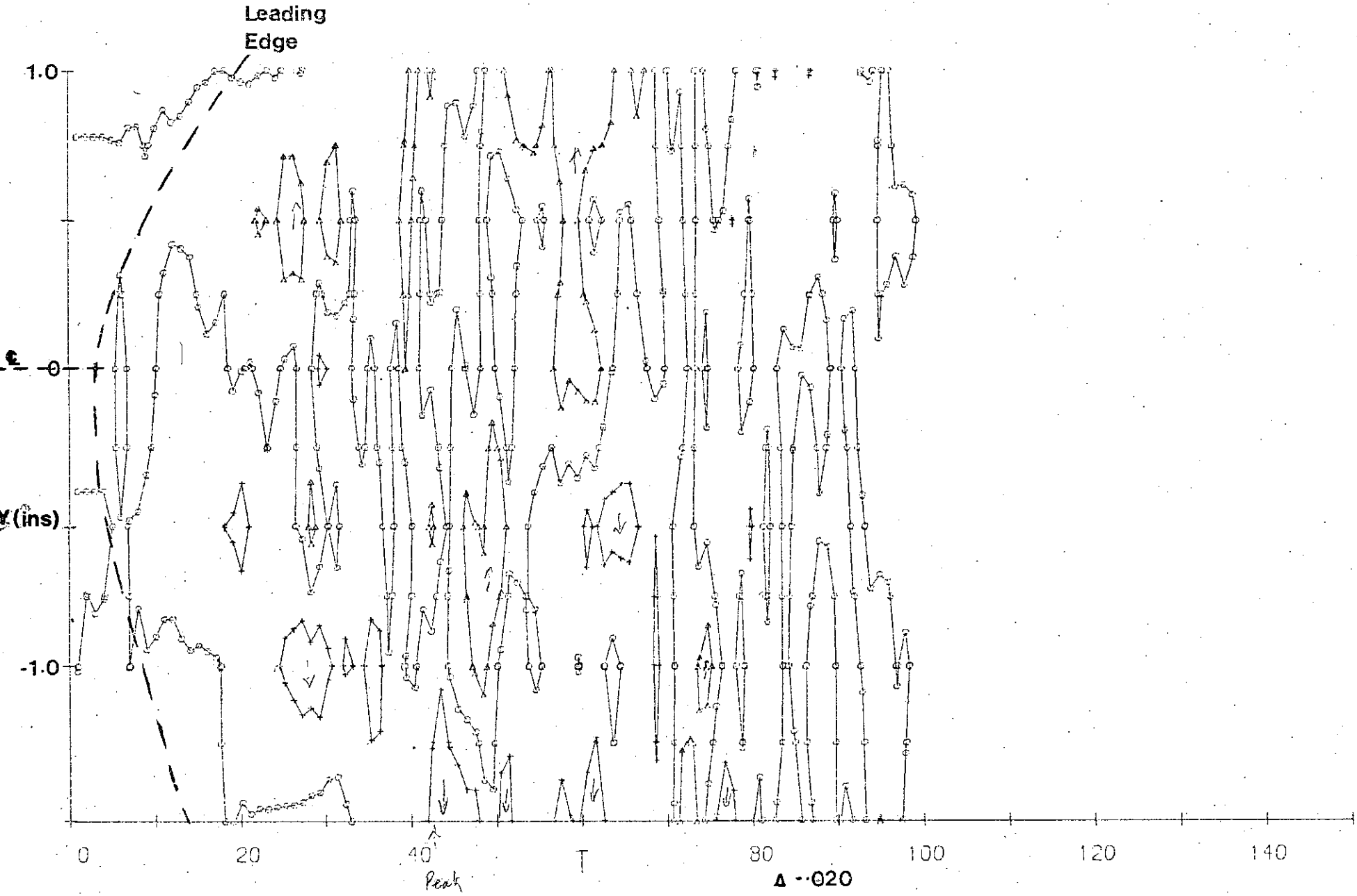

Fig B1a : V/U_o , Spanwise Mean Velocity ; $z/\delta = 0.8$. Legend o 0 , T is in 1/1500s. $R_\delta = 1385$.
Δ -·020
+ ·020

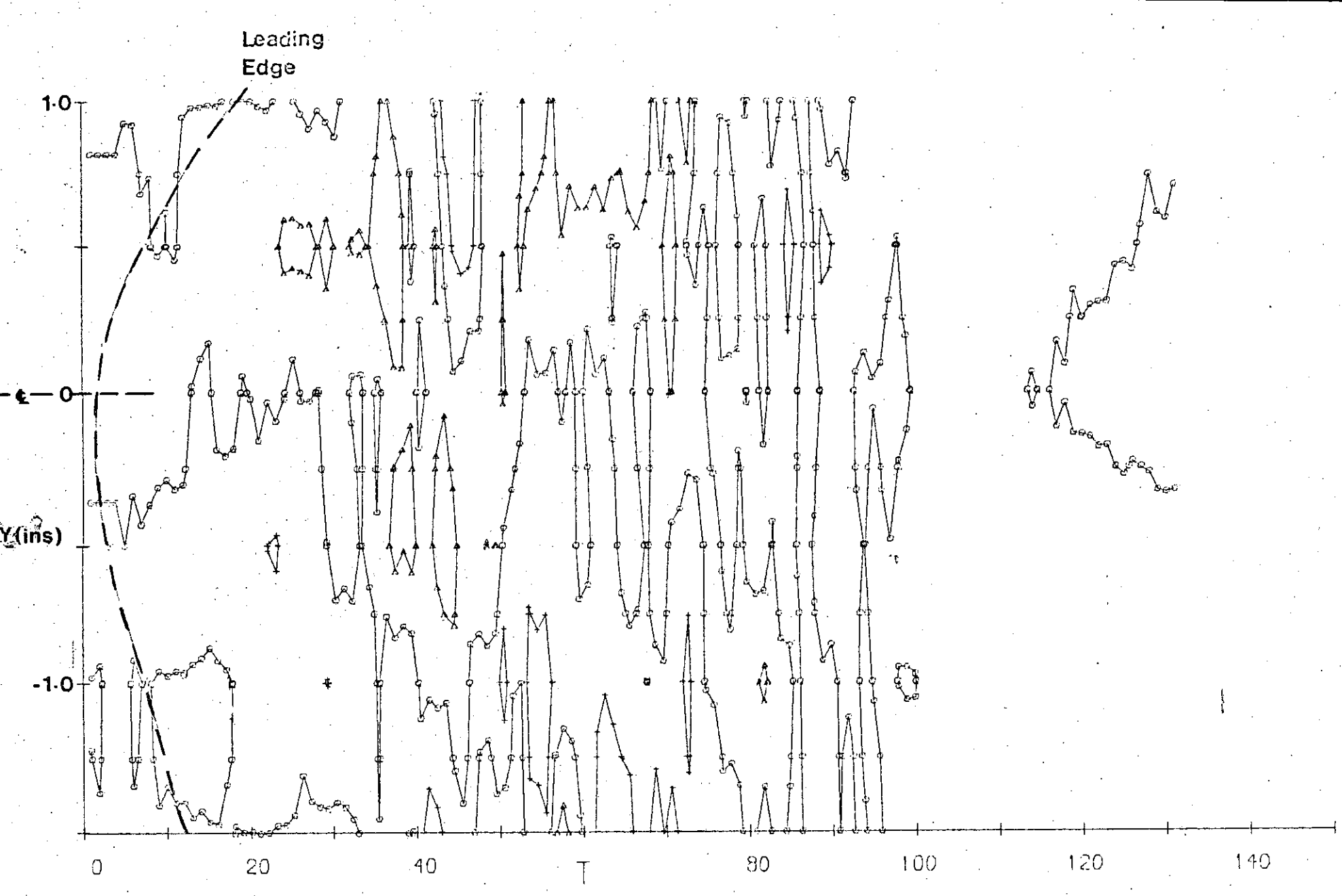

Fig B1b : V/U_o , Spanwise Mean Velocity ; $z/\delta = 0.9$. Legend o 0 , Δ -·020 , T is in 1/1500s. $R_\delta = 1385$.

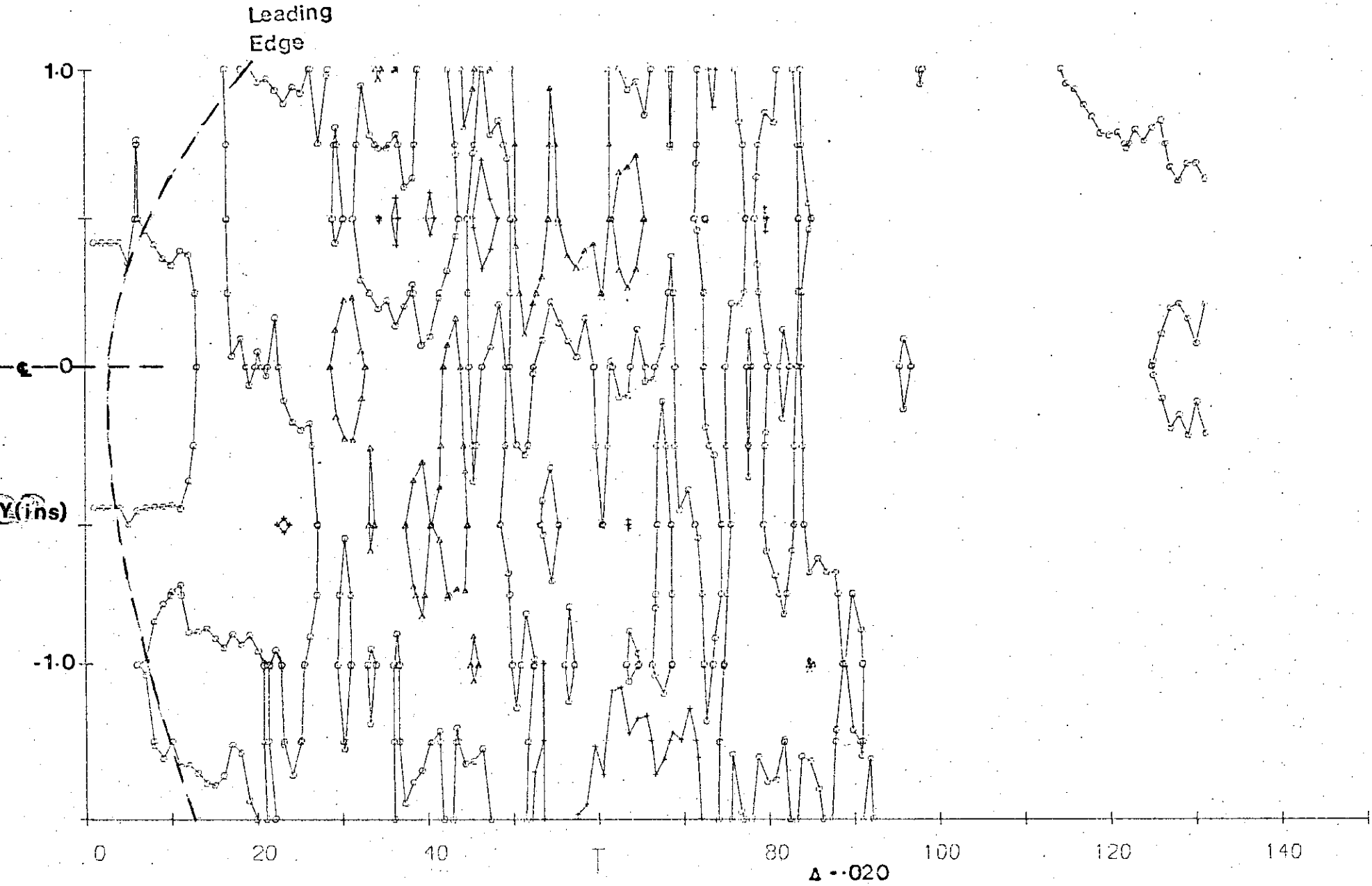

Fig B1c : V/U_o , Spanwise Mean Velocity ; $z/\delta = 1.0$. Legend o 0 , T is in 1/1500s. $R_\delta = 1385$.
Δ ··020

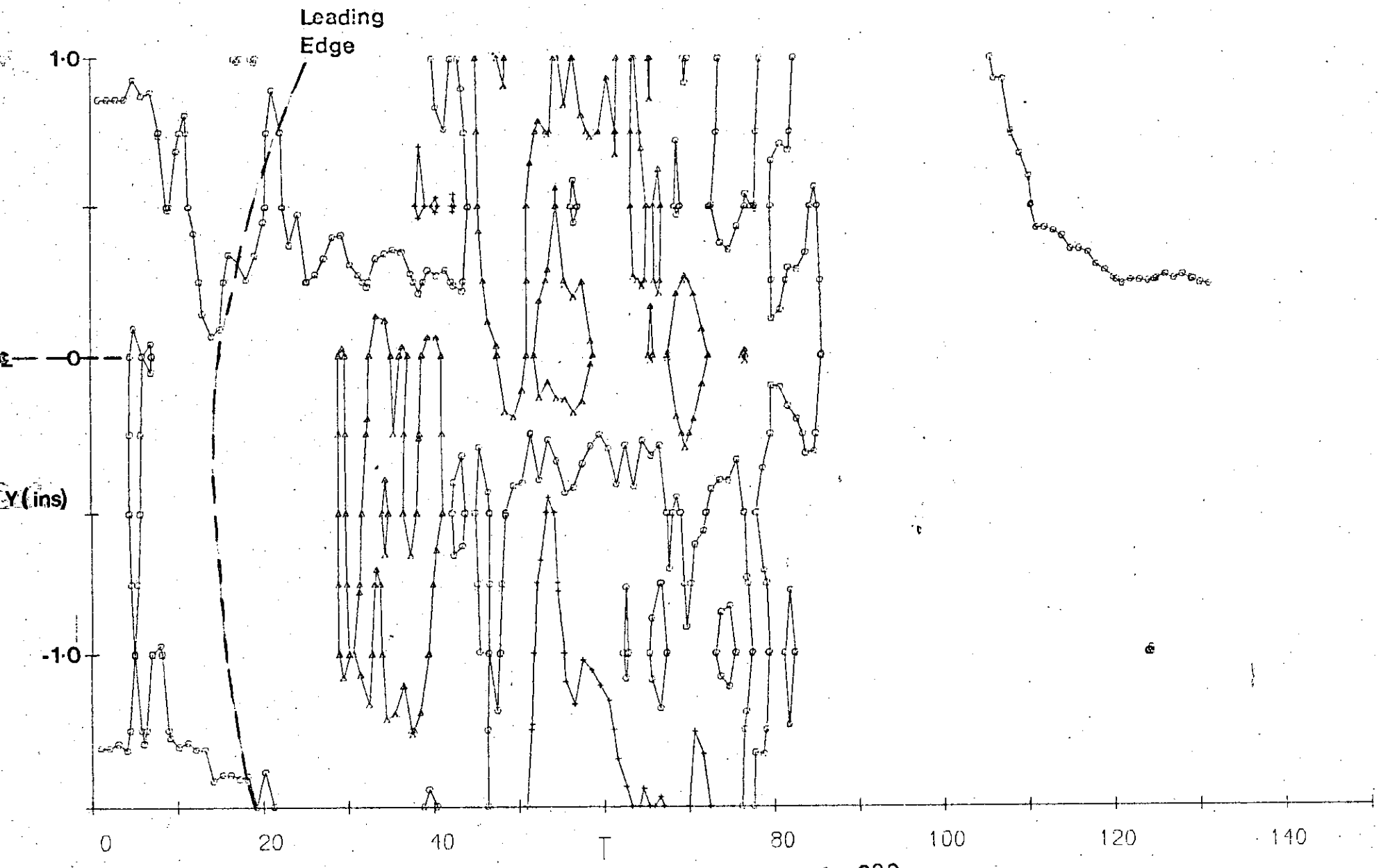

Fig B1d : V/U_o , Spanwise Mean Velocity ; $z/\delta = 1.5$. Legend Δ ·-020 o 0 + ·020 , T is in 1/1500s. $R_\delta = 1385$.

z/δ decreases from 1.5 to 0.8 (see figs. B2a-d). This region lies almost symmetrically about the spot centre line and the leading edge of the spot.

Thus, as stated on page 45 of the text, this data, when looked at in conjunction with the swept back shape of the leading edge, indicates a spanwise vortex directed upwards across the plate and following the outline of the leading edge of the spot.

The contour maps of the streamwise component of mean vorticity (fig. B3) confirm this view in the way this component of mean vorticity changes sign above and below the spot centre line. Below the spot centre line the streamwise component of mean vorticity is directed downstream while above the centre line the opposite is the case.

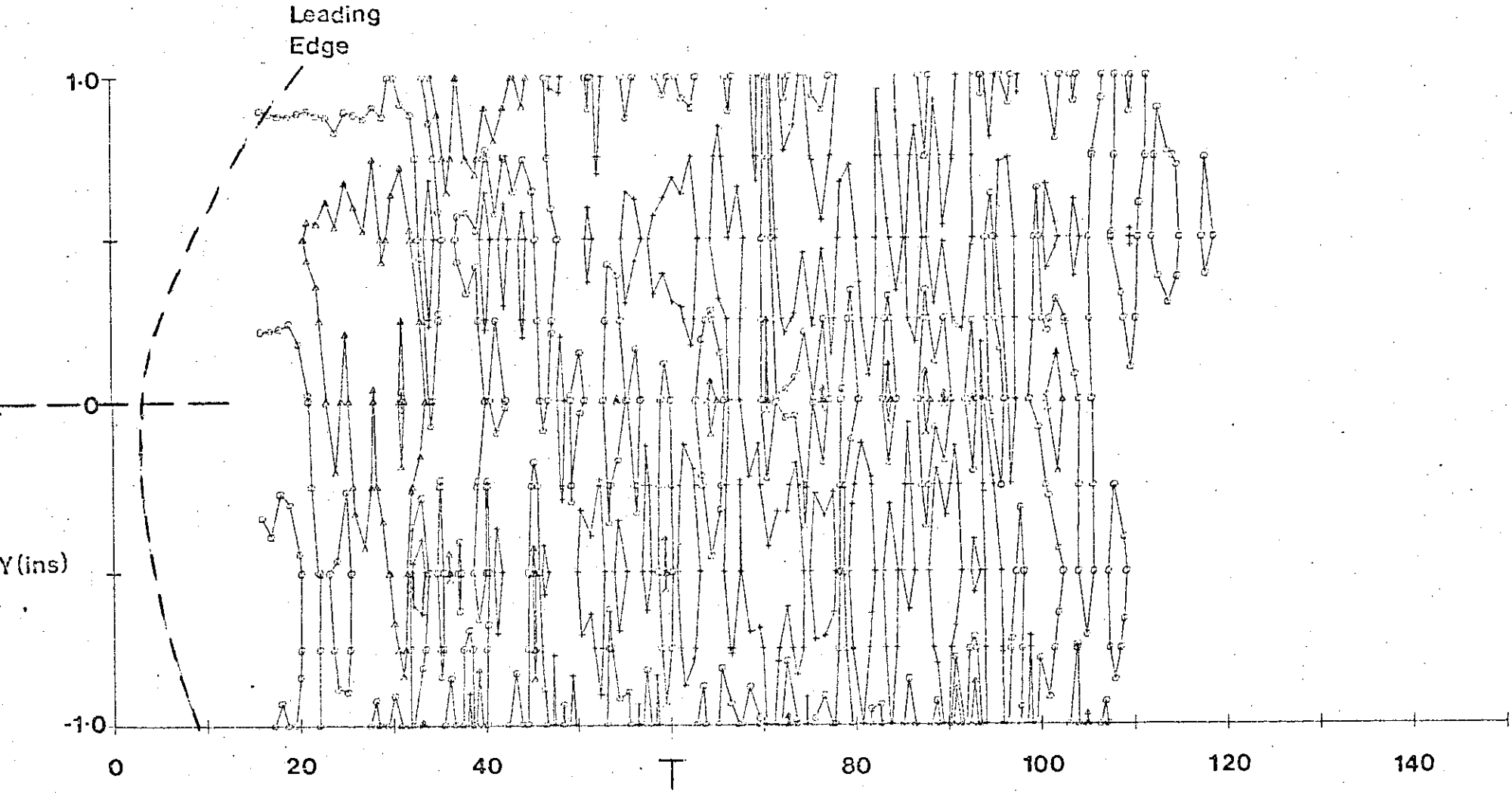

Δ -·01

Fig B2a : W/U_o, Normal Mean Velocity; $z/\delta = 0{\cdot}8$. Legend o 0 , T is in 1/1500s. $R_\delta = 1385$.

+ ·01

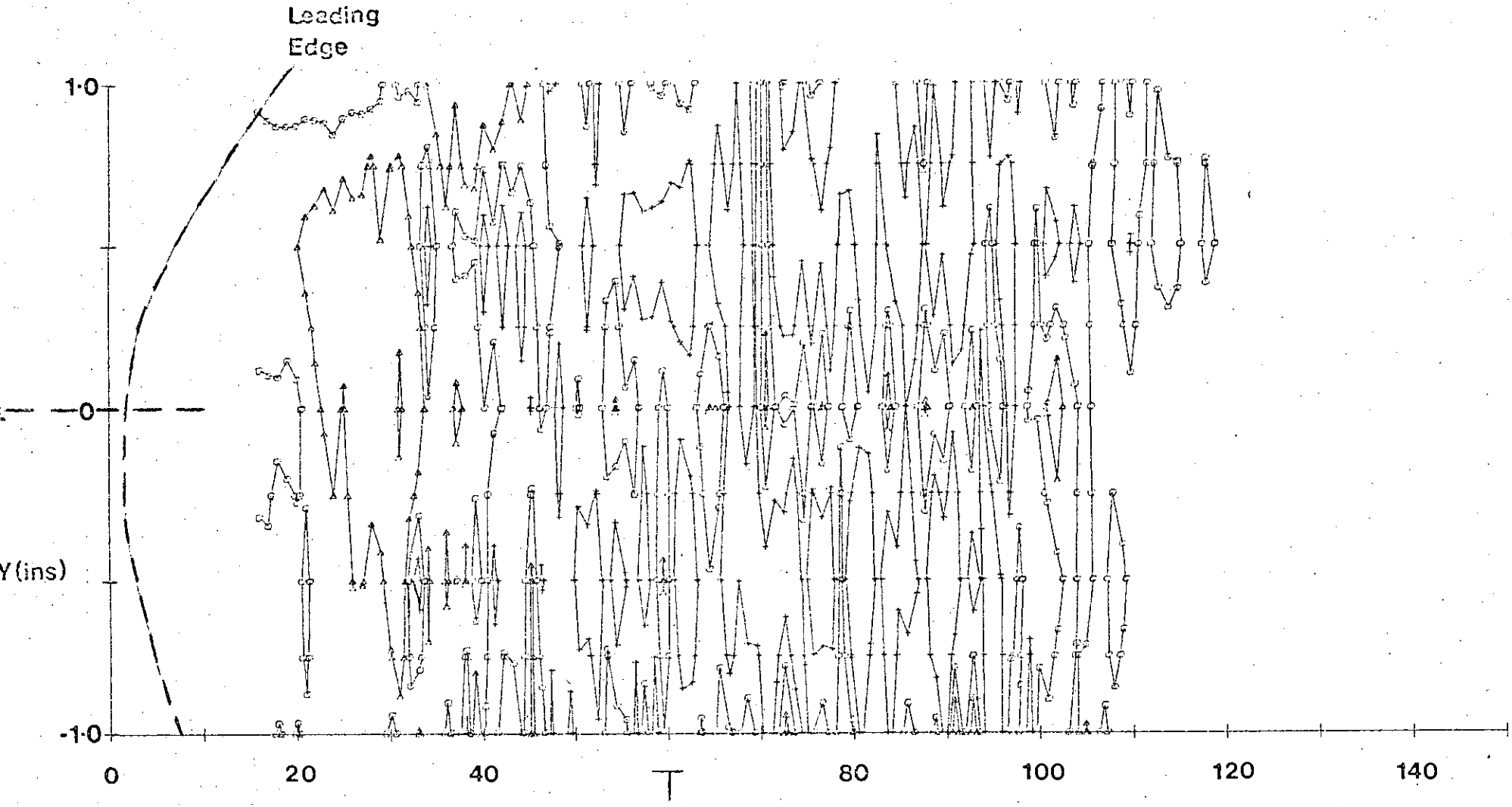

Δ ·01

Fig B2b : W/U_o, Normal Mean Velocity; $z/\delta = 0{\cdot}9$. Legend o 0 , T is in 1/1500s. $R_\delta = 1385$.

+ ·01

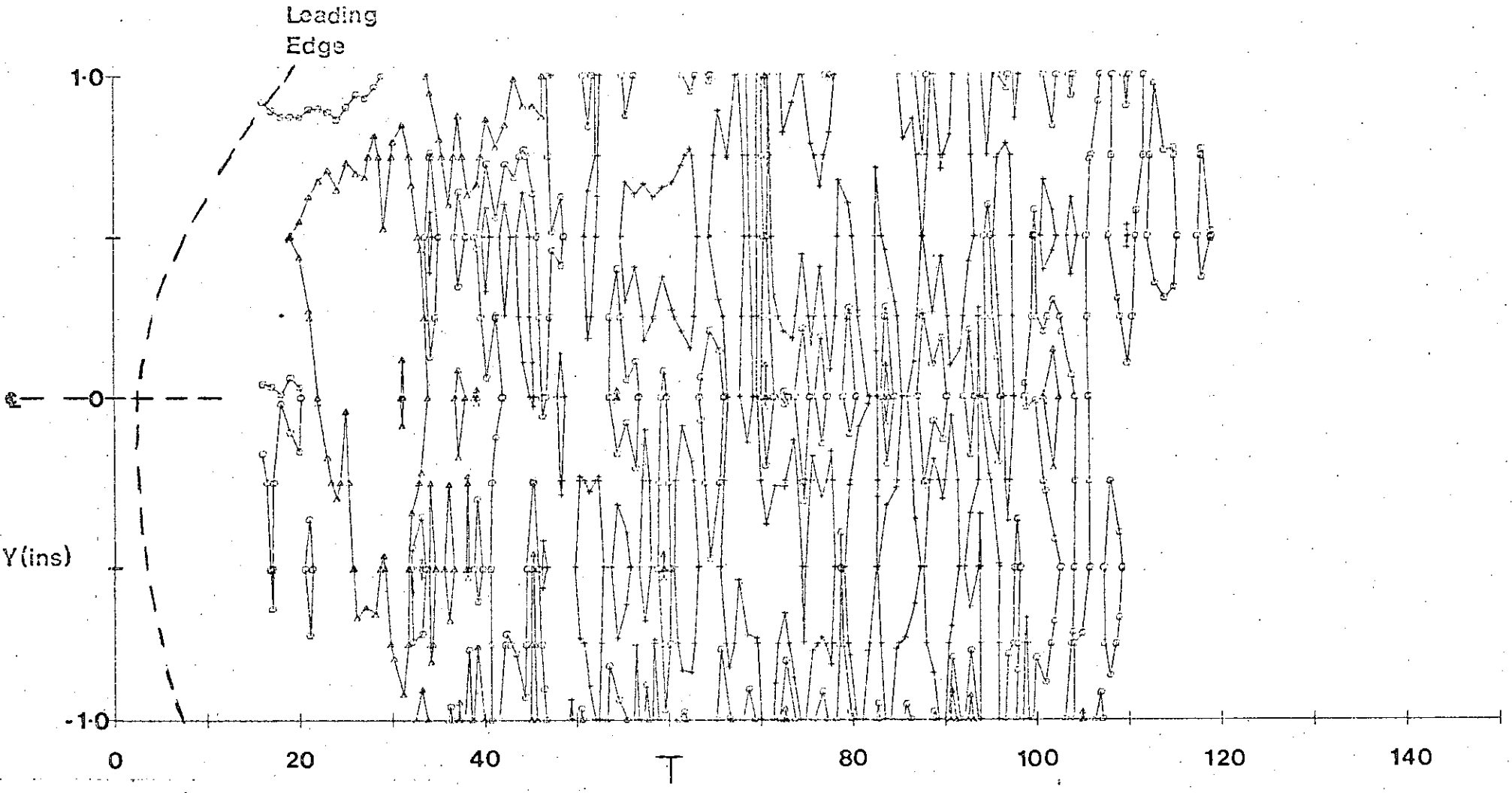

Fig B2c : W/U_o, Normal Mean Velocity; $z/\delta = 1{\cdot}0$. Legend o 0 , T is in 1/1500s. $R_\delta = 1385$.

+ ·01

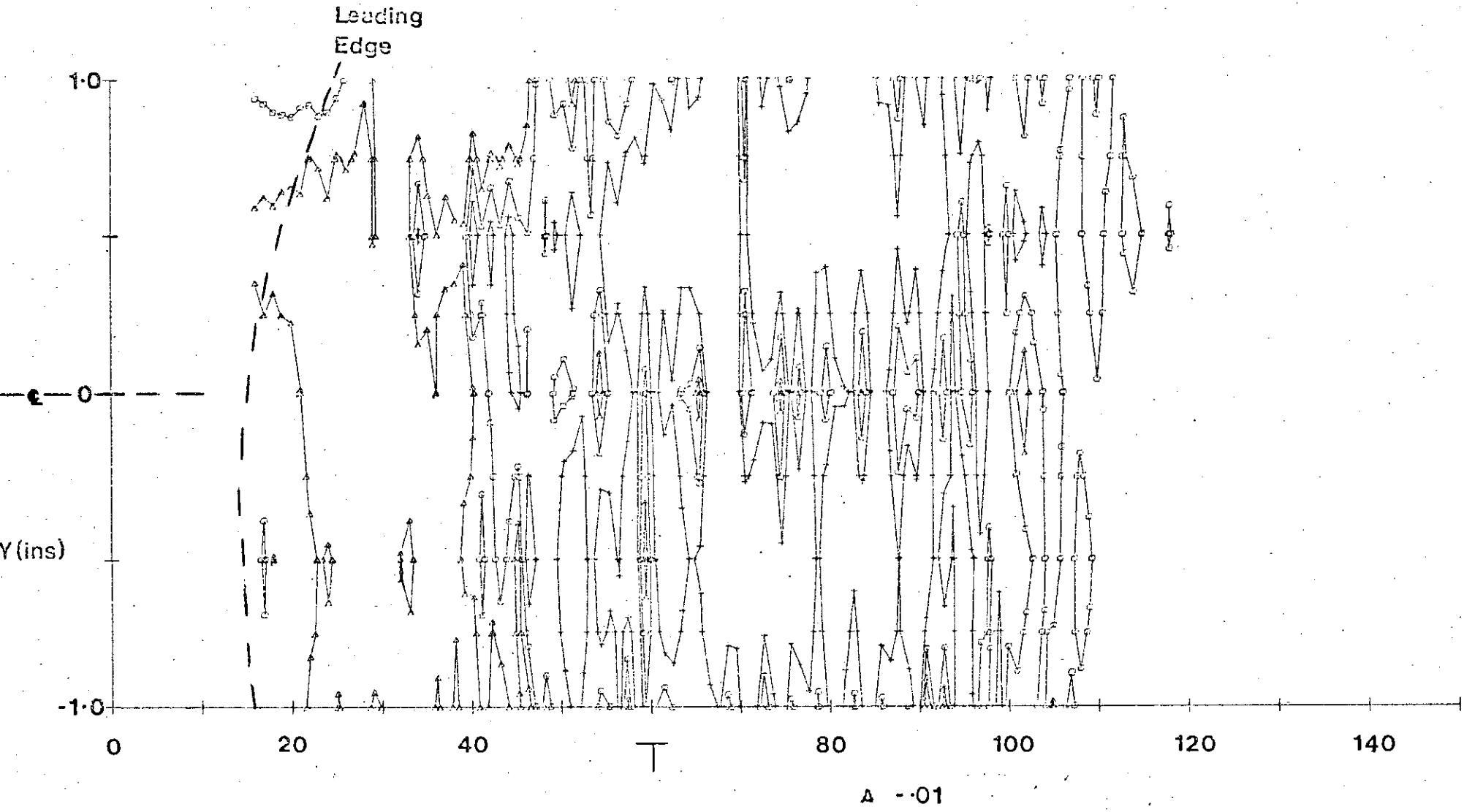

Fig B2d : W/U_o, Normal Mean Velocity; $z/\delta = 1{\cdot}5$. Legend

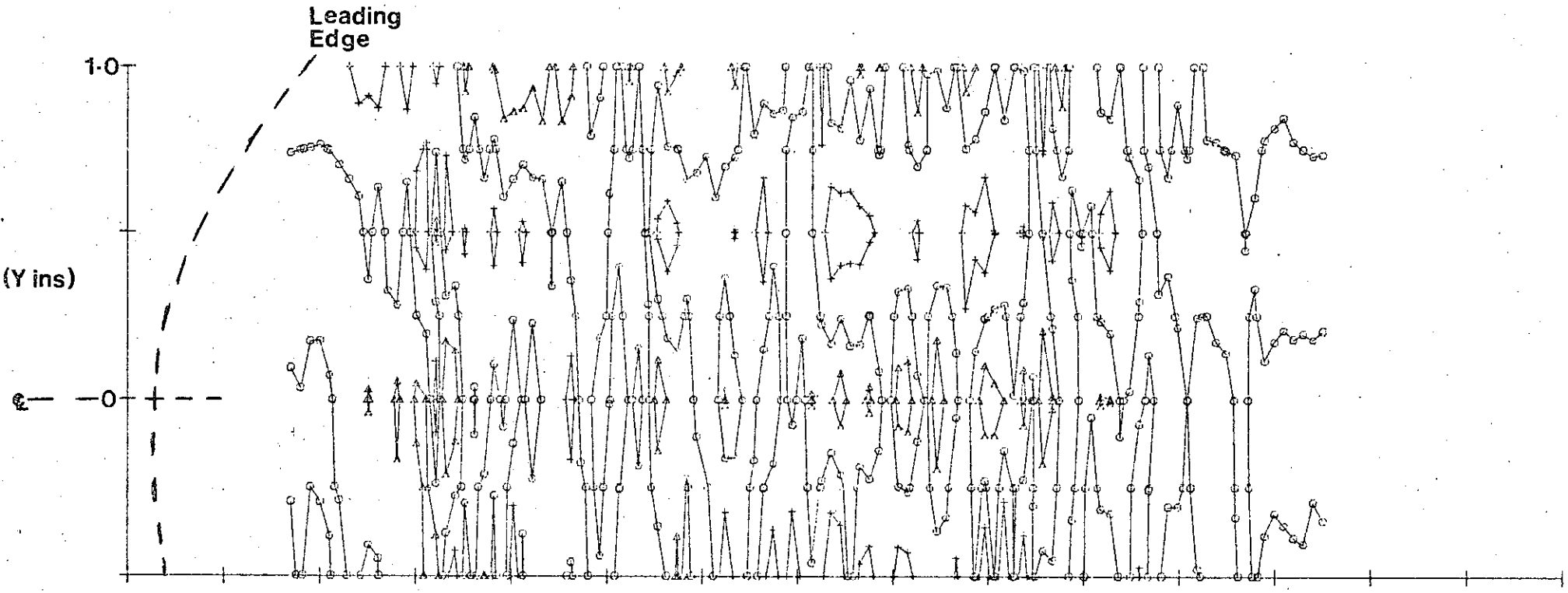

Fig B3: Streamwise Mean Vorticity; $z/\delta = 1.0$. Legend $\begin{matrix} \Delta & -.01 \\ o & 0 \\ + & .01 \end{matrix}$, T is in 1/1500s. $R_\delta = 1385$.

REFERENCES

1. F.H. Barnes, Ph.D. Thesis, Edinburgh University (1966).
2. R.F. Blackwelder and L.S.G. Kovasznay, Phys. Fluids 15, No. 9, p. 1545 (1972).
3. F.H. Champagne and C.A. Sleicher, J. Fluid Mech. 28, 177 (1967).
4. E.R. Corino and R.S. Brodkey, J. Fluid Mech. 37, 1 (1969).
5. H.W. Emmons, J. Aero Sci. 18, No. 7, 490 (July 1951).
6. F.R. Hama, J.D. Long and J.C. Hagarty, J. Appl. Phys. 28, 388 (1957).
7. R.E. Kaplan and J. Laufer, Proc. 12th International Congress on Appl. Mech. (Springer-Verlag, Berlin, 1969), p. 236.
8. H.T. Kim, S.J. Kline and W.C. Reynolds, J. Fluid Mech. 50, 133 (1971).
9. P.S. Klebanoff, K.D. Tidstrom and L.M. Sargent, J. Fluid Mech. 12, 1, (1962).
10. L.S.G. Kovasznay, V. Kibens and R.F. Blackwelder, J. Fluid Mech. 41, 283 (1970).
11. L.S.G. Kovasznay, H. Komoda and B.R. Vasudeva, Proc. 1962 Heat Transfer and Fluid Mech. Inst., Stanford Univ. Press, 1962.
12. O. Reynolds, Phil. Trans. Roy. Soc. 1883.
13. T.G. Robertson and J.G. Burns, Jour. Phys. E; Sci. Instr. 5 (1972).
14. J.A. Ross, Ph.D. Thesis, Edinburgh University (1969).
15. G.B. Schubauer and P.S. Klebanoff, N.A.C.A. Tech. Note 3489 (1955).
16. G.I. Taylor, Proc. Roy. Soc. A 156, No. 858, 301 (1936).
17. A.A. Townsend, The Structure of Turbulent Shear Flow, Cambridge, 1956.
18. W.W. Willmarth and S.S. Lu, J. Fluid Mech. 55, 65 (1972).

ACKNOWLEDGEMENTS

I should like to thank Dr. M.A.S. Ross for suggesting the topic of this thesis and for her help, encouragement and supervision during the course of the work.

I am also grateful for the many helpful discussions with Dr. F.H. Barnes, Dr. I. Grant and Dr. D. Corner. The technical assistance of Mr. R.F. Lawson and Mr. P. McInnes was gratefully received.

I should like to thank Professor N. Feather, F.R.S., for the use of the facilities in the Department of Physics, University of Edinburgh.

I should also like to thank my wife for her help and patience during this work.

Finally, I would like to thank the Ministry of Defence for the grant which supported me in the initial stages of this work.

SUMMARY.

The on-line facility of the wind tunnel was used to control experiments and collect digitised data. The shape and velocity of propagation of the turbulent spot were determined and the streamwise and spanwise components of mean velocity and the streamwise turbulent component were measured. The mean velocity component normal to the flat plate was derived using the equation of continuity and the measured mean velocity components. Contour maps of the mean velocity components and the turbulent fluctuations were drawn using a computer controlled graph plotter. From these maps it is deduced that the mean structure of the turbulent spots consists of three spanwise vortices on top of each other. It is proposed that the action of the vortices maintains the high level of turbulence in the turbulent spot by entraining fluid from the free stream.

Turbulent bursting events were alsc observed and are discussed in the light of reports by other workers.